Neutrino Oscillations and Non-standard Interactions

Yasaman Farzan[1] and Mariam Tórtola[2]*

[1] *School of Physics, Institute for Research in Fundamental Sciences, Tehran, Iran,* [2] *AHEP Group, Institut de Física Corpuscular—Universitat de València/CSIC, Paterna, Spain*

Current neutrino experiments are measuring the neutrino mixing parameters with an unprecedented accuracy. The upcoming generation of neutrino experiments will be sensitive to subdominant neutrino oscillation effects that can in principle give information on the yet-unknown neutrino parameters: the Dirac CP-violating phase in the PMNS mixing matrix, the neutrino mass ordering and the octant of θ_{23}. Determining the exact values of neutrino mass and mixing parameters is crucial to test various neutrino models and flavor symmetries that are designed to predict these neutrino parameters. In the first part of this review, we summarize the current status of the neutrino oscillation parameter determination. We consider the most recent data from all solar neutrino experiments and the atmospheric neutrino data from Super-Kamiokande, IceCube, and ANTARES. We also implement the data from the reactor neutrino experiments KamLAND, Daya Bay, RENO, and Double Chooz as well as the long baseline neutrino data from MINOS, T2K, and NOνA. If in addition to the standard interactions, neutrinos have subdominant yet-unknown Non-Standard Interactions (NSI) with matter fields, extracting the values of these parameters will suffer from new degeneracies and ambiguities. We review such effects and formulate the conditions on the NSI parameters under which the precision measurement of neutrino oscillation parameters can be distorted. Like standard weak interactions, the non-standard interaction can be categorized into two groups: Charged Current (CC) NSI and Neutral Current (NC) NSI. Our focus will be mainly on neutral current NSI because it is possible to build a class of models that give rise to sizeable NC NSI with discernible effects on neutrino oscillation. These models are based on new $U(1)$ gauge symmetry with a gauge boson of mass $\lesssim 10$ MeV. The UV complete model should be of course electroweak invariant which in general implies that along with neutrinos, charged fermions also acquire new interactions on which there are strong bounds. We enumerate the bounds that already exist on the electroweak symmetric models and demonstrate that it is possible to build viable models avoiding all these bounds. In the end, we review methods to test these models and suggest approaches to break the degeneracies in deriving neutrino mass parameters caused by NSI.

Keywords: neutrino oscillations, leptonic CP violation, non-standard neutrino interactions, neutrino masses, neutrino physics

1. INTRODUCTION

In the framework of "old" electroweak theory, formulated by Glashow, Weinberg and Salam, lepton flavor is conserved and neutrinos are massless. As a result, a neutrino of flavor α ($\alpha \in \{e, \mu, \tau\}$) created in charged current weak interactions in association with a charged lepton of flavor α will maintain its flavor. Various observations have however shown that the flavor of neutrinos change upon propagating long distances. Historically, solar neutrino anomaly (deficit of the solar neutrino flux relative to standard solar model predictions) [1] and atmospheric neutrino anomaly (deviation of the ratio of muon neutrino flux to the electron neutrino flux from 2 for atmospheric neutrinos that cross the Earth before reaching the detector) [2] were two main observations that showed the lepton flavor was violated in nature. This conclusion was further confirmed by observation of flavor violation of man-made neutrinos after propagating sizable distances in various reactor [3–5] and long baseline experiments [6, 7]. The established paradigm for flavor violation which impressively explain all these anomalies is the three neutrino mass and mixing scheme. According to this scheme, each neutrino flavor is a mixture of different mass eigenstates. As neutrinos propagate, each component mass eigenstate acquires a different phase so neutrino of definite flavor will convert to a mixture of different flavors; hence, lepton flavor violation takes place.

Within this scheme, the probability of conversion of ν_α to ν_β (as well as that of $\bar{\nu}_\alpha$ to $\bar{\nu}_\beta$) in vacuum or in matter with constant density has a oscillatory dependence on time or equivalently on the distance traveled by neutrinos[1]. For this reason, the phenomenon of flavor conversion in neutrino sector is generally known as neutrino oscillation. Neutrino flavor eigenstates are usually denoted by ν_α. That is ν_α is defined as a state which appears in W boson vertex along with charged lepton l_α ($\alpha \in \{e, \mu, \tau\}$). The latter corresponds to charged lepton mass eigenstates. Neutrino mass eigenstates are denoted by ν_i with mass m_i where $i \in \{1, 2, 3\}$. The flavor eigenstates are related to mass eigenstate by a 3×3 unitary matrix, U, known as PMNS after Pontecorvo-Maki-Nakagawa-Sakata: $\nu_\alpha = \sum_i U_{\alpha i} \nu_i$. The unitary mixing matrix can be decomposed as follows

$$U \equiv \begin{pmatrix} 1 & 0 & 0 \\ 0 & \cos\theta_{23} & \sin\theta_{23} \\ 0 & -\sin\theta_{23} & \cos\theta_{23} \end{pmatrix} \begin{pmatrix} \cos\theta_{13} & 0 & \sin\theta_{13}e^{-i\delta} \\ 0 & 1 & 0 \\ -\sin\theta_{13}e^{i\delta} & 0 & \cos\theta_{13} \end{pmatrix}$$
$$\begin{pmatrix} \cos\theta_{12} & \sin\theta_{12} & 0 \\ -\sin\theta_{12} & \cos\theta_{12} & 0 \\ 0 & 0 & 1 \end{pmatrix}, \quad (1)$$

where the mixing angles θ_{ij} are defined to be in the $[0, \pi/2]$ range while the phase δ can vary in $[0, 2\pi]$. In this way, the whole physical parameter space is covered. Historically, ν_1, ν_2 and ν_3 have been defined according to their contribution to ν_e. In other words, they are ordered such that $|U_{e1}| > |U_{e2}| > |U_{e3}|$ so ν_1 (ν_3)

---

[1]One should bear in mind that in a medium with varying density, such as the Sun interior, the conversion may not have an oscillatory behavior for a certain energy range. Likewise, the presence of strong matter effects may suppress the oscillatory behavior even in the case of constant density [8].

provides largest (smallest) contribution to ν_e. Notice that with this definition, $\theta_{12}, \theta_{13} \leq \pi/4$. It is then of course a meaningful question to ask which ν_i is the lightest and which one is the heaviest; or equivalently, what is the sign of $\Delta m_{ij}^2 = m_i^2 - m_j^2$. The answer to this question comes from observation. Time evolution of ultra-relativistic neutrino state is governed by the following Hamiltonian: $H_{vac} + H_m$, where the effective Hamiltonian in vacuum is given by

$$H_{vac} = U \cdot \text{Diag}\left(\frac{m_1^2}{2E}, \frac{m_2^2}{2E}, \frac{m_3^2}{2E}\right) \cdot U^\dagger. \quad (2)$$

Within the Standard Model (SM) of particles, the effective Hamiltonian in matter H_m in the framework of the medium in which neutrinos are propagating can be written as

$$H_m = \begin{pmatrix} \sqrt{2}G_F N_e - \frac{\sqrt{2}}{2}G_F N_n & 0 & 0 \\ 0 & -\frac{\sqrt{2}}{2}G_F N_n & 0 \\ 0 & 0 & -\frac{\sqrt{2}}{2}G_F N_n \end{pmatrix}, \quad (3)$$

where it is assumed that the medium is electrically neutral ($N_e = N_p$), unpolarized and composed of non-relativistic particles. In vacuum, $H_m = 0$ and we can write

$$P(\nu_\alpha \rightarrow \nu_\beta) = \left| \sum_{ij} U_{\alpha i} U_{\beta j}^* e^{i\Delta m_{ij}^2 L/(2E)} \right|^2. \quad (4)$$

By adding or subtracting a matrix proportional to the identity $I_{3\times 3}$ to the Hamiltonian, neutrinos obtain an overall phase with no observable physical consequences. That is why neutrino oscillation probabilities (both in vacuum and in matter) are sensitive only to Δm_{ij}^2 rather than to m_i^2. As a result, it is impossible to derive the mass of the lightest neutrino from oscillation data alone. Similarly, neutrino oscillation pattern within the SM only depends on N_e not on N_n. Similar arguments can be repeated for antineutrinos by replacing U with U^* (or equivalently $\delta \rightarrow -\delta$) and replacing $H_m \rightarrow -H_m$. The phase δ, similarly to its counterpart in the CKM mixing matrix of quark sector, violates CP. Just like in the quark sector, CP violation in neutrino sector is given by the Jarlskog invariant: $\mathcal{J} = \sin\theta_{13}\cos^2\theta_{13}\sin\theta_{12}\cos\theta_{12}\cos\theta_{23}\sin\theta_{23}\sin\delta$.

As we will see in detail in section 2, the mixing angles θ_{12}, θ_{13} and θ_{23} are derived from observations with remarkable precision. The mixing angle θ_{23} has turned out to be close $45°$ but it is not clear within present uncertainties whether $\theta_{23} < \pi/4$ or $\theta_{23} > \pi/4$. This uncertainty is known as the octant degeneracy. The value of δ is also unknown for the time being, although experimental data start indicating a preferred value close to $3\pi/2$. The absolute value and the sign of Δm_{21}^2 are however determined. While $|\Delta m_{31}^2|$ is measured, the sign of Δm_{31}^2 is not yet determined. If $\Delta m_{31}^2 > 0$ ($\Delta m_{31}^2 < 0$), the scheme is called normal (inverted) ordering or normal (inverted) mass spectrum. The main goals of current and upcoming neutrino oscillation experiments are determining $sgn(\cos 2\theta_{23})$, $sgn(\Delta m_{31}^2)$ and the value of the CP–violating phase δ.

The neutrino oscillation program is entering a precision era, where the known parameters are being measured with an ever increasing accuracy. Next generation of long–baseline neutrino experiments will resolve the subdominant effects in oscillation data sensitive to the yet unknown oscillation parameters (e.g., δ). Of course, all these derivations are within 3×3 neutrino mass and mixing scheme under the assumption that neutrinos interact with matter only through the SM weak interactions (plus gravity which is too weak to be relevant). Allowing for Non-Standard Interaction (NSI) can change the whole picture. Non-Standard Interaction of neutrinos can be divided into two groups: Neutral Current (NC) NSI and Charged Current (CC) NSI. While the CC NSI of neutrinos with the matter fields (e, u, d) affects in general the production and detection of neutrinos, the NC NSI may affect the neutrino propagation in matter. As a result, both types of interaction may show up at various neutrino experiments. In recent years, the effects of both types of NSI on neutrino experiments have been extensively studied in the literature, formulating the lower limit on the values of couplings in order to have a resolvable impact on the oscillation pattern in upcoming experiments. On the other hand, non-standard interaction of neutrinos can crucially affect the interpretation of the experimental data in terms of the relevant neutrino mass parameters. Indeed, as it will be discussed in this work, the presence of NSI in the neutrino propagation may give rise, among other effects, to a degeneracy in the measurement of the solar mixing angle θ_{12} [9–11]. Likewise, CC NSI at the production and detection of reactor antineutrinos can affect the very precise measurement of the mixing angle θ_{13} in Daya Bay [12, 13]. Moreover, it has been shown that NSI can cause degeneracies in deriving the CP–violating phase δ [14–17], as well as the correct octant of the atmospheric mixing angle θ_{23} [18] at current and future long–baseline neutrino experiments. Along this review, we will discuss possible ways to resolve the parameter degeneracies due to NSI, by exploiting the capabilities of some of the planned experiments such as the intermediate baseline reactor neutrino experiments JUNO and RENO50 [19].

Most of the analyses involving NSI in neutrino experiments parameterize such interactions in terms of effective four-Fermi couplings. However, one may ask whether it is possible to build viable renormalizable electroweak symmetric UV complete models that underlay this effective interaction with coupling large enough to be discernible at neutrino oscillation experiments. Generally speaking if the effective coupling comes from integrating out a new state (X) of mass m_X and of coupling g_X, we expect the strength of the effective four-Fermi interaction to be given by g_X^2/m_X^2. We should then justify why X has not been so far directly produced at labs. As far as NC NSI is concerned, two solutions exist: (i) X is too heavy; i.e., $m_X \gg m_{EW}$. Recent bounds from the LHC imply $m_X > 4 - 5$ TeV [20] which for even $g_X \sim 1$ implies $g_X^2/m_X^2 \ll G_F$ [21, 22]. Moreover, as shown in Friedland et al. [23], in the range 10 GeV $< m_{Z'} <$ TeV, the monojet searches at the LHC constrain this ratio to values much smaller than 1. (ii) Second approach is to take $m_X \ll m_{EW}$ and $g_X \ll 1$ such that $g_X^2/m_X^2 \sim G_F$. In this approach, the null result for direct production of X is justified with its very small coupling. In Farzan [24], Farzan and Heeck [25], and Farzan

and Shoemaker [26], this approach has been evoked to build viable models for NC NSI with large effective couplings. For CC NSI, the intermediate state, being charged, cannot be light. That is, although its Yukawa couplings to neutrinos and matter fields can be set to arbitrarily small values, the gauge coupling to the photon is set by its charge so the production at LEP and other experiments cannot be avoided. We are not aware of any viable model that can lead to a sizable CC NSI. Interested reader may see Agarwalla et al. [13], Vanegas Forero [27], Bakhti and Khan [28], Khan and Tahir [29], Kopp et al. [30], Bellazzini et al. [31], Akhmedov et al. [32], Biggio and Blennow [33]. Notice that throughout this review, we focus on the interaction of neutrinos with matter fields. Das et al. [34] and Dighe and Sen [35] study the effects of non-standard self-interaction of neutrinos in supernova. de Salas et al. [36], Brdar et al. [37] discuss propagation of neutrino in presence of interaction with dark matter. The effect of NSI on the decoupling of neutrinos in the early Universe has been considered in Mangano et al. [38].

This review is organized as follows. In section 2, we review the different neutrino oscillation experiments and discuss how neutrino oscillation parameters within the standard three neutrino scheme can be derived. We then discuss the prospect of measuring yet unknown parameters: δ, $sgn(\Delta m_{31}^2)$ and $sgn(\cos 2\theta_{23})$. In section 3, we discuss how NSI can affect this picture and review the bounds that the present neutrino data sets on the effective ϵ parameters. We then discuss the potential effects of NSI on future neutrino experiments and suggest strategies to solve the degeneracies. In section 4, we introduce models that can lead to effective NSI of interest and briefly discuss their potential effects on various observables. In section 5, we review methods suggested to test these models. Results will be summarized in section 6.

2. NEUTRINO OSCILLATIONS

In this section, we will present the current status of neutrino oscillation data in the standard three–neutrino framework. Most recent global neutrino fits to neutrino oscillations can be found in de Salas et al. [39], Capozzi et al. [40], and Esteban et al. [41]. Here we will focus on the results of de Salas et al. [39], commenting also on the comparison with the other two analysis. First, we will describe the different experiments entering in the global neutrino analysis, grouped in the solar, reactor, atmospheric and long–baseline sectors. For each of them we will also discuss their main contribution to the determination of the oscillation parameters.

2.1. The Solar Neutrino Sector: ($\sin^2 \theta_{12}$, Δm_{21}^2)

Under the denomination of *solar neutrino sector*, one finds traditionally not only all the solar neutrino experiments, but also the reactor KamLAND experiment, sensitive to the same oscillation channel, under the assumption of CPT conservation. Solar neutrino analysis include the historical radiochemical experiments Homestake [42], Gallex/GNO [43], SAGE [44], sensitive only to the interaction rate of electron neutrinos, but not to their energy or arrival time to the detector. This more detailed

information became available with the start-up of the real–time solar neutrino experiment Kamiokande [45], that confirmed the solar neutrino deficit already observed by the previous experiments. Its successor Super–Kamiokande, with a volume 10 times larger, has provided very precise observations in almost 20 years of operation. Super–Kamiokande is a Cherenkov detector that uses 50 kton of ultra pure water as target for solar neutrino interactions, that are detected through elastic neutrino-electron scattering. This process is sensitive to all neutrino flavors, with a larger cross section for ν_e due to the extra contribution from the charged–current neutrino–electron interaction. The correlation between the incident neutrino and the recoil electron in the observed elastic scattering makes possible the reconstruction of the incoming neutrino energy and arrival direction. After its first three solar phases [46–48], Super-Kamiokande is already in its fourth phase, where a very low energy detection threshold of 3.5 MeV has been achieved [49]. Moreover, during this last period, Super–Kamiokande has reported a 3σ indication of Earth matter effects in the solar neutrino flux, with the following measured value of the day–night asymmetry [50, 51]

$$A_{DN} = \frac{\Phi_D - \Phi_N}{(\Phi_D + \Phi_N)/2} = (-3.3 \pm 1.0 \, (\text{stat}) \pm 0.5 \, (\text{syst})) \, \% \, . \quad (5)$$

Likewise, they have reconstructed a neutrino survival probability consistent with the MSW prediction at 1σ [52, 53].

The Sudbury Neutrino Observatory (SNO) used a similar detection technique with 1 kton of pure heavy water as neutrino target. The use of the heavy water allowed the neutrino detection through three different processes: charged–current ν_e interactions with the deuterons in the heavy water (CC), neutral–current ν_α with the deuterons (NC), and as well as elastic scattering of all neutrino flavors with electrons (ES). The measurement of the neutrino rate for each of the three reactions allows the determination of the ν_e flux and the total active ν_α flux of ^{8}B neutrinos from the Sun. SNO took data during three phases, each of them characterized by a different way of detecting the neutrinos produced in the neutrino NC interaction with the heavy water [54, 55].

Apart from Super–Kamiokande, the only solar neutrino detector at work nowadays is the Borexino experiment. Borexino is a liquid–scintillator experiment sensitive to solar neutrinos through the elastic neutrino–electron scattering, with a design optimized to measure the lower energy part of the spectrum. During its first detection phase, Borexino has reported precise observations of the ^{7}Be solar neutrino flux, as well as the first direct observation of the mono-energetic *pep* solar neutrinos and the strongest upper bound on the *CNO* component of the solar neutrino flux [56]. Moreover, Borexino has also measured the solar ^{8}B rate with a very low energy threshold of 3 MeV [57] and it has also provided the first real–time observation of the very low energy *pp* neutrinos [58].

The simulation of the production and propagation of solar neutrinos requires the knowledge of the neutrino fluxes produced in the Sun's interior. This information is provided by the Standard Solar Model (SSM), originally built by Bahcall [59]. The more recent versions of the SSM offer at least two different

versions according to the solar metallicity assumed [60, 61]. de Salas et al. [39] uses the low metallicity model while Esteban et al. [41] reports its main results for the high–metallicity model. For a discussion on the impact of the choice of a particular SSM over the neutrino oscillation analysis see for instance Esteban et al. [41] and Schwetz et al. [62].

KamLAND is a reactor neutrino experiment designed to probe the existence of neutrino oscillations in the so-called LMA region, with $\Delta m_{21}^2 \sim 10^{-5} \text{eV}^2$. KamLAND detected reactor antineutrinos produced at an average distance of 180 km, providing the first evidence for the disappearance of neutrinos traveling to a detector from a power reactor [63]. In KamLAND, neutrinos are observed through the inverse beta decay process $\bar{\nu}_e + p \rightarrow e^+ + n$, with a delayed coincidence between the positron annihilation and the neutron capture in the medium that allows the efficient reduction of the background. The final data sample released by KamLAND contains a total live time of 2,135 days, with a total of 2,106 reactor antineutrino events observed to be compared with $2,879 \pm 118$ reactor antineutrino events plus 325.9 ± 26.1 background events expected in absence of neutrino oscillations [64].

Figure 1 reports the allowed region in the $\sin^2 \theta_{12} - \Delta m_{21}^2$ plane from the analysis of all solar neutrino data (black lines), from the analysis of the KamLAND reactor experiment (blue lines) and from the combined analysis of solar + KamLAND data (colored regions). Here the value of the θ_{13} has been marginalized following the most recent short–baseline reactor experiments which will be described in the next subsection. From the figure, one can see that the determination of θ_{12} is mostly due to solar neutrino experiments, while the very
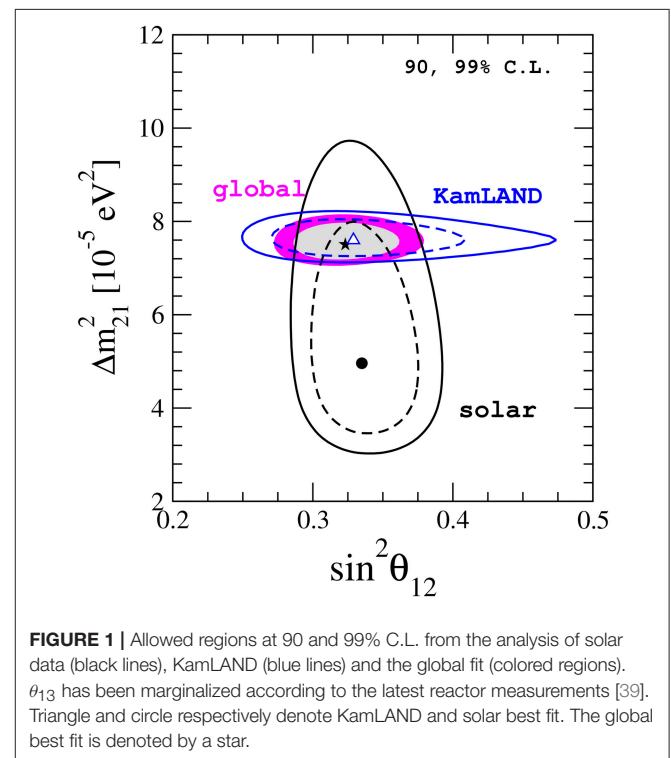

FIGURE 1 | Allowed regions at 90 and 99% C.L. from the analysis of solar data (black lines), KamLAND (blue lines) and the global fit (colored regions). θ_{13} has been marginalized according to the latest reactor measurements [39]. Triangle and circle respectively denote KamLAND and solar best fit. The global best fit is denoted by a star.

accurate measurement of Δm_{21}^2 is obtained thanks to the spectral information from KamLAND. There is also a mild but noticeable tension between the preferred values of Δm_{21}^2 by KamLAND and by solar experiments. While the first one shows a preference for $\Delta m_{21}^2 = 4.96 \times 10^{-5}$ eV^2, the combination of all solar experiments prefer a lower value: $\Delta m_{21}^2 = 7.6 \times 10^{-5}$ eV^2. This discrepancy appears at the 2σ level. As we will see in the next section, non–standard neutrino interactions have been proposed as a way to solve the tension between solar and KamLAND data.

The best fit point for the global analysis corresponds to:

$$\sin^2\theta_{12} = 0.321^{+0.018}_{-0.016}, \ \Delta m_{21}^2 = 7.56 \pm 0.19 \times 10^{-5}\text{eV}^2. \quad (6)$$

Maximal mixing is excluded at more than 7σ.

2.2. Short–Baseline Reactor Neutrino Experiments and θ_{13}

Until recently, the mixing angle θ_{13} was pretty much unknown. Indeed, the only available information about the reactor angle was an upper-bound obtained from the non-observation of antineutrino disappearance at the CHOOZ and Palo Verde reactor experiments [65, 66]: $\sin^2\theta_{13} < 0.039$ at 90% C.L. for $\Delta m_{31}^2 = 2.5 \times 10^{-3}$eV^2. Later on, the interplay between different data samples in the global neutrino oscillation analyses started showing some sensitivity to the reactor mixing angle θ_{13}. In particular, from the combined analysis of solar and KamLAND neutrino data, a non-zero θ_{13} value was preferred [62, 67, 68]. The non-trivial constraint on θ_{13} mainly appeared as a result of the different correlation between $\sin^2\theta_{12}$ and $\sin^2\theta_{13}$ present in the solar and KamLAND neutrino data samples [69, 70]. Moreover, a value of θ_{13} different from zero helped to reconcile the tension between the Δm_{21}^2 best fit points for solar and KamLAND separately. Another piece of evidence for a non-zero value of θ_{13} was obtained from the combination of atmospheric and long-baseline neutrino data [71, 72]. Due to a small tension between the preferred values of $|\Delta m_{31}^3|$ at $\theta_{13} = 0$ by MINOS experiment and Super-Kamiokande atmospheric neutrino data, the combined analysis of both experiments showed a preference for $\theta_{13} > 0$ [73–75].

Nevertheless, the precise determination of θ_{13} was possible thanks to the new generation of reactor neutrino experiments, Daya Bay, RENO and Double Chooz. The main features of these new reactor experiments are, on one side, their increased reactor power compared to their predecessors and, on the other side, the use of several identical antineutrino detectors located at different distances from the reactor cores. Combining these two features results in an impressive increase on the number of detected events. Moreover, the observed event rate at the closest detectors is used to predict the expected number of events at the more distant detectors, without relying on the theoretical predictions of the antineutrino flux at reactors. Several years ago, in the period between 2011 and 2012, the three experiments found evidence for the disappearance of reactor antineutrinos over short distances, providing the first measurement of the angle θ_{13} [3–5]. We will now briefly discuss the main details of each experiment as well as their latest results.

The Daya Bay reactor experiment [4] in China is a multi-detector and multi-core reactor experiment. Electron antineutrinos produced at six reactor cores with 2.9 GW thermal power are observed at eight antineutrino 20 ton Gadolinium-doped liquid scintillator detectors, located at distances between 350 and 2,000 m from the cores. The latest data release from Daya Bay has reported the detection of more than 2.5 millions of reactor antineutrino events, after 1,230 days of data taking [76]. This enormous sample of antineutrino events, together with a significant reduction of systematical errors has made possible the most precise determination of the reactor mixing angle to date [76]

$$\sin^2 2\theta_{13} = 0.0841 \pm 0.0027\,(\text{stat.}) \pm 0.0019\,(\text{syst.}). \quad (7)$$

Likewise, the sensitivity to the effective mass splitting Δm_{ee}^2 has been substantially improved[2],

$$|\Delta m_{ee}^2| = 2.50 \pm 0.06\,(\text{stat.}) \pm 0.06\,(\text{syst.}) \times 10^{-3}\,\text{eV}^2, \quad (8)$$

reaching the accuracy of the long–baseline accelerator experiments, originally designed to measure this parameter.

The RENO experiment [5] in South Korea consists of six aligned reactor cores, equally distributed over a distance of 1.3 km. Reactor antineutrinos are observed by two identical 16 ton Gadolinium-doped Liquid Scintillator detectors, located at approximately 300 (near) and 1,400 m (far detector) from the reactor array center. The RENO Collaboration has recently reported their 500 live days observation of the reactor neutrino spectrum [78, 79], showing an improved sensitivity to the atmospheric mass splitting, $|\Delta m_{ee}^2| = 2.62^{+0.24}_{-0.26} \times 10^{-3}$ eV^2. Their determination for θ_{13} is consistent with the results of Daya Bay:

$$\sin^2 2\theta_{13} = 0.082 \pm 0.009\,(\text{stat.}) \pm 0.006\,(\text{syst.}) \quad (9)$$

The Double Chooz experiment in France detects antineutrinos produced at two reactor cores in a near and far detectors located at distances of 0.4 and 1 km from the neutrino source, respectively [3]. The latest results presented by the Double Chooz collaboration correspond to a period of 818 days of data at far detector plus 258 days of observations with the near detector. From the spectral analysis of the multi-detector neutrino data, the following best fit value for θ_{13} is obtained [80]

$$\sin^2 2\theta_{13} = 0.119 \pm 0.016\,(\text{stat.} + \text{syst.}). \quad (10)$$

Figure 2 illustrates the sensitivity to $\sin^2\theta_{13}$ obtained from the analysis of reactor and global neutrino data for normal and inverted mass ordering. The black line corresponds to the result obtained from the combination of all the reactor neutrino data samples while the others correspond to the individual reactor data samples, as indicated. One can see from the figure that the more constraining results come from Daya Bay and RENO experiments, while Double Chooz shows a more limited sensitivity to θ_{13}. Moreover, the global constraint on

---

[2]Parke [77] discusses the correct form of the definition of Δm_{ee}^2.
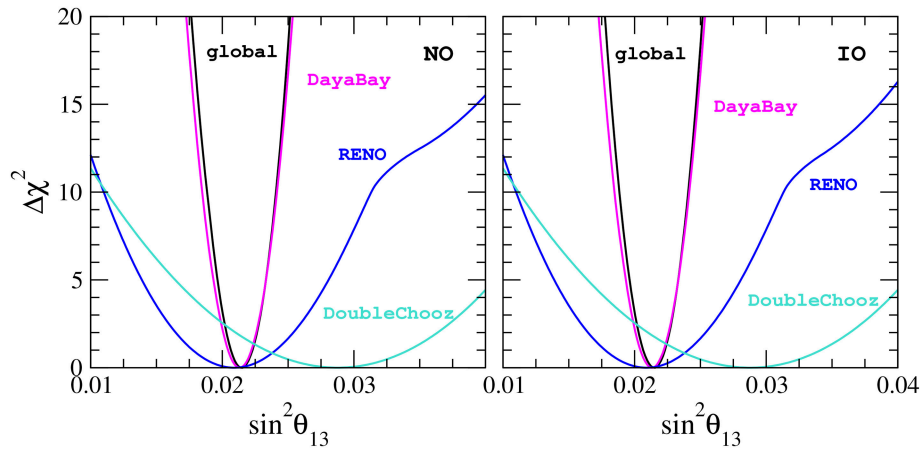
FIGURE 2 | $\Delta\chi^2$ profile as a function of $\sin^2\theta_{13}$ from the analysis of global neutrino data (black line), as well as from the separate analysis of the reactor experiments: Daya Bay (magenta), RENO (blue) and Double Chooz (turquoise). **Left** (**Right**) panel corresponds to normal (inverted) mass ordering. Figure adapted from de Salas et al. [39].

θ_{13} is totally dominated by the Daya Bay measurements, with some contributions from RENO to its lower bound. Notice also that global analyses of neutrino data do not show relevant differences between the preferred value of θ_{13} for normal or inverted mass ordering, as we will discuss later. For more details on the analysis of reactor data presented in **Figure 2**, see de Salas et al. [39].

2.3. The Atmospheric Neutrino Sector: ($\sin^2\theta_{23}$, Δm_{31}^2)

The atmospheric neutrino flux was originally studied as the main source of background for the nucleon-decay experiments [81–83]. For several years, most of the dedicated experiments observed a deficit in the detected number of atmospheric neutrinos with respect to the predictions. The solution to this puzzling situation arrived in 1998, when the observation of the zenith angle dependence of the μ-like atmospheric neutrino data in Super-Kamiokande indicated an evidence for neutrino oscillations [2]. Some years later, the Super-Kamiokande Collaboration reported a L/E distribution of the atmospheric ν_μ data sample characteristic of neutrino oscillations [84]. Super-Kamiokande has been taking data almost continuously since 1996, being now in its fourth phase. Super-Kamiokande is sensitive to the atmospheric neutrino flux in the range from 100 MeV to TeV. The observed neutrino events are classified in three types, fully contained, partially contained and upward-going muons, based on the topology of the event. The subsequent data releases by the Super-Kamiokande Collaboration have increased in complexity. Currently it is very complicated to analyze the latest results by independent groups [39, 41]. From the analysis of the latest Super-Kamiokande atmospheric data, the following best fit values have been obtained for the oscillation parameters [85]:

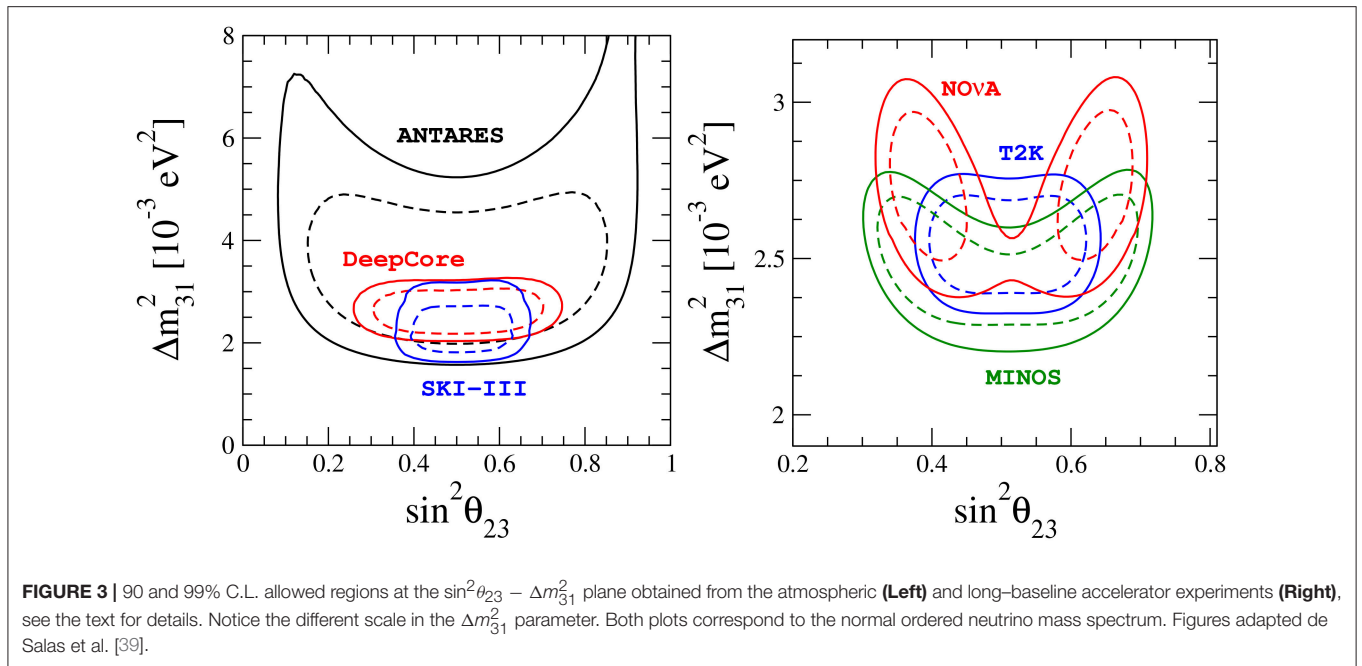$$\sin^2\theta_{23} = 0.587\,, \quad \Delta m_{32}^2 = 2.5 \times 10^{-3}\text{eV}^2. \quad (11)$$

Thus, a slight preference for $\theta_{23} > \pi/4$ is reported. Likewise, the normal mass ordering (i.e., $\Delta m_{31}^2 > 0$) is preferred over the inverted one (i.e., $\Delta m_{31}^2 < 0$).

In recent years, atmospheric neutrinos are also being detected by neutrino telescope experiments. IceCube and ANTARES, originally designed to detect higher energy neutrino fluxes, have reduced their energy threshold in such a way that they can measure the most energetic part of the atmospheric neutrino flux.

The ANTARES telescope [86], located under the Mediterranean Sea, observes atmospheric neutrinos with energies as low as 20 GeV. Neutrinos are detected via the Cherenkov light emitted after the neutrino interaction with the medium in the vicinity of the detector. In Adrian-Martinez et al. [87], the ANTARES Collaboration has analyzed the atmospheric neutrino data collected during a period of 863 days. Their results for the oscillation parameters are in good agreement with current world data. For the first time, ANTARES results have also been included in a global neutrino oscillation fit [39].

The IceCube DeepCore detector is a sub-array of the IceCube neutrino observatory, operating at the South Pole [88]. DeepCore was designed with a denser instrumentation compared to IceCube, with the goal of lowering the energy threshold for the detection of atmospheric muon neutrino events below 10 GeV. Neutrinos are identified trough the Cherenkov radiation emitted by the secondary particles produced after their interaction in the ice. The most recent data published by DeepCore correspond to a live time of 3 years [89]. A total of 5,174 atmospheric neutrino events were observed, compared to a total 6,830 events expected in absence of neutrino oscillations. The obtained best fit values for the atmospheric neutrino parameters $\sin^2\theta_{23} = 0.53^{+0.09}_{-0.12}$ and $\Delta m_{32}^2 = 2.72^{+0.19}_{-0.20} \times 10^{-3}$ eV^2 are also compatible with the atmospheric results of the Super–Kamiokande experiment.

The left panel of **Figure 3** shows the allowed regions at 90 and 99% C.L. in the atmospheric neutrino oscillation parameters $\sin^2\theta_{23}$ and Δm_{31}^2 obtained from ANTARES, DeepCore and Super-Kamiokande phases I to III [39]. From the combination

FIGURE 3 | 90 and 99% C.L. allowed regions at the $\sin^2\theta_{23} - \Delta m_{31}^2$ plane obtained from the atmospheric **(Left)** and long–baseline accelerator experiments **(Right)**, see the text for details. Notice the different scale in the Δm_{31}^2 parameter. Both plots correspond to the normal ordered neutrino mass spectrum. Figures adapted de Salas et al. [39].

one sees that DeepCore results start being competitive with the determination of the atmospheric oscillation parameters by long-baseline experiments. Indeed, a recent reanalysis of DeepCore atmospheric data [90] shows an improved sensitivity with respect to the region plotted in **Figure 3**. The sensitivity of ANTARES shown in **Figure 3** is not yet competitive with the other experiments. However, it is expected that the ANTARES collaboration will publish an updated analysis that will certainly improve their sensitivity to the atmospheric neutrino parameters.

2.4. Long–Baseline Accelerator Experiments

After the discovery of neutrino oscillations in the atmospheric neutrino flux, several long-baseline accelerator experiments were planned to confirm the oscillation phenomenon with a man–made neutrino source. The first two experiments trying to probe the ν_μ disappearance oscillation channel in the same region of Δm^2 as explored by atmospheric neutrinos were K2K and MINOS. Their successors, T2K and NOνA are still at work today.

The KEK to Kamioka (K2K) experiment used a neutrino beam produced by a 12 GeV proton beam from the KEK proton synchrotron. The neutrino beam was detected by a near detector 300 m away from the proton target and by the Super–Kamiokande detector, at a distance of 250 km. The number of detected neutrino events, as well as the spectral distortion of the neutrino flux observed by K2K was fully consistent with the hypothesis of neutrino oscillation [91].

The Main Injector Neutrino Oscillation Search (MINOS) experiment observed neutrino oscillations from a beam produced by the NuMI (Neutrinos at Main Injector) beamline at Fermilab in an underground detector located at the Soudan Mine, in Minnesota, 735 km away. MINOS searched for oscillations in the disappearance ($\nu_\mu \rightarrow \nu_\mu$) and appearance channels ($\nu_\mu \rightarrow \nu_e$),

for neutrinos and antineutrinos as well. After a period of 9 years, the MINOS experiment collected a data sample corresponding to an exposure of 10.71×10^{20} protons on target (POT) in the neutrino mode, and 3.36×10^{20} POT in the antineutrino mode [92, 93]. The combined analysis of all MINOS data shows a slight preference for inverted mass ordering and θ_{23} below maximal as well as a disfavored status for maximal mixing with $\Delta\chi^2 = 1.54$ [94]. The allowed ranges for the atmospheric parameters from the joint analysis of all MINOS data are the following

$$\sin^2\theta_{23} \in [0.35, 0.65] \ (90\% \ \text{C.L.}),$$
$$|\Delta m_{32}^2| \in [2.28, 2.46] \times 10^{-3} \ \text{eV}^2 \ (1\sigma) \ \text{for normal ordering} \tag{12}$$

$$\sin^2\theta_{23} \in [0.34, 0.67] \ (90\% \ \text{C.L.}),$$
$$|\Delta m_{32}^2| \in [2.32, 2.53] \times 10^{-3} \ \text{eV}^2 \ (1\sigma) \ \text{for inverted ordering.} \tag{13}$$

The Tokai to Kamioka (T2K) experiment uses a neutrino beam consisting mainly of muon neutrinos, produced at the J-PARC accelerator facility and observed at a distance of 295 km and an off-axis angle of $2.5°$ by the Super-Kamiokande detector. The most recent results of the T2K collaboration for the neutrino and antineutrino channel have been published in Abe et al. [95, 96]. A separate analysis of the disappearance data in the neutrino and antineutrino channels has provided the determination of the best fit oscillation parameters for neutrinos and antineutrinos [96]. The obtained results are consistent so, no hint for CPT violation in the neutrino sector has been obtained [97, 98][3]. In both cases, the preferred value of the atmospheric angle is compatible with maximal mixing. The combined analysis of the neutrino and

---

[3]See Barenboim et al. [99] for updated bounds on CPT violation from neutrino oscillation data.

antineutrino appearance and disappearance searches in T2K, that corresponds to a total sample of 7.482×10^{20} POT in the neutrino mode, and 7.471×10^{20} POT in the antineutrino mode, results in the best determination of the atmospheric oscillation parameters to date [95]

$$\sin^2 \theta_{23} = 0.532 \, (0.534) \,, \; |\Delta m_{32}^2| = 2.545 \, (2.510) \times 10^{-3} \, \text{eV}^2 \,, \tag{14}$$

for normal (inverted) mass ordering spectrum. Furthermore, thanks to the combination of neutrino and antineutrino data, T2K has already achieved a mild sensitivity to the CP violating phase, reducing the allowed 90% C.L. range of δ in radians to $[-3.13, -0.39]$ for normal and $[-2.09, -0.74]$ for inverted mass ordering [95].

In the NOνA (NuMI Off-Axis ν_e Appearance) experiment, neutrinos produced at the Fermilab's NuMI beam are detected in Ash River, Minnesota, after traveling 810 km through the Earth. In the same way as the T2K experiment, the NOνA far detector is located slightly off the centerline of the neutrino beam coming from Fermilab. Thanks to this configuration, a large neutrino flux is obtained at energies close to 2 GeV, where the maximum of the muon to electron neutrino oscillations is expected. The most recent data release from the NOνA collaboration corresponds to an accumulated statistics of 6.05×10^{20} POT in the neutrino run [100, 101]. For the muon antineutrino disappearance channel, 78 events have been observed, to be compared with 82 events expected for oscillation and 473 ± 30 events predicted under the no-oscillation hypothesis. The searches for $\nu_\mu \rightarrow \nu_e$ transitions in the accelerator neutrino flux have reported the observation of 33 electron neutrino events, with an expected background of 8.2 ± 0.8 ν_e events. The analysis of the NOνA Collaboration disfavors maximal values of θ_{23} at the 2.6σ level [100]. On the other hand, from the analysis of the appearance channel it is found that the inverted mass ordering is disfavored at 0.46σ, due to the small number of event predicted for this ordering in comparison to the observed results [101]. Furthermore, the combination of appearance and disappearance NOνA data with the θ_{13} measurement at the reactor experiments results disfavors the scenario with inverted neutrino mass ordering and $\theta_{23} < \pi/2$ at 93% C.L., regardless of the value of δ [101].

The right panel of **Figure 3** shows the 90 and 99% C.L. allowed region in the atmospheric neutrino oscillation parameters $\sin^2 \theta_{23}$ and Δm_{31}^2 according to the MINOS, T2K and NOνA data for normal mass ordering [39]. Note the different scale for Δm_{31}^2 with respect to the left panel. The three long–baseline experiments provide similar constraints on this parameter, while the constraint on θ_{23} obtained from T2K is a bit stronger. One can also see some small differences between the preferred values of θ_{23} by the three experiments. While T2K prefers maximal mixing, MINOS and NOνA show a slight preference for non-maximal θ_{23}. In any case, these differences are not significant and the agreement among the three experiments is quite good. Although not shown here, the agreement for inverted mass ordering is a bit worse, since in that case the rejection of NOνA against maximal mixing is stronger, whereas the preference for $\theta_{23} \sim \pi/4$ in T2K remains the same as for normal ordering.

2.5. Global Fit to Neutrino Oscillations

In the previous subsections, we have reviewed the different experimental neutrino data samples, discussing their dominant sensitivity to one or two oscillation parameters. However, every data sample offers subleading sensitivities to other parameters as well. Although the information they can provide about such parameters may be limited, in combination with the rest of data samples, relevant information can emerge. This constitutes the main philosophy behind global analyses of neutrino oscillation data: joint analyses trying to exploit the complementarity of the different experiments to improve our knowledge on the neutrino oscillation parameters. Here, we will show the results of a combined analysis of neutrino oscillation data in the framework of the three-flavor neutrino oscillation scheme.

Figure 4 reports the 90, 95, and 99% C.L. allowed regions in the parameters $\sin^2 \theta_{23}$, $\sin^2 \theta_{13}$, $|\Delta m_{31}^2|$ and δ from the global fit in de Salas et al. [39] for normal and inverted mass ordering. For the allowed regions in the solar plane $\sin^2 \theta_{12} - \Delta m_{21}^2$, see **Figure 1**. The best fit points, along with the corresponding 1σ uncertainties and 90% C.L. ranges for each parameter, are quoted in **Table 1**. The relative uncertainties on the oscillation parameters at 1σ range from around 2% for the mass splittings to 7–10% (depending on the mass ordering) for $\sin^2 \theta_{23}$. In case of the CP phase, the 1σ uncertainties are of the order of 15–20%. Note also that, at the 3σ level, the full range of δ is still allowed for normal ordering. For the case of inverted ordering, a third of the total range is now excluded at the 3σ level. These results are in good agreement with Capozzi et al. [40] and Esteban et al. [41].

Despite the remarkable sensitivity reached in the determination of most of the neutrino oscillation parameters, there are still three unknown parameters in the oscillation of standard three neutrino scheme: the octant of θ_{23}, the value of the CP phase δ and the neutrino mass ordering. The current status of these still unknown parameters will be discussed next.

Let us now comment on the maximality/non-maximality and octant preference for the atmospheric mixing angle. So far, experimental neutrino data have not shown a conclusive preference for values of θ_{23} smaller, equal or larger than $\pi/4$. Different experiments may show a limited preference for one of the choices, but for the moment all the results are consistent at the 3σ level. On the other hand, one finds that the available global analyses of neutrino data [39–41], using very similar data samples show slightly different results for the octant preference. For this particular case, one can find the origin of the possible discrepancies in the different treatment of the Super–Kamiokande atmospheric data. See the previous references for more details on the chosen approach at each work. The results in **Figure 4** and **Table 1**, corresponding to the analysis in de Salas et al. [39], show a preference for θ_{23} in the first octant. This global best fit point corresponds to normal mass ordering, but a local minimum can also be found with $\theta_{23} > \pi/4$ and inverted mass ordering with a $\Delta \chi^2 = 4.3$. In the same way, additional local minima can be found with θ_{23} in the second octant and inverted mass spectrum and the other way around. All these possibilities are allowed at 90% C.L. as can be seen in the right panel of **Figure 4**. With current data, the status of the maximal atmospheric mixing is a bit delicate, being allowed only at 99%
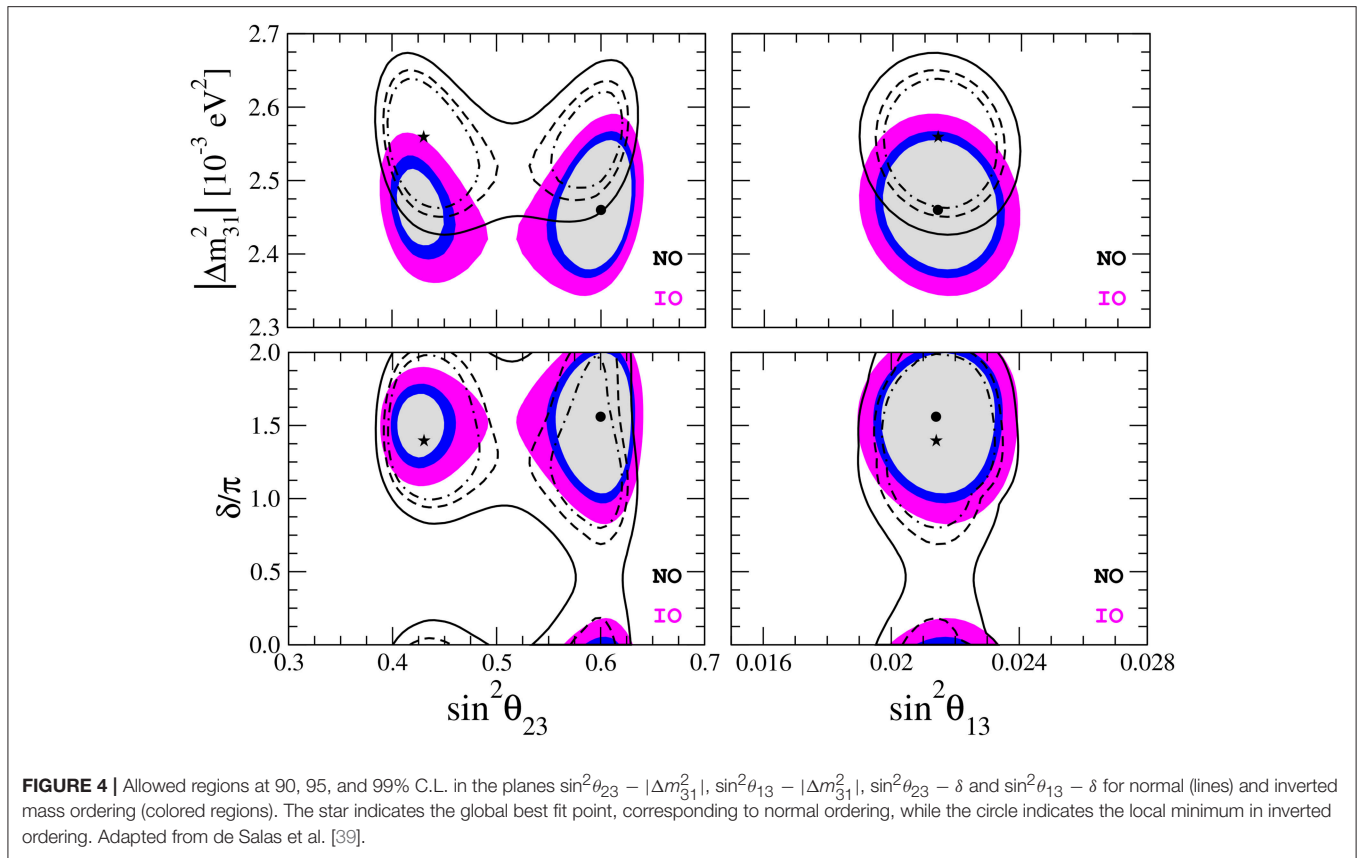
FIGURE 4 | Allowed regions at 90, 95, and 99% C.L. in the planes $\sin^2\theta_{23} - |\Delta m^2_{31}|$, $\sin^2\theta_{13} - |\Delta m^2_{31}|$, $\sin^2\theta_{23} - \delta$ and $\sin^2\theta_{13} - \delta$ for normal (lines) and inverted mass ordering (colored regions). The star indicates the global best fit point, corresponding to normal ordering, while the circle indicates the local minimum in inverted ordering. Adapted from de Salas et al. [39].

TABLE 1 | Neutrino oscillation parameters summary determined from the global analysis in de Salas et al. [39]. The ranges for inverted ordering refer to the local minimum of this neutrino mass ordering.

Parameter	Best fit $\pm 1\sigma$	90% C.L. range
Δm^2_{21} [10^{-5}eV^2]	7.56 ± 0.19	7.26–7.87
Δm^2_{31} [10^{-3}eV^2] (NO)	2.55 ± 0.04	2.48–2.62
$|\Delta m^2_{31}|$ [10^{-3}eV^2] (IO)	$2.47^{+0.04}_{-0.05}$	2.40–2.53
$\sin^2\theta_{12}/10^{-1}$	$3.21^{+0.18}_{-0.16}$	0.294–0.352
$\sin^2\theta_{23}/10^{-1}$ (NO)	$4.30^{+0.20}_{-0.18}$a	0.403–0.466 & 0.577–0.608
$\sin^2\theta_{23}/10^{-1}$ (IO)	$5.98^{+0.17}_{-0.15}$b	0.569–0.623
$\sin^2\theta_{13}/10^{-2}$ (NO)	$2.155^{+0.090}_{-0.075}$	0.0201–0.0228
$\sin^2\theta_{13}/10^{-2}$ (IO)	$2.155^{+0.076}_{-0.092}$	0.0201–0.0228
δ/π (NO)	$1.40^{+0.31}_{-0.20}$	0.98–2.00
δ/π (IO)	$1.56^{+0.22}_{-0.26}$	1.15–1.90

[a]Local min. at $\sin^2\theta_{23} = 0.596$ with $\Delta\chi^2 = 2.1$ w.r.t. the global min.
[b]Local min. at $\sin^2\theta_{23} = 0.426$ with $\Delta\chi^2 = 3.0$ w.r.t. the global min. for IO.

C.L. However, this result may change after the implementation of the partially published data release of T2K [102] in the global fit.

In the same way, the current neutrino oscillation data do not offer a definitive determination for the neutrino mass ordering. Individual neutrino experiments show in general a limited sensitivity to the mass ordering, with the exception of

the latest atmospheric data from Super-Kamiokande, that prefer normal mass ordering with a significance of $\Delta\chi^2 = 4.3$. Note however that this data sample is not included in some of the global analyses of neutrino oscillations [39, 41]. The sensitivity to the mass ordering in the global analysis arises instead from the interplay of the different neutrino data, as a result of the existing correlations and tensions among the other neutrino parameters. Indeed, the three global analysis discussed in this review show a preference for normal mass ordering, although the significance may be different in each case, depending on the particular details of the specific global fit. In the work in de Salas et al. [39], discussed in a bit more details here, a preference for normal ordering over inverted is obtained, with a significance of $\Delta\chi^2 = 4.3$. In any case, the results reported are not conclusive yet, and we will have to wait for the next generation of experiments devoted to this purpose (among others), such as DUNE [103], PINGU [104], ORCA [105], JUNO [106], or RENO-50 [107].

Finally, we comment on the sensitivity to the CP-violating phase δ. Prior to the publication of the antineutrino run data from T2K, combined analyses were already showing a weak preference for $\delta = 3\pi/2$, while $\delta = \pi/2$ was disfavored above the 2σ level [108–110]. This sensitivity, absent in all the individual data samples, emerged from the tension between the value of θ_{13} measured at the reactor experiments and the preferred value of θ_{13} for $\delta = \pi/2$ in T2K. This scenario has changed after the release of T2K results from its antineutrino run and now the sensitivity to δ comes mainly from the combined analysis of

the neutrino and antineutrino channel in T2K. The remaining experiments contribute only marginally to the determination of the CP–violating phase.

3. CURRENT BOUNDS ON NON–STANDARD INTERACTIONS

New neutrino interactions beyond the Standard Model are natural features in most neutrino mass models [111, 112]. As commented in the introduction, these Non–Standard Interactions (NSI) may be of Charged-Current (CC) or of Neutral-Current (NC) type. In the low energy regime, neutrino NSI with matter fields can be formulated in terms of the effective four-fermion Lagrangian terms as follows:

$$\mathcal{L}_{\text{CC–NSI}} = -2\sqrt{2}G_F \epsilon_{\alpha\beta}^{ff'X} \left(\bar{\nu}_\alpha \gamma^\mu P_L \ell_\beta\right)\left(\bar{f}' \gamma_\mu P_X f\right), \quad (15)$$

$$\mathcal{L}_{\text{NC–NSI}} = -2\sqrt{2}G_F \epsilon_{\alpha\beta}^{fX} \left(\bar{\nu}_\alpha \gamma^\mu P_L \nu_\beta\right)\left(\bar{f} \gamma_\mu P_X f\right). \quad (16)$$

where G_F is the Fermi constant and P_X denote the left and right chirality projection operators $P_{R,L} = (1 \pm \gamma_5)/2$. The dimensionless coefficients $\epsilon_{\alpha\beta}^{ff'X}$ and $\epsilon_{\alpha\beta}^{fX}$ quantify the strength of the NSI between leptons of α and β flavor and the matter field $f \in \{e, u, d\}$ (for NC-NSI) and $f \neq f' \in \{u, d\}$ (for CC-NSI). At the limit $\epsilon_{\alpha\beta}^{fX} \to 0$, we recover the standard interactions, while $\epsilon_{\alpha\beta} \sim 1$ corresponds to new interactions with strength comparable to that of SM weak interactions. If $\epsilon_{\alpha\beta}$ is non-zero for $\alpha \neq \beta$, the NSIs violate lepton flavor. If $\epsilon_{\alpha\alpha} - \epsilon_{\beta\beta} \neq 0$, the lepton flavor universality is violated by NSI.

The presence of neutrino NSI may affect the neutrino production and detection at experiments as well as their propagation in a medium through modified matter effects [52, 53]. In the literature, it is common denoting the CC-NSI couplings as $\epsilon_{\alpha\beta}^s$ or $\epsilon_{\alpha\beta}^d$ since they may often affect the source (s) and detector (d) interactions at neutrino experiments. On the other hand, $\epsilon_{\alpha\beta}^{mf}$ is used to refer to the NC-NSI couplings with the fundamental fermion f generally affecting the neutrino propagation in matter (m). In this case, what is relevant for neutrino propagation in a medium is the vector part of interaction $\epsilon_{\alpha\beta}^{fV} = \epsilon_{\alpha\beta}^{fL} + \epsilon_{\alpha\beta}^{fR}$. In fact, the neutrino propagation in a medium is sensitive to the following combinations[4]

$$\epsilon_{\alpha\beta} \equiv \epsilon_{\alpha\beta}^{eV} + \frac{N_u}{N_e}\epsilon_{\alpha\beta}^{uV} + \frac{N_d}{N_e}\epsilon_{\alpha\beta}^{dV} \quad (17)$$

so most of the bounds from oscillation experiments are presented in the literature in terms of $\epsilon_{\alpha\beta}$ rather than in terms of $\epsilon_{\alpha\beta}^{fV}$. Inside the Sun, $N_u/N_e \simeq 2N_d/N_e \simeq 1$ [60] and inside the Earth, $N_u/N_e \simeq N_d/N_e \simeq 3$ [113]. When studying the effect of NSI at

---

[4]Note that some references use the definition $\epsilon_{\alpha\beta} = \sum_f \frac{N_f}{N_d}\epsilon_{\alpha\beta}^{fV}$. It is very relevant to distinguish between both notations, since the reported bounds will be different by a factor of 3. For this reason, we prefer to quote directly the results in terms of the effective lagrangian coefficients $\epsilon_{\alpha\beta}^{fV}$. In any case, for the analysis including Earth matter effects, the relation between the corresponding NSI couplings is straightforward.

neutrino detection, there will be independent sensitivity for the left and right chirality coefficients $\epsilon_{\alpha\beta}^{fL}$ and $\epsilon_{\alpha\beta}^{fR}$.

Although this kind of interactions has not been confirmed experimentally, their potential effects have been extensively studied in a large variety of physical scenarios. As a result, stringent bounds on their strength have been derived [11, 111, 112]. Moreover, it has been shown that NSI may interfere with neutrino oscillations in different contexts, giving rise to parameter degeneracies that can affect the robustness of the neutrino parameter determination. In this section, we will review these results.

3.1. NSI in Solar Experiments

NSI may affect the propagation of solar neutrinos within the Sun and the Earth as well as the detection, depending on the type of NSI considered. Before the confirmation of neutrino oscillation as the phenomenon responsible for the solar neutrino anomaly by the KamLAND experiment, NSI with massless neutrinos was also proposed as the mechanism behind this anomaly [114–118]. After KamLAND confirmed the phenomenon of mass–induced electron neutrino (antineutrino) oscillation, NSI was excluded as the main mechanism behind the solar neutrino oscillations, although its presence has been considered at subleading level in solar neutrino experiments, see for instance [9–11, 119, 120]. These analyses have found that a small amount of NSI, $\epsilon_{ee}^{dV} \simeq 0.3$, is in better agreement with data than the standard solution at the level of 2σ. Palazzo [121] finds the best fit value to lie at $\epsilon_{e\tau}^{dV} - \epsilon_{e\mu}^{dV} = 0.23$. On one hand, this result is due to the non–observation of the upturn of the solar neutrino spectrum predicted by the standard LMA–MSW solution at around 3 MeV [9, 119, 121]. On the other hand, there exists a small tension between the preferred value of Δm_{21}^2 by KamLAND and by solar experiments that can be eased by introducing NSI. More surprisingly, these studies revealed an alternative solution to the standard LMA–MSW, known as LMA-Dark or LMA-D solution [9–11], requiring NSI with strength $\epsilon_{\tau\tau}^{dV} - \epsilon_{ee}^{dV} \simeq 1$. The presence of this new degenerate solution to the solar neutrino anomaly, shown in **Figure 5**, can be understood in the framework of two-neutrino mixing as follows. Under this approximation (justified by the fact that $\sin^2\theta_{13} \ll 1$), the two by two Hamiltonian matrix can be diagonalized with an effective mixing angle given by

$$\tan 2\theta_{12}^m = \frac{\sin 2\theta_{12}(\Delta m_{12}^2/2E)}{\cos 2\theta_{12}(\Delta m_{12}^2/2E) - (H_m)_{ee}}. \quad (18)$$

The splitting between two eigenvalues is given by

$$\Delta^m = \left((H_m)_{ee}^2 + \left(\frac{\Delta m_{21}^2}{2E}\right)^2 - \frac{\Delta m_{21}^2}{E}(H_m)_{ee}\cos 2\theta_{12}\right)^{1/2}. \quad (19)$$

Under the simultaneous transformations $\cos 2\theta_{12} \to -\cos 2\theta_{12}$ and $(H_m)_{ee} \to -(H_m)_{ee}$, we find $\theta_{12}^m \to \pi/2 - \theta_{12}^m$ and $\Delta^m \to \Delta^m$ which means that the off-diagonal elements of the 2×2 Hamiltonian remains the same but the diagonal elements (the 11 and 22 elements) flip. That is, $P(\nu_e \to \nu_e)$ changes to
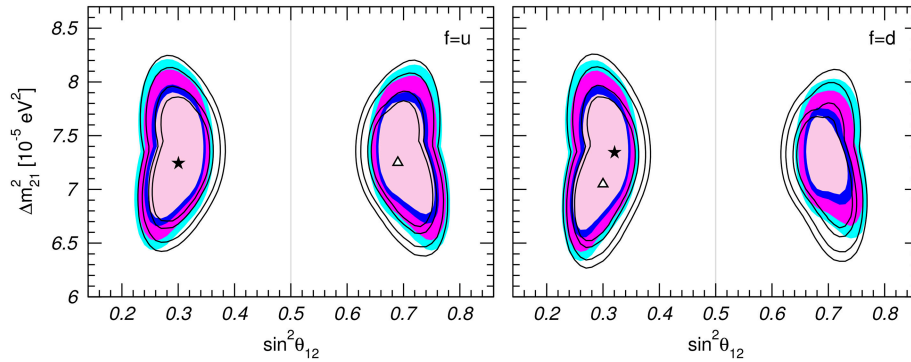
FIGURE 5 | Allowed regions at 90, 95, 99% and 3σ C.L. (2 d.o.f.) from the analysis of solar and KamLAND data in the presence of NSI with up **(Left)** and down **(Right)** quarks. The colored filled and contour regions in each panel correspond to different analysis of solar SNO data. Star and triangle denote the corresponding best fits. This figure has been taken from Gonzalez-Garcia and Maltoni [11], published under the terms of the Creative Commons Attribution Noncommercial License and therefore no copyright permissions were required for its inclusion in this manuscript. See this reference for further details.

$P(\nu_c \to \nu_c)$ where $\nu_c \equiv c_{23}\nu_\mu - s_{23}\nu_\tau$ is the combination that ν_e converts to (that is $\langle \nu_c | \nu_3 \rangle = \langle \nu_c | \nu_e \rangle = 0$). Since in two neutrino approximation, we can write $P(\nu_e \to \nu_e) + P(\nu_e \to \nu_c) = 1$, $P(\nu_c \to \nu_e) + P(\nu_c \to \nu_c) = 1$ and $P(\nu_e \to \nu_c) = P(\nu_c \to \nu_e)$. We therefore conclude $P(\nu_e \to \nu_e) = P(\nu_c \to \nu_c)$. As a result, under the transformation described above, $P(\nu_e \to \nu_e)$ remains invariant. This transformation is not possible for the case of standard matter effects, where the value of $(H_m)_{ee}$ is fixed to $\sqrt{2}G_F N_e$. However, if one considers the presence of neutrino NSI with the matter field f, the effective Hamiltonian in the medium is modified to:

$$H'_m = H_m + H_{NSI} = \sqrt{2}G_F N_e \begin{pmatrix} 1 & 0 & 0 \\ 0 & 0 & 0 \\ 0 & 0 & 0 \end{pmatrix}$$

$$+ \sqrt{2}G_F \sum_f N_f \begin{pmatrix} \epsilon_{ee}^{fV} & \epsilon_{e\mu}^{fV} & \epsilon_{e\tau}^{fV} \\ \epsilon_{e\mu}^{fV*} & \epsilon_{\mu\mu}^{fV} & \epsilon_{\mu\tau}^{fV} \\ \epsilon_{e\tau}^{fV*} & \epsilon_{\mu\tau}^{fV*} & \epsilon_{\tau\tau}^{fV} \end{pmatrix}. \qquad (20)$$

Allowing for sufficiently large values of the ϵ_{ee}^{fV} coupling in the effective Hamiltonian in matter H'_m, it is now possible to apply the transformation described above, obtaining a degenerate solution to the solar neutrino anomaly with $\cos 2\theta_{12} < 0$. Notice that, letting $\cos 2\theta_{12}$ to change sign, we are violating the historical choice of keeping θ_{12} in the first octant and, therefore, ν_1 will not be anymore the state giving the largest contribution to ν_e, but the lighter one between those two eigenstates that give the main contribution to ν_e. This change of definition is in fact equivalent to maintain the same convention regarding the allowed range for the mixing angle, but allowing Δm_{21}^2 to be negative. Indeed, changing $\Delta m_{21}^2 \to -\Delta m_{21}^2$ instead of $\cos 2\theta_{12} \to -\cos 2\theta_{12}$, we would find the same degeneracy. In other words, for a given H_m, solar neutrino data only determine the sign of the product $\Delta m_{21}^2 \cos 2\theta_{12}$, not the signs of Δm_{21}^2 and $\cos 2\theta_{12}$ separately, and therefore there is a freedom in definition. Since the LMA-D solution was introduced in the literature keeping Δm_{21}^2 positive while allowing θ_{12} to vary in the range $(0, \pi/2)$ [9] and this

convention has become popular in the literature since then, we will use it along this review. Note also that the degeneracy found at the neutrino oscillation probability is exact only for a given composition of matter (i.e., for a given $N_n/N_p = N_n/N_e$). The composition slightly varies across the Sun radius and of course is quite different for the Sun and the Earth. Because of this, the allowed regions in the neutrino oscillation parameter space for the LMA and LMA-D solutions are not completely degenerate. A small χ^2 difference between the best fit point of the LMA solution and the local minimum of LMA-Dark solution appears because the relevant data analyses take into account the varying composition of the Sun and the day-night asymmetry due to propagation in the Earth.

Unfortunately, the degeneracy between the LMA and LMA-Dark solutions could not be lifted by the KamLAND reactor experiment because KamLAND was not sensitive to the octant of the solar mixing angle due to the lack of matter effects. A possible way to solve this problem was proposed in Escrihuela et al. [10]. There, it was found that the combination of solar experiments, KamLAND and neutrino neutral–current scattering experiments, such as CHARM [122], may help to probe the LMA-D solution. The relevance of the degeneracy in the solar neutrino parameter determination has been explored recently in Coloma and Schwetz [123]. As discussed in this analysis, the ambiguity of LMA-D does not affect only the octant of the solar mixing angle but it also makes impossible the determination of the neutrino mass ordering at oscillation experiments. More recently, a global analysis of neutrino scattering and solar neutrino experiments was performed to further investigate the situation of the LMA-D solution [124]. Besides the accelerator experiment CHARM, the authors also considered the NuTeV experiment [125]. They found that the degenerate LMA-D solution may be lifted for NSI with down quarks, although it does not disappear for the case of neutrino NSI with up quarks. As discussed in that work, constraints from CHARM and NuTeV experiments can be however directly applied only for NSI with relatively heavy mediators. For the case of NSI mediated by lighter particles (above 10 MeV), constraints coming from

coherent neutrino-nucleus scattering experiments may be used to resolve the degeneracy. Indeed, after the recent observation of such process at the COHERENT experiment [126], a combined analysis of neutrino oscillation data including the observed number of events in this experiment has excluded the LMA-D solution (for up and down quarks) at the 3σ level [127][5]. One should, however, bear in mind that the analysis [127] assumes the mediator of interaction in Equation (16) is heavier than 50 MeV. As we shall see in sect V, for light mediator, their conclusion should be revised. Besides that, COHERENT data along with neutrino oscillation data has been used to improve the current bounds on the flavor–diagonal NSI parameters [127][6]:

$$-0.09 < \epsilon_{\tau\tau}^{uV} < 0.38 \, , \, -0.075 < \epsilon_{\tau\tau}^{dV} < 0.33 \quad (90\% \text{ C.L.}) \,.$$
(21)

These limits on NC vector interactions of ν_τ improve previous bounds by one order of magnitude [10, 11, 128]. For the flavor–changing NC NSI couplings, however, the improvement is much smaller[7]:

$$-0.073 < \epsilon_{e\mu}^{uV} < 0.044 \, , \, -0.07 < \epsilon_{e\mu}^{dV} < 0.04 \quad (90\% \text{ C.L.}),$$
(22)

$$-0.15 < \epsilon_{e\tau}^{uV} < 0.13 \, , \, -0.13 < \epsilon_{e\tau}^{dV} < 0.12 \quad (90\% \text{ C.L.}).$$ (23)

The spectrum of coherent elastic neutrino–nucleus scattering events at COHERENT has also been analyzed to constrain the amplitude of NSI in Liao and Marfatia [130].

Besides their impact on solar neutrino propagation, NSI can also affect the detection processes at solar neutrino experiments. In experiments like Super–Kamiokande and Borexino, for instance, the presence of NSI may modify the cross section of neutrino elastic scattering on electrons, used to observe solar neutrinos. Analyzing data from solar neutrino experiments, and in particular the effect of NSI on neutrino detection in Super-Kamiokande, in combination with KamLAND, Bolanos et al. [131] reported limits on the NSI parameters which are competitive and complementary to the ones obtained from laboratory experiments. For the case of ν_e NSI interaction with electrons, the reported bounds (taking one parameter at a time) are:

$$-0.021 < \epsilon_{ee}^{eL} < 0.052 \, , \quad -0.18 < \epsilon_{ee}^{eR} < 0.51 \quad (90\% \text{ C.L.}),$$
(24)

while for the case of ν_τ NSI interaction with electrons, looser constraints are obtained:

$$-0.12 < \epsilon_{\tau\tau}^{eL} < 0.060 \, , \quad -0.99 < \epsilon_{\tau\tau}^{eR} < 0.23 \quad (90\% \text{ C.L.}).$$
(25)

---

[5]The analysis of atmospheric neutrino data performed in Coloma et al. [127] employs two simplifying assumptions. First, the solar mass splitting is neglected. Second, rather than taking the most general matter potential, it is assumed that two of eigenvalues of this matrix are degenerate. As a result, the derived constraints on the NSI couplings are more stringent than what we expect in the most general case.

[6]Notice that since the beam at COHERENT does not contain ν_τ, this experiment cannot directly probe $\epsilon_{\tau\tau}$. The bounds on $\epsilon_{\tau\tau}$ come from combining the limits on $\epsilon_{\mu\mu}$ and ϵ_{ee} by COHERENT with the bounds on $\epsilon_{\tau\tau} - \epsilon_{ee}$ and $\epsilon_{\tau\tau} - \epsilon_{\mu\mu}$ from oscillation experiments.

[7]Note that the existing bounds on $\epsilon_{e\mu}^{qV}$ were revised in Biggio et al. [129] showing that previously derived loop bounds do not hold in general.

The sensitivity of the Borexino solar experiment to NSI has also been investigated in Berezhiani et al. [132] and Agarwalla et al. [133]. Using [7]Be neutrino data from Borexino Phase I, the following 90% C.L. bounds have been derived [133]

$$-0.046 < \epsilon_{ee}^{eL} < 0.053, \quad -0.21 < \epsilon_{ee}^{eR} < 0.16,$$
(26)

$$-0.23 < \epsilon_{\tau\tau}^{eL} < 0.87, \quad -0.98 < \epsilon_{\tau\tau}^{eR} < 0.73.$$
(27)

As can be seen, the NSI constraints obtained from Borexino and the combined analysis of solar (mainly Super-Kamiokande) and KamLAND data are comparable. It is expected that future results from Borexino Phase II, as well as the combination of all solar data, including Borexino, plus KamLAND data would allow a significant improvement on the current knowledge of neutrino NSI with matter [134].

3.2. NSI in Atmospheric Neutrino Experiments

The impact of non-standard neutrino interactions on atmospheric neutrinos was originally considered in Fornengo et al. [135, 136] and Friedland et al. [137, 138]. Assuming a two–flavor neutrino system, it was shown [136] that the presence of large NSI couplings together with the standard mechanism of neutrino oscillation can spoil the excellent description of the atmospheric neutrino anomaly given by neutrino oscillations. Thus, quite strong bounds on the magnitude of the non–standard interactions were derived. Using atmospheric neutrino data from the first and second phase of the Super–Kamiokande experiment, the following constraints were obtained, under the two–flavor neutrino approach [139]:

$$|\epsilon_{\mu\tau}^{dV}| < 0.011 \, , \quad |\epsilon_{\mu\mu}^{dV} - \epsilon_{\tau\tau}^{dV}| < 0.049 \quad (90\% \text{ C.L.}).$$
(28)

However, Friedland et al. [137, 138] showed that a three–family analysis significantly relaxes the previous bounds in such a way that the values of the NSI couplings with quarks comparable to the standard neutral current couplings can be still compatible with the Super–Kamiokande atmospheric data. A more recent three–neutrino analysis of NSI in the atmospheric neutrino flux can be found in Gonzalez-Garcia et al. [140], where the following limits on the effective NSI couplings with electrons have been obtained:

$$-0.035 \, (-0.035) < \epsilon_{\mu\tau}^{eV} < 0.018 \, (0.035),$$
$$|\epsilon_{\tau\tau}^{eV} - \epsilon_{\mu\mu}^{eV}| < 0.097 \, (0.11) \quad (90\% \text{ C.L.})$$
(29)

for the case of real (complex) $\epsilon_{\mu\tau}^{eV}$ coupling.

The IceCube extension to lower energies, DeepCore, has made possible the observation of atmospheric neutrinos down to 5 GeV with unprecedented statistics. Indeed, with only 3 years of data, DeepCore allows the determination of neutrino oscillation parameters with similar precision as the one obtained from the long–lived Super–Kamiokande or the long–baseline accelerator experiments [90]. Focusing now on its sensitivity to NSI, the idea of using IceCube data to constrain the $\mu - \tau$ submatrix of ϵ was first proposed in Esmaili and Smirnov [141]. Using the most

recent data release from DeepCore, the IceCube collaboration has reported the following constraints on the flavor–changing NSI coupling [142]:

$$-0.0067 < \epsilon_{\mu\tau}^{dV} < 0.0081 \quad (90\% \text{ C.L.}). \quad (30)$$

From a different data sample containing higher energy neutrino data from IceCube, the authors of Salvado et al. [143] have derived somewhat more restrictive bounds on the same NSI interactions:

$$-0.006 < \epsilon_{\mu\tau}^{dV} < 0.0054 \quad (90\% \text{ C.L.}). \quad (31)$$

Both results are fully compatible and constitute the current best limits on NSI in the $\nu_\mu - \nu_\tau$ sector.

Future prospects on NSI searches in atmospheric neutrino experiments have been considered in the context of PINGU, the future project to further lower the energy threshold at the IceCube observatory. Choubey and Ohlsson [144] shows that, after three years of data taking in PINGU in the energy range between 2 and 100 GeV, the Super–Kamiokande constraints on the NSI couplings may be improved by one order of magnitude:

$$-0.0043 < \epsilon_{\mu\tau}^{eV} < 0.0047, \quad -0.03 < \epsilon_{\tau\tau}^{eV} < 0.017 \quad (90\% \text{ C.L.}). \quad (32)$$

Likewise, the impact of NSI interactions on atmospheric neutrinos on the future India-based Neutrino Observatory (INO) has been analyzed in Choubey et al. [145]. Besides discussing its constraining potential toward NSI, this work studies how the sensitivity to the neutrino mass hierarchy of INO, one of the main goals of the experiment, may change in the presence of NSI.

Notice that the above bounds have been derived from the study of the atmospheric neutrinos flux at neutrino telescopes. Gonzalez-Garcia et al. [146] discusses the effects of NSI on high energy astrophysical neutrinos detected by IceCube when they propagate through the Earth.

3.3. NSI in Reactor Experiments

Modern reactor neutrino experiments, like Daya Bay, RENO and Double Chooz, provide a very accurate determination of the reactor mixing angle θ_{13} [78, 147, 148]. Being at the precision era of the neutrino parameter determination, it is imperative to investigate the robustness of this successful measurement in the presence of NSI. Leitner et al. [12], Agarwalla et al. [13], Ohlsson and Zhang [149], Girardi and Meloni [150], and Khan et al. [151] have addressed this point. In principle, short–baseline reactor experiments may be affected by the presence of new neutrino interactions in β and inverse-β decay processes, relevant for the production and detection of reactor antineutrinos [152]. The NSI parameters relevant for these experiments are the CC NSI couplings between up and down quarks, positrons and antineutrinos of flavor α, $\epsilon_{e\alpha}^{ud}$. Considering unitarity constraints on the CKM matrix as well as the non-observation of neutrino oscillations in the NOMAD experiment, one may find the following constraints on these CC NSI couplings [33]:

$$|\epsilon_{e\alpha}^{udV}| < 0.041, \ |\epsilon_{e\mu}^{udL}| < 0.026, \ |\epsilon_{e\mu}^{udR}| < 0.037, (90\% \text{ C.L.}). \quad (33)$$

Agarwalla et al. [13] explored the correlations between the NSI parameters and the reactor mixing angle determination, showing that the presence of NSI may lead to relatively large deviations in the measured value of θ_{13} in Daya Bay, as it can be seen in **Figure 6**. Conversely, the total number of events observed in Daya Bay was used to constrain the corresponding NSI couplings under two assumptions: (i) perfect theoretical knowledge of the reactor neutrino flux in absence of NSI and (ii) assuming a conservative error on its total normalization. In the latter case, it was shown that assuming an uncertainty of 5% on the reactor flux can relax the bounds by one order of magnitude, obtaining the following conservative limits on the NSI strengths[8]

$$|\epsilon_{ee}^{udP}| < 0.015, \ |\epsilon_{e\mu}^{udP}| < 0.18, \ |\epsilon_{e\tau}^{udP}| < 0.18, (90\% \text{ C.L.}), \quad (34)$$

with P = L,R,V,A. Note that these results improve the existing bounds on the ϵ_{ee}^{ud} coupling reported above. On the other hand, one finds that an improved knowledge of the standard absolute neutrino flux from nuclear reactors together with a larger data sample from Daya Bay will result in a more stringent bound on the other two couplings in the near future. Notice also that previous results have been obtained assuming that the NSI couplings at neutrino production and detection satisfy $\epsilon_{\alpha\beta}^s = \epsilon_{\alpha\beta}^{d*}$. In this case, the presence of NSI would only produce a shift in the oscillation amplitude without altering the L/E pattern of the oscillation probability, and therefore, the analysis of the total neutrino rate in Daya Bay provides enough information. The investigation of more exotic scenarios where $\epsilon_{\alpha\beta}^s \neq \epsilon_{\alpha\beta}^{d*}$ will require the spectral analysis of the Daya Bay data [12].

NSI at future intermediate baseline reactor experiments like JUNO and RENO-50 (see for instance, Ohlsson et al. [153] and Khan et al. [151]) are discussed at section 5.

3.4. NSI in Long–Baseline Neutrino Experiments

Besides neutrino production and detection, NSI can also modify the neutrino propagation through the Earth in long–baseline accelerator experiments[9]. This effect will be larger for experiments with larger baselines such as MINOS or NOνA. Using their neutrino and antineutrino data sample, the MINOS Collaboration reported the following bounds on the flavor-changing NC NSI with electrons [154]:
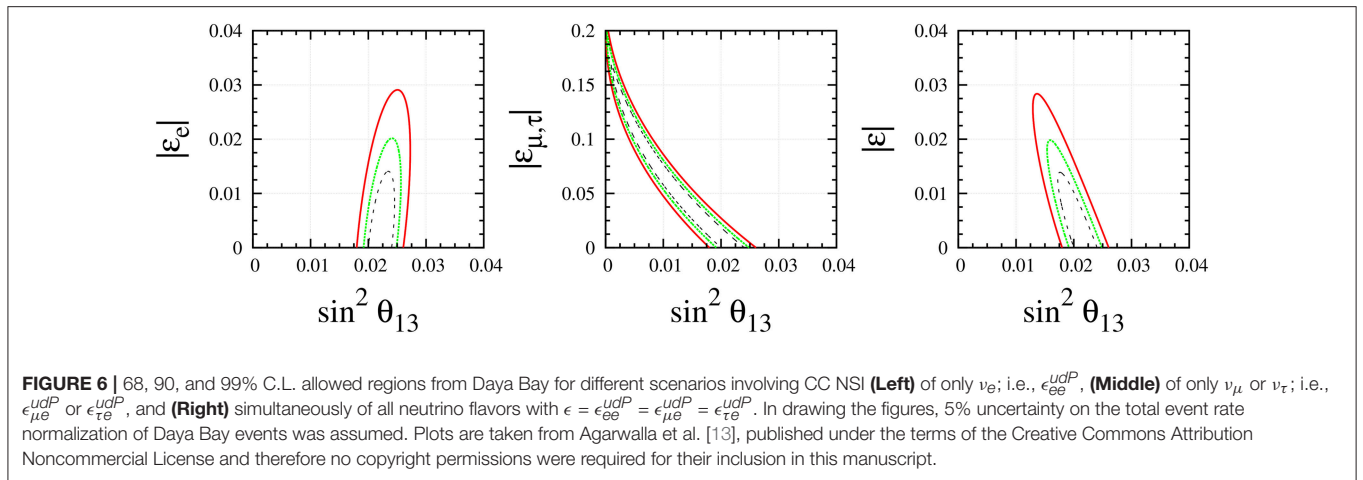
$$-0.20 < \epsilon_{\mu\tau}^{eV} < 0.07 \ (90\% \text{ C.L.}). \quad (35)$$

MINOS appearance data were also used to constrain NSI interactions between the first and third family [155], although the reported bound, $|\epsilon_{e\tau}^{eV}| < 3.0$ (90% C.L.) does not improve the previous limits on that parameter [33].

Regarding the long–baseline experiment NOνA, the presence of NSI in the neutrino propagation has been proposed as a way to solve the mild tension between the measured values of the

---

[8]The NSI parameters probed in this kind of analysis obtain contributions from the (V±A) operators in Equation 15 so, taking one parameter at a time, the derived bounds apply to all the chiralities.

[9]See for instance Kopp et al. [152], where the impact of NSI on long–baseline experiment is analyzed in detail.

FIGURE 6 | 68, 90, and 99% C.L. allowed regions from Daya Bay for different scenarios involving CC NSI **(Left)** of only ν_e; i.e., ϵ_{ee}^{udP}, **(Middle)** of only ν_μ or ν_τ; i.e., $\epsilon_{\mu e}^{udP}$ or $\epsilon_{\tau e}^{udP}$, and **(Right)** simultaneously of all neutrino flavors with $\epsilon = \epsilon_{ee}^{udP} = \epsilon_{\mu e}^{udP} = \epsilon_{\tau e}^{udP}$. In drawing the figures, 5% uncertainty on the total event rate normalization of Daya Bay events was assumed. Plots are taken from Agarwalla et al. [13], published under the terms of the Creative Commons Attribution Noncommercial License and therefore no copyright permissions were required for their inclusion in this manuscript.

atmospheric mixing angle in T2K and NOνA [156]. Under this hypothesis, the deviation of the NOνA preferred value for θ_{23} from maximal mixing would be explained through the NSI-modified matter effects. The T2K experiment, with a shorter baseline, has a limited sensitivity to matter effects in the neutrino propagation so, its θ_{23} measurement would be unaffected by NSI. Note, however, that the size of the NSI required to reproduce the observed results is of the same order as the standard neutrino interaction [to be more precise $\epsilon_{e\tau}, (\epsilon_{\tau\tau} - \epsilon_{\mu\mu}) \simeq (\epsilon_{\tau\tau} - \epsilon_{ee}) \sim O(1)$].

The presence of NSI has also been considered to reconcile the measured value of θ_{13} in reactor experiments and T2K [157]. In that case, it is suggested that CC-NSI in the neutrino production and detection processes may be responsible for the different values of the reactor mixing angle measured in Daya Bay and T2K.

Finally, it has been shown that long–baseline neutrino facilities can also suffer from degeneracies in the reconstruction of some parameters due to the existence of new neutrino interactions with matter. For instance, Forero and Huber [14] states that NC NSI may affect the sensitivity to the CP–violating phase δ in experiments like T2K and NOνA. According to this analysis, it would be possible confusing signals of NSI with a discovery of CP violation, even if CP is conserved in nature. This result is illustrated in **Figure 7**, where it is shown how the standard CP–violating scenario may be confused with an hybrid standard plus NSI CP–conserving scenario.

Future sensitivities to NSI as well as the presence of new degeneracies due to NSI in future long–baseline experiments such as DUNE, T2HK and T2HKK are analyzed in more detail in section 5. It is worth mentioning that CC-NSI, affecting the production and detection of neutrinos can show up also in short baseline experiments [158–160].

3.5. NSI in Non-oscillation Neutrino Experiments

Neutrino scattering experiments constitute a very precise tool toward the understanding of neutrino interactions with matter. Indeed, this kind of experiments has been often used to measure

the electroweak mixing angle θ_W [161]. Non–standard neutrino interactions may contribute significantly to the neutrino–electron elastic scattering cross section and therefore they cannot be ignored when studying this process. Barranco et al. [162] compiled most of the neutrino scattering experiments potentially modified by the presence of NSI, from the neutrino accelerator–based experiments LSND and CHARM to the short–baseline neutrino reactor experiments Irvine, Rovno and MUNU, including as well as the measurement of the process $e^+ e^- \rightarrow \nu\bar{\nu}\gamma$ at LEP. From a combined analysis of all experimental data, allowed ranges on the $\epsilon_{\alpha\beta}^e$ were obtained. Some of these results are among the current strongest constraints on NSI couplings, and are reported in **Table 2**. The antineutrino–electron scattering data collected by the TEXONO Collaboration has been also used to constrain the presence of neutrino NC NSI with electrons [163] as well as CC NSI at neutrino production and detection [164].

In order to constrain the NSI between neutrinos and quarks, one may use data from the neutrino–nucleus experiments NuTeV, CHARM and CDHS. From the combination of atmospheric and accelerator data from NuTeV, CHARM and CDHS, the following limits on the non–universal vectorial and axial NSI parameters were derived [165]:

$$|\epsilon_{\mu\mu}^{dV}| < 0.042, \qquad -0.072 < \epsilon_{\mu\mu}^{dA} < 0.057 \quad (90\% \text{ C.L.}). \quad (36)$$

For the case of the flavor changing NSI couplings (with $q = u, d$)

$$|\epsilon_{\mu\tau}^{qV}| < 0.007, \qquad |\epsilon_{\mu\tau}^{qA}| < 0.039 \quad (90\% \text{ C.L.}). \quad (37)$$

Under this category we include also the first observation of coherent neutrino–nucleus scattering observed at the COHERENT experiment recently [126]. As discussed above, the COHERENT data have been used to constrain neutrino NSI with quarks in Coloma et al. [127] and Liao and Marfatia [130]. The combination of solar neutrino oscillation data with COHERENT has been exploited to investigate the status of the solar degenerate solution LMA-D.
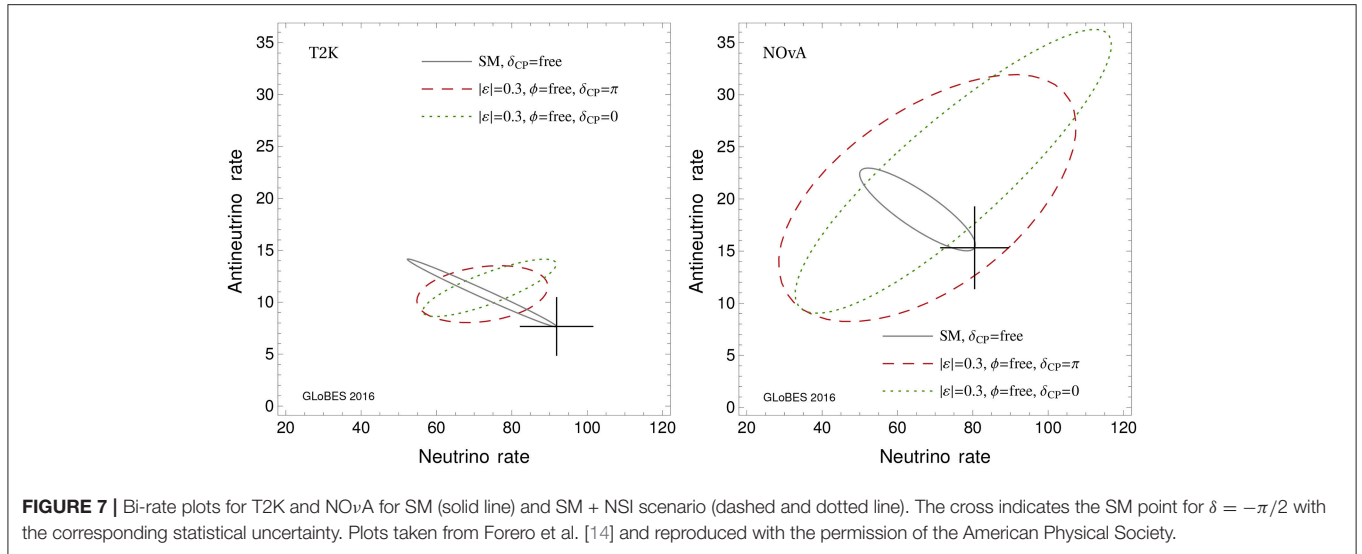
FIGURE 7 | Bi-rate plots for T2K and NOvA for SM (solid line) and SM + NSI scenario (dashed and dotted line). The cross indicates the SM point for $\delta = -\pi/2$ with the corresponding statistical uncertainty. Plots taken from Forero et al. [14] and reproduced with the permission of the American Physical Society.

TABLE 2 | Bounds on flavor diagonal NC NSI couplings.

	90% C.L. range	Origin	References
NSI WITH QUARKS			
ϵ_{ee}^{dL}	[−0.3, 0.3]	CHARM	[128]
ϵ_{ee}^{dR}	[−0.6, 0.5]	CHARM	[128]
ϵ_{ee}^{dV}	[0.030, 0.55]	Oscillation data + COHERENT	[127]
ϵ_{ee}^{uV}	[0.028, 0.60]	Oscillation data + COHERENT	[127]
$\epsilon_{\mu\mu}^{dV}$	[−0.042, 0.042]	Atmospheric + accelerator	[165]
$\epsilon_{\mu\mu}^{uV}$	[−0.044, 0.044]	Atmospheric + accelerator	[165]
$\epsilon_{\mu\mu}^{dA}$	[−0.072, 0.057]	Atmospheric + accelerator	[165]
$\epsilon_{\mu\mu}^{uA}$	[−0.094, 0.14]	Atmospheric + accelerator	[165]
$\epsilon_{\tau\tau}^{dV}$	[−0.075, 0.33]	Oscillation data + COHERENT	[127]
$\epsilon_{\tau\tau}^{uV}$	[−0.09, 0.38]	Oscillation data + COHERENT	[127]
$\epsilon_{\tau\tau}^{qV}$	[−0.037, 0.037]	Atmospheric	[140][a]
NSI WITH ELECTRONS			
ϵ_{ee}^{eL}	[−0.021, 0.052]	Solar + KamLAND	[131]
ϵ_{ee}^{eR}	[−0.07, 0.08]	TEXONO	[163]
$\epsilon_{\mu\mu}^{eL}, \epsilon_{\mu\mu}^{eR}$	[−0.03, 0.03]	Reactor + accelerator	[128, 162]
$\epsilon_{\tau\tau}^{eL}$	[−0.12, 0.06]	Solar + KamLAND	[131]
$\epsilon_{\tau\tau}^{eR}$	[−0.98, 0.23]	Solar + KamLAND and Borexino	[131, 133]
	[−0.25, 0.43]	Reactor + accelerator	[162]
$\epsilon_{\tau\tau}^{eV}$	[−0.11, 0.11]	Atmospheric	[140]

[a] Bound adapted from $\epsilon_{\tau\tau}^{eV}$.

3.6. Summary of Current Bounds on NSI Parameters

Here we summarize the current constraints on the NSI couplings from different experiments discussed throughout this section. For more details about the assumptions considered in each case, we refer the reader to the previous subsections as well as to the original references where the constraints have been calculated. The limits summarized in **Tables 2–4** have been obtained assuming only one nonzero NSI coupling at a time.

Table 2 contains the limits on the flavor diagonal NC NSI couplings between neutrinos and electrons $\epsilon_{\alpha\alpha}^{eP}$ and neutrinos and quarks $\epsilon_{\alpha\alpha}^{qP}$, with $P = L, R, V, A$ being the chirality index and $q = u, d$. The table indicates the origin of the reported bound as well as the reference where it has been obtained as well. Most of the limits have been derived from the combination of neutrino oscillation and detection or production experimental results. For instance, the joint analysis of atmospheric neutrino data and accelerator measurements in NuTeV, CHARM and CDHS [165], or solar and KamLAND data together with the recent bounds of COHERENT [127][10]. In other cases the constraints reported in the table come just from one type of experiment, as the limits derived only from CHARM [128], TEXONO [163] or atmospheric data [140]. Note that, for the latter case, we have adapted the bound on $\epsilon_{\tau\tau}^{eV}$ reported in Gonzalez-Garcia et al. [140] to the corresponding bound for quarks, $\epsilon_{\tau\tau}^{qV}$.

Table 3 collects the limits of the flavor changing NC NSI couplings between neutrinos and electrons $\epsilon_{\alpha\beta}^{eP}$ and neutrinos and quarks $\epsilon_{\alpha\beta}^{qP}$, with the same conventions indicated above for P and q. As discussed before, in this case most of the bounds also emerge from the complementarity of different types of experiments, as the combination of reactor and accelerator non-oscillation experiments in Barranco et al. [162]. On the other hand, the first analyses on NSI obtained from IceCube data [142, 143] offer very strong bounds on $\epsilon_{\mu\tau}^{qV}$. This last constraint has also been adapted to get the equivalent bound for NSI with electrons, $\epsilon_{\mu\tau}^{eV}$.

Finally, **Table 4** contains the limits on the neutrino CC NSI with quarks and electrons (*semileptonic* CC NSI) and the CC NSI with leptons only (*purely-leptonic* CC NSI) in terms of the couplings $\epsilon_{\alpha\beta}^{udP}$ and $\epsilon_{\alpha\beta}^{ll'P}$, respectively. The former ones, have been discussed in the context of the neutrino production and detection in the Daya Bay reactor experiment, as analyzed in Agarwalla

---

[10] The bounds in Coloma et al. [127] assume mediator mass to be heavier than ∼50 MeV. As we shall discuss in the next section, these bounds do not apply for mediator mass lighter than ∼10 MeV.

TABLE 3 | Bounds on flavor changing NC NSI couplings.

	90% C.L. range	Origin	References
NSI WITH QUARKS			
$\epsilon_{e\mu}^{qL}$	[−0.023, 0.023]	Accelerator	[112, 165]
$\epsilon_{e\mu}^{qR}$	[−0.036, 0.036]	Accelerator	[112, 165]
$\epsilon_{e\mu}^{uV}$	[−0.073, 0.044]	Oscillation data + COHERENT	[127]
$\epsilon_{e\mu}^{dV}$	[−0.07, 0.04]	Oscillation data + COHERENT	[127]
$\epsilon_{e\tau}^{qL}$, $\epsilon_{e\tau}^{qR}$	[−0.5, 0.5]	CHARM	[128]
$\epsilon_{e\tau}^{uV}$	[−0.15, 0.13]	Oscillation data + COHERENT	[127]
$\epsilon_{e\tau}^{dV}$	[−0.13, 0.12]	Oscillation data + COHERENT	[127]
$\epsilon_{\mu\tau}^{qL}$	[−0.023, 0.023]	Accelerator	[165]
$\epsilon_{\mu\tau}^{qR}$	[−0.036, 0.036]	Accelerator	[165]
$\epsilon_{\mu\tau}^{qV}$	[−0.006, 0.0054]	IceCube	[143]
$\epsilon_{\mu\tau}^{qA}$	[−0.039, 0.039]	Atmospheric + accelerator	[165]
NSI WITH ELECTRONS			
$\epsilon_{e\mu}^{eL}$, $\epsilon_{e\mu}^{eR}$	[−0.13, 0.13]	Reactor + accelerator	[162]
$\epsilon_{e\tau}^{eL}$	[−0.33, 0.33]	Reactor + accelerator	[162]
$\epsilon_{e\tau}^{eR}$	[−0.28, −0.05] & [0.05, 0.28]	Reactor + accelerator	[162]
	[−0.19, 0.19]	TEXONO	[163]
$\epsilon_{\mu\tau}^{eL}$, $\epsilon_{\mu\tau}^{eR}$	[−0.10, 0.10]	Reactor + accelerator	[128, 162]
$\epsilon_{\mu\tau}^{eV}$	[−0.018, 0.016]	IceCube	[143][a]

[a]Bound adapted from $\epsilon_{\mu\tau}^{qV}$.

TABLE 4 | Bounds on CC NSI couplings.

	90% C.L. range	Origin	References
SEMILEPTONIC NSI			
ϵ_{ee}^{udP}	[−0.015, 0.015]	Daya Bay	[13]
$\epsilon_{e\mu}^{udL}$	[−0.026, 0.026]	NOMAD	[33]
$\epsilon_{e\mu}^{udR}$	[−0.037, 0.037]	NOMAD	[33]
$\epsilon_{\tau e}^{udL}$	[−0.087, 0.087]	NOMAD	[33]
$\epsilon_{\tau e}^{udR}$	[−0.12, 0.12]	NOMAD	[33]
$\epsilon_{\tau\mu}^{udL}$	[−0.013, 0.013]	NOMAD	[33]
$\epsilon_{\tau\mu}^{udR}$	[−0.018, 0.018]	NOMAD	[33]
PURELY LEPTONIC NSI			
$\epsilon_{\alpha e}^{\mu eL}$, $\epsilon_{\alpha e}^{\mu eR}$	[−0.025, 0.025]	KARMEN	[33]
$\epsilon_{\alpha\beta}^{\mu eL}$, $\epsilon_{\alpha\beta}^{\mu eR}$	[−0.030, 0.030]	kinematic G_F	[33]

et al. [13]. Previous bounds on this type of NSI have been derived using the negative searches for neutrino oscillations at short distances in the NOMAD experiment [166, 167], as reported in the table [33]. Constraints on leptonic CC NSI using the results of the KARMEN experiment [168] as well as the deviations of Fermi's constant G_F in the presence of these interactions, have also been obtained in Biggio et al. [33]. We refer the reader to that work for further details on the derivation of these constraints.

4. VIABLE MODELS LEADING TO SIZEABLE NSI

As we saw in the previous section, neutral current NSI of neutrinos with matter fields can lead to observable effect on neutrino oscillation provided that the NSI parameters $\epsilon_{\alpha\beta}$ are large enough. As briefly discussed in the introduction, it is possible to build viable models for NSI by invoking an intermediate state of relatively light mass ($\sim$10 MeV) which has escaped detection so far because of its very small coupling. In this chapter, we review the models that give rise to sizeable NSI through integrating out a new gauge boson Z' with a mass smaller than $\sim$100 MeV. We however note that an alternative model has been suggested [169] in which NSI are obtained from $SU(2)_L$ scalar doublet-singlet mixing. We shall not cover this possibility in the present review. The models described in this chapter introduce a new $U(1)'$ gauge interaction which is responsible for NSI between neutrinos and quarks.

In section 4.1, we describe the general features of the model gauging a linear combination of lepton flavors and Baryon number with a light $O(10$ MeV) gauge boson. We then outline general phenomenological consequences. We show how a simple economic model can be reconstructed to reproduce the NSI pattern that gives the best fit to neutrino data, solving the small tension between KamLAND and solar neutrino by explaining the suppression of the upturn in the low energy part of the solar neutrino spectrum. In section 4.2, we describe another model which can provide arbitrary flavor structure $\epsilon_{\alpha\beta}^{u} = \epsilon_{\alpha\beta}^{d}$ (both lepton flavor violating and lepton flavor conserving) without introducing new interactions for charged leptons. In section 4.3, the impact of the recent results from the COHERENT experiment is outlined.

4.1. NSI from New $U(1)'$

In this section, we show how we can build a model based on $U(1)' \times SU(2)_L \times U(1)_Y$ gauge symmetry which gives rise to NSI for neutrinos. Notice that the NSI of interest for neutrino oscillation involves only neutrinos and quarks of first generation which make up the matter. However, to embed the scenario within a gauge symmetric theory free from anomalies, the interaction should involve other fermions.

Let us first concentrate on quark sector and discuss the various possibilities of $U(1)'$ charge assignment. Remember that, in the flavor basis by definition, the interaction of W_μ boson with quarks is diagonal: $W_\mu \sum_{i=1}^{3} \bar{u}_{iL} \gamma^\mu d_{iL}$, where i is the flavor index. To remain invariant under $U(1)'$, u_{iL} and d_{iL} should have the same values of $U(1)'$ charge. As discussed in sect II.A, the SNO experiment has measured the rate of neutral current interaction of solar neutrinos by Deuteron dissociation $\nu + D \rightarrow \nu + p + n$. In general, a large contribution to neutral current interaction from new physics should have affected the rate measured by SNO but this process, being a Gamow-Teller transition, is only sensitive to the axial interaction. In order to maintain the SM prediction for the total neutrino flux measured at the SNO experiment via NC interactions, the coupling to (at least the first generation of) quarks should be non-chiral. Thus, the $U(1)'$ charges of u_{1L}, u_{1R}, d_{1L} and d_{1R} should be all equal. In principle, different generations of quarks can have different $U(1)'$ charges. Such a freedom opens up abundant possibilities for anomaly cancelation. However, if the coupling of the new gauge bosons to different quark generations is non-universal, in the quark mass basis, off-diagonal couplings of form $Z'_\mu \bar{q}_i \gamma^\mu q_j|_{i \neq j}$ appear which

can lead to $q_i \rightarrow Z'q_j$ with a rate enhanced by $m_{q_i}^3/m_{Z'}^2$ due to longitudinal component of Z'. These bounds are discussed in great detail in Babu et al. [170]. To avoid these decays, we assume the quarks couple to Z' universally. In other words, the $U(1)'$ charges of quarks are taken to be proportional to baryon number, B. Yukawa couplings of quarks to the SM Higgs will then be automatically invariant under $U(1)'$.

Let us now discuss the couplings of leptons to the new gauge boson. There are two possibilities: (1) $U(1)'$ charges are assigned to a combination of lepton numbers of different flavors. In this case, the $U(1)'$ charges of charged leptons and neutrinos will be equal. (2) Neutrinos couple to Z' through mixing with a new fermion with mass larger than $m_{Z'}$. In this case charged leptons do not couple to Z' at tree level. We shall return to the second case in section 4.2. In the present section, we focus on the first case. As discussed in Farzan and Shoemaker [26], it is possible to assign $U(1)'$ charge to linear combinations of leptons which do not even correspond to charged lepton mass eigenstates. However, let us for the time being study the charge assignment as follows

$$a_e L_e + a_\mu L_\mu + a_\tau L_\tau + B. \tag{38}$$

Denoting the new gauge coupling by g', the coupling of each generation of leptons and quarks to Z' are, respectively, $g'a_\alpha$ and $g'/3$. There are strong bounds on the new couplings of the electrons. If $a_e \neq 0$, Z' with a mass of ~ 10 MeV will dominantly decay into $e^- e^+$ so strong bounds from beam dump experiments apply. These bounds combined with supernova cooling study yield $g'a_e < 3 \times 10^{-11}$ (see Figure 4 of Harnik et al. [171].) On the other hand, for $m_{Z'} < m_\pi$, the bound from $\pi^0 \rightarrow \gamma Z'$ is $g' < 3 \times 10^{-3}$ [172] (see **Figure 8** which is taken from Farzan and Heeck [25]). These bounds are too stringent to lead to a discernible ϵ_{ee}. We therefore set $a_e = 0$ which means at tree level, neither electron nor ν_e couple to Z'. With such charge assignment, we obtain

$$\epsilon_{\alpha\alpha}^u = \epsilon_{\alpha\alpha}^d = \frac{g'^2 a_\alpha}{6\sqrt{2}G_F m_{Z'}^2} \quad \text{and} \quad \epsilon_{\alpha\beta}^u = 0|_{\alpha\neq\beta}. \tag{39}$$
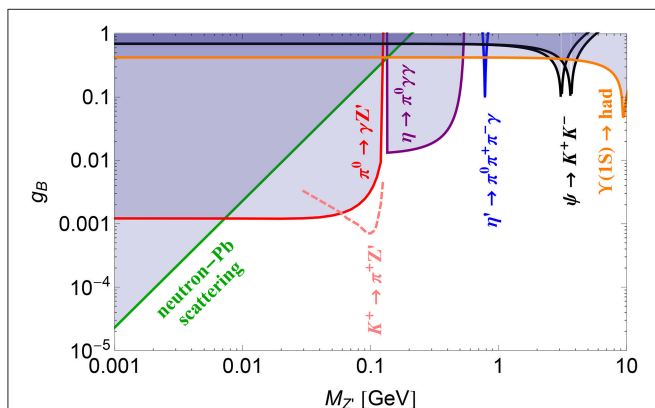

FIGURE 8 | Parameter space of a gauge boson Z' coupled to quarks with coupling $g'/3 = g_B/3$. The shaded areas are excluded at 90% C.L. Plot taken from Farzan and Heeck [25] and reproduced with the permission of the American Physical Society.

Notice that, with this technique, we only obtain lepton flavor conserving NSI. For neutrino oscillation not only the absolute value of $\epsilon_{\alpha\alpha} - \epsilon_{\beta\beta}$ but also its sign is important. In fact, neutrino oscillation data favor positive value of $\epsilon_{ee} - \epsilon_{\mu\mu} \simeq \epsilon_{ee} - \epsilon_{\tau\tau} \sim 0.3$. If $a_\mu + a_\tau = -3$, the anomalies cancel without any need for new generations of leptons and/or quarks. However, just like in $B - L$ and $L_\mu - L_\tau$ gauge theories, the presence of right-handed neutrinos is necessary to cancel the $U(1)' - U(1)' - U(1)'$ anomaly. Let us take $a_\mu = a_\tau = -3/2$ so that anomalies cancel; moreover, we obtain $\epsilon_{\mu\mu} = \epsilon_{\tau\tau}$. We can then accommodate the best fit with

$$g' = 4 \times 10^{-5} \frac{m_{Z'}}{10 \text{ MeV}} \left(\frac{\epsilon_{ee} - \epsilon_{\mu\mu}}{0.3} \right)^{1/2}. \tag{40}$$

For the LMA-Dark solution $\epsilon_{ee} - \epsilon_{\mu\mu} < 0$ is required, so the value of $a_\mu \simeq a_\tau$ should be positive. As a result, more chiral fermions are needed to be added to cancel anomalies. We will return to this point later.

Since the $U(1)'$ charges of the left-handed and right-handed charged leptons are equal, their Yukawa coupling (and therefore their mass terms) preserve $U(1)'$ automatically. We should however consider the mass matrix of neutrinos with more care. While the flavor diagonal elements of neutrino mass matrix can be produced without any need for $U(1)'$ breaking, if a_α is not universal, obtaining the neutrino mass mixing requires symmetry breaking. As mentioned above, right-handed neutrinos are also required to cancel anomalies. If the masses of neutrinos are of Dirac type, right-handed neutrinos will be as light as left-handed neutrinos. They can be produced in the early universe via $U(1)'$ coupling so, if they are light, they can contribute to the relativistic degrees of freedom. To solve both problems at one shot, we can invoke the seesaw mechanism. For simplicity, we take $a_\mu = a_\tau$ so that the mixing between the second and third generation does not break $U(1)'$. Generalization to $a_\mu \neq a_\tau$ will be straightforward. Let us denote the right-handed neutrino of generation "i" by N_i. Under $U(1)'$,

$$N_1 \rightarrow N_1, \ N_2 \rightarrow e^{ia_\mu\alpha}N_2 \text{ and } N_3 \rightarrow e^{ia_\tau\alpha}N_3 = e^{ia_\mu\alpha}N_3. \tag{41}$$

Dirac mass terms come from

$$\lambda_1 N_1^T H^c c L_e + \lambda_2 N_2^T H^c c L_\mu + \lambda_3 N_3^T H^c c L_\tau + \lambda_4 N_2^T H^c c L_\tau + \lambda_5 N_3^T H^c c L_\mu + H.c. \tag{42}$$

By changing the basis, either of λ_4 and λ_5 can be set to zero, but the nonzero one will mix the second and the third generations. Moreover, we add electroweak singlet scalars S_1 and S_2 with $U(1)'$ charges $-2a_\mu$ and $-a_\mu$, respectively. We can then write the following potential

$$M_1 N_1^T c N_1 + S_1(A_2 N_2^T c N_2 + A_3 N_3^T c N_3 + A_{23} N_2^T c N_3) + S_2(B_2 N_1^T c N_2 + B_3 N_1^T c N_3) + H.c \tag{43}$$

Once S_1 and S_2 develop a vacuum expectation value (VEV), $U(1)'$ will be broken leading to the desired neutrino mass and mixing scheme. The VEVs of S_1 and S_2 induce a mass of

$$g'a_\mu(4\langle S_1\rangle^2 + \langle S_2\rangle^2)^{1/2} \tag{44}$$

for the Z' boson. Taking $g'a_\mu \sim 10^{-5} - 10^{-4}$, we find that as long as $\langle S_1 \rangle \sim \langle S_2 \rangle \sim 100$ GeV$(10^{-4}/g'a_\mu)$, the contribution to the Z' mass will be ~ 10 MeV as desired. In case that more scalars charged under $U(1)'$ are added to the model (we shall see examples in section 4.2), the Z' mass receives further contributions.

For $m_{Z'} < m_\pi$, the Z' can decay only to neutrino pair at tree level with a lifetime of

$$c\tau_{Z'} \sim 10^{-9} \text{ km} \left(\frac{7 \times 10^{-5}}{g'} \right)^2 \left(\frac{10 \text{ MeV}}{m_{Z'}} \right) \frac{1}{a_\mu^2 + a_\tau^2}.$$

As a result, Z' evades the bounds from the beam dump experiments. In the following, we go through possible experiments that can search for the Z' boson.

In the presence of new interactions, new decay modes for charged mesons open up: $K^+ \rightarrow l^+ + \nu + Z'$ and $\pi^+ \rightarrow l^+ + \nu + Z'$. The typical upper bounds from meson decay are of order of $O(0.001)$ [173–176] which are too weak to be relevant for our models; see **Figures 10**, **11**, which are taken from Bakhti and Farzan [173]. As shown in Bakhti and Farzan [173], the bound on the ν_e coupling to the Z' boson can be dramatically improved by customized searches for three body decays ($K^+ \rightarrow e^+$ + missing energy) and ($\pi^+ \rightarrow e^+$ + missing energy).

In principle, Z' can kinetically mix with the hypercharge gauge boson which gives rise to Z' mixings both with the photon and the Z bosons. Even if we set the kinetic mixing to zero at tree level, it can be produced at loop level as long as there are particles charged under both $U(1)$ gauge symmetries. Going to a basis where the kinetic terms of gauge bosons is canonical, the Z' boson obtains a coupling to the electron given by $e\epsilon$ where ϵ is the kinetic mixing between Z' and the photon. This coupling can affect neutrino interaction with the electron on which there are strong bounds from solar experiments (mostly Super-Kamiokande and Borexino) [131, 133]. Kamada and Yu [177], setting the tree level kinetic mixing equal to zero, has calculated the kinetic mixing for the $L_\mu - L_\tau$ models and has found it to be finite and of order of $eg'/8\pi^2$. The Borexino bound [133] can then be translated into $g'e \overset{<}{\sim} 10^{-4}$ which can be readily satisfied for $g' < 10^{-4}$. The loop contribution to the photon Z' mixing from a charged particle is very similar to its contribution to the vacuum polarization (photon field renormalization) replacing $(qe)^2$ with $(qe)(a_\alpha g')$. In case of the $L_\mu - L_\tau$ gauge symmetry, $a_e = 0$, $a_\mu = -a_\tau$ and since the electric charges of μ and τ are the same, the infinite parts of their contribution to the mixing cancels out. In general, we do not however expect such a cancelation and counter terms are therefore required. Once we open up the possibility of tree level kinetic mixing, the sum of tree level and loop level mixing can be set to arbitrarily small value satisfying any bound.

The above discussion on the $Z' - \gamma$ kinetic mixing also applies to the $Z' - Z$ kinetic mixing. Here, we should also check the $Z - Z'$ mass mixing [178]. It is straightforward to show that, since the Z' couplings are taken to be non-chiral, there is no contribution to the $Z - Z'$ mass mixing at one loop level. If the model contains scalars that are charged both under electroweak and $U(1)'$ and develop VEV, mass mixing between Z and Z' appears even at tree level. In the minimal version of the model that is described above

there is no such scalar but we shall come back to this point in section 4.2.

Decay of Z' to neutrino pairs can warm up the neutrino background during and right after the Big Bang Nucleosynthesis (BBN) era. The effect can be described by the contribution to the effective extra relativistic degrees of freedom ΔN_{eff}. As shown in Kamada and Yu [177], BBN bounds rule out $m_{Z'} < 5$ MeV. Of course, this lower bound on $m_{Z'}$ applies only if the coupling is large enough to bring Z' to thermal equilibrium with neutrinos before they decouple from the plasma at $T \sim 1$ MeV. That is, for 1 MeV $< m_{Z'} < 5$ MeV the coupling should be smaller than $\sim 3 \times 10^{-10}$ [179].

NSI can leave its imprint on the flavor composition of supernova neutrino flux [34, 180, 181]. Moreover, Z' particle can be produced and decay back to neutrinos within the supernova core. This leads to a shortening of the mean free path of neutrinos inside the supernova core [177]. This, in turn, results in prolonging the duration of neutrino emission from supernova. To draw a quantitative conclusion and bound, a full simulation is required.

Once we introduce the new interaction for neutrinos, high energy neutrinos (or antineutrinos) traveling across the universe resonantly interact with cosmic background antineutrinos (or neutrinos) producing Z' which decays back to $\nu\bar\nu$ pair with energies lower than that of initial neutrino (or antineutrino). This will result in a dip in the spectrum of high energy neutrinos. Taking the cosmic background neutrinos as non-relativistic, we expect the position of the dip to be given by $E_\nu \sim$ PeV$(m_{Z'}/10 \text{ MeV})^2 (0.05 \text{ eV}/m_\nu)$. The value is tantalizingly close to the observed (but by no means established) gap in the high energy IceCube data. Moreover, as shown in Kamada and Yu [177] with $g' \sim 10^{-5} - 10^{-4}$ (the range of interest to us), the optical depth is larger than one. Thus, this rather robust prediction can be eventually tested by looking for the dip in the high energy neutrino data.

The contribution from the Z' loop to $(g-2)_\mu$ can be estimated as $g'^2/(8\pi)$ up to corrections of order $O(m_{Z'}^2/m_\mu^2) \sim 0.01$. For $g' < 10^{-4}$, the contribution is too small to explain the claimed discrepancy [182].

Let us now discuss the neutrino scattering experiments. The amplitude of the contribution from t-channel Z' exchange to neutrino quark scattering is suppressed relative to that from SM by a factor of $m_{Z'}^2/(t - m_{Z'}^2)$, where t is the Mandelstam variable. At CHARM and NuTeV experiments, the energy momentum exchange was about 10 GeV ($t \gg m_{Z'}^2$), so the new effects were suppressed. As a result, the bound found in Escrihuela et al. [10], Coloma et al. [124], and Davidson et al. [128] does not apply to the model with a light gauge boson. However, as discussed in Farzan and Heeck [25], Coloma et al. [124], and Dutta et al. [183], low energy scattering experiments can be sensitive to low mass gauge interactions. Three categories of scattering experiments have been studied in this regard: (1) Scattering of solar neutrino at direct dark matter search experiments [25, 183–185]. As shown in Farzan and Heeck [25], the upcoming Xenon based experiments such as LUX-Zeplin and the future Germanium based experiments such as superCDMS at SNOLAB can test most of the parameter space of our interest (see **Figure 9**, adapted
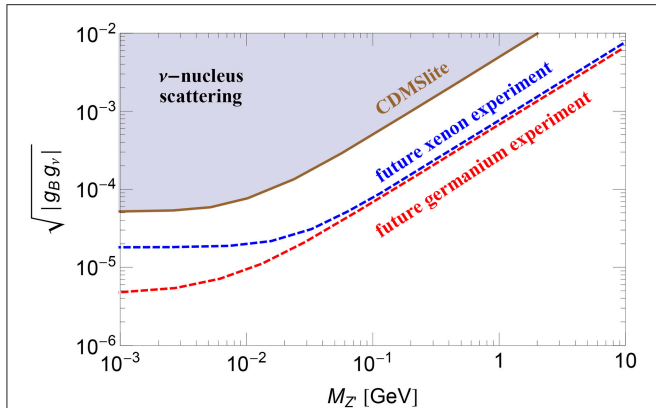
FIGURE 9 | Approximate 90% C.L. bounds on the product of couplings of neutrinos and quarks to Z' from solar-neutrino nuclear recoils in CDMSlite and optimistic projections for second-generation Xenon (e.g., LUX–ZEPLIN) and Germanium experiments (e.g., SuperCDMS SNOLAB), adapted from Cerdeno et al. [184]. Plot taken from Farzan and Heeck [25] and reproduced with the permission of the American Physical Society.

from Farzan and Heeck [25]). (2) As shown in detail in Coloma et al. [124] and Shoemaker [186], the running COHERENT experiment [187] is an ideal setup to probe NSI with a light mediator. At this experiment, low energy ν_μ and ν_e fluxes are produced via pion and muon decay at rest. The LMA-Dark solution can be entirely probed by this experiment [124]. The COHERENT experiment has recently released its preliminary results, ruling out a significant part of the parameter space. We shall discuss the new results in section 4.3. (3) Scattering of reactor $\bar{\nu}_e$ flux off nuclei can also probe NSI of the type we are interested in Wong [188], Aguilar-Arevalo et al. [189, 190], Agnolet et al. [191], Billard et al. [192], Lindner et al. [193], Barranco et al. [194], and Kerman et al. [195].

The Z' gauge boson coupled to ν and μ can contribute to the so-called neutrino trident production $\nu + A \rightarrow \nu + A + \mu^+ + \mu^-$, where A is a nucleus. The rate of such interaction was measured by the CCFR [196] and CHARM II [197] collaborations, and is found to be consistent with the SM prediction. This observation sets the bound $g'a < 9 \times 10^{-4}$ for $m_{Z'} \sim 10$ MeV [198, 199].

As we saw earlier, taking $a_\mu = a_\tau = -3/2$, the contributions from the field content of the SM to anomalies cancel out. We can then obtain any negative values of $\epsilon_{\mu\mu} - \epsilon_{ee} = \epsilon_{\tau\tau} - \epsilon_{ee} \sim -1$ by choosing $g' \sim 10^{-4}(|\epsilon_{\mu\mu} - \epsilon_{ee}|)^{1/2}$ (see Equation 40). Let us now discuss if with this mechanism we can reconstruct a model that embeds the LMA-Dark solution with positive $\epsilon_{\mu\mu} - \epsilon_{ee} = \epsilon_{\tau\tau} - \epsilon_{ee} \sim 1$. The condition $\epsilon_{\mu\mu} - \epsilon_{ee} = \epsilon_{\tau\tau} - \epsilon_{ee} \sim 1$ can be satisfied if $a_e = 0$, $a_\mu = a_\tau > 0$ and

$$g' \sim 10^{-4} \left(\frac{m_{Z'}}{10\,\text{MeV}} \right) \left(\frac{1}{a_\mu} \right)^{1/2}. \tag{45}$$

We should however notice that with $a_\mu = a_\tau > 0$, the cancelation of $U(1)' - SU(2) - SU(2)$ and $U(1)' - U(1) - U(1)$ anomalies require new chiral fermions. A new generation of leptons with $U(1)'$ charge equal to $-(3 + a_\mu + a_\tau)$ can cancel

the anomalies but in order for these new fermions to acquire masses large enough to escape bounds from direct production at colliders, their Yukawa couplings enter the non-perturbative regime. Similar argument holds if we add a new generation of quarks instead of leptons. Another option is to add a pair of new generations of leptons (or quarks) with opposite $U(1)_Y$ charges but equal $U(1)'$ charge of $-(3 + a_\mu + a_\tau)/2$. Let us denote the field content of the fourth generation with ν_{R4}, e_{R4} and L_4, and similarly that of the fifth generation with ν_{R5}, e_{R5} and L_5. As pointed out, the hypercharges of fourth and fifth generation are opposite so we can write Yukawa terms of type

$$Y_1 S e_{R4}^T c e_{5R} + Y_2 S L_4^T c L_5 + \text{H.c.},$$

where S is singlet of the electroweak symmetry group, $SU(2) \times U(1)$ with a $U(1)'$ charge of $3 + a_\mu + a_\tau$. Even for $Y_1 \sim Y_2 \sim 1$, in order to obtain heavy enough mass, $\langle S \rangle$ should be of order of TeV. On the other hand, $\langle S \rangle$ contributes to Z' mass so

$$\text{Masses of 4th and 5th generation} \lesssim \langle S \rangle$$

$$< 5\,\text{TeV}\, \frac{m_{Z'}}{10\,\text{MeV}} \frac{2 \times 10^{-6}}{g'(3 + a_\mu + a_\tau)}.$$

In other words, $g' \lesssim \frac{5\,\text{TeV}}{M_{4,5}} \frac{2 \times 10^{-6}}{3 + a_\mu + a_\tau} \frac{m_{Z'}}{10\,\text{MeV}}$, where $M_{4,5}$ are the typical masses of the fourth and fifth generation leptons. Inserting this in Equation (39), we find $\epsilon_{\mu\mu} = \epsilon_{\tau\tau} \lesssim 0.01$.

In general, the cancelation of $U(1)' - SU(2) - SU(2)$ and $U(1)' - U(1) - U(1)$ anomalies requires new chiral fermions charged under $U(1)'$ and $SU(2) \times U(1)'$ (or both). In the former case, we need new $U(1)'$ charged scalars whose VEV contribute to the Z' mass. The lower bounds on the masses of new particles set a lower bound on the VEV of new scalars which, in turn, can be translated into an upper bound on $g'/m_{Z'}$ which leads to $\epsilon_{\mu\mu} \lesssim 0.01$. In the second case, large masses of the 4th and 5th generations requires non-perturbative Yukawa coupling to the Higgs. If masses of the new fermions could be about few hundred GeV, none of these obstacles would exist. Fortunately, there is a trick to relax the strong lower bounds from colliders on the masses of new particles. Let us suppose the charged particles are just slightly heavier than their neutral counterparts. Their decay modes can be then of type $e_{4(5)}^- \rightarrow \nu_{4(5)} l \nu, \nu_{4(5)} q' \bar{q}$ with a final charged lepton or jet too soft to be detected at colliders. In this case, the new generation can be as light as few 100 GeV so their mass can come from a perturbative Yukawa coupling to the SM Higgs or new scalars charged under $U(1)'$ and VEV of ~100 GeV opening up a hope for $g'/m_{Z'} \sim 10^{-5}$ MeV^{-1} and therefore for $\epsilon_{\mu\mu} = \epsilon_{\tau\tau} \sim 1$.

4.2. A Model Both for LF Conserving and LFV NSI

As mentioned in section 4.1, the coupling of Z' to neutrinos can be achieved with two mechanisms: (i) The $(\nu_\alpha\ \ell_{L\alpha})$ doublet is assigned a charge under $U(1)'$, so neutrinos directly obtain a gauge coupling to the Z' boson. This route was discussed in section 4.1. (ii) Active neutrinos mix with a new fermion singlet under electroweak group symmetry but charged under

new $U(1)'$. In this section, we focus on the second route. Using the notation in Equation (38), in the present scenario one has $a_e = a_\mu = a_\tau = 0$ so to cancel the $U(1)' - SU(2) - SU(2)$ and $U(1)' - U(1) - U(1)$ anomalies, we should add new fermions. As discussed in the previous section, in order to make these new fermions heavier than ~ 1 TeV, we need new scalars charged under $U(1)'$ with a VEV of 1 TeV. To keep the contribution from the new VEV to Z' mass under control,

$$g' < 10^{-5} \frac{m_{Z'}}{10 \text{ MeV}}. \tag{46}$$

Notice that this tentative bound is stronger than the bound from $\pi \to Z'\gamma$ (see **Figure 8**). Let us introduce a new Dirac fermion Ψ which is neutral under electroweak symmetry but charged under $U(1)'$. Its $U(1)'$ charge denoted by a_Ψ can be much larger than one. Since we take equal $U(1)'$ charges for Ψ_L and Ψ_R, no anomaly is induced by this Dirac fermion. Let us denote the mixing of Ψ with neutrino of flavor α with κ_α. Such a mixing of course breaks $U(1)'$. Mixing can be obtained in two ways:

- We add a sterile Dirac N (neutral both under electroweak and under $U(1)'$) and a scalar (S) to break $U(1)'$. The $U(1)'$ charge of the S is taken to be equal to that of Ψ. We can then add terms like the following to the Lagrangian:

$$m_\Psi \bar{\Psi}\Psi + m_N \bar{N}N + Y_\alpha \bar{N}_R H^T c L_\alpha + \lambda_L S \bar{\Psi}_R N_L. \tag{47}$$

Notice that we were allowed to add a term of $\lambda_R S \bar{\Psi}_L N_R$ too, but this term is not relevant for our discussion. Taking $Y_\alpha \langle H \rangle, \lambda_L \langle S \rangle, m_\Psi \ll m_N$, we can integrate out N and obtain

$$\kappa_\alpha = \frac{Y_\alpha \langle H \rangle \lambda_L \langle S \rangle}{m_N m_\Psi}. \tag{48}$$

Since we take $\lambda_L \langle S \rangle < m_N$, in order to have sizeable κ_α, the mass of Ψ cannot be much larger than $Y_\alpha \langle H \rangle$. On the other hand, Y_α determines the new decay mode of $H \to \nu N$ which is observationally constrained [200]. We therefore find an upper bound on m_Ψ of few GeV. For example, taking $m_\Psi = 2$ GeV, $m_N = 20$ GeV, $Y_\alpha \langle H \rangle = 0.1$ GeV, $\lambda_L = 1$ and $\langle S \rangle \sim 4$ GeV, we obtain $\kappa_\alpha \simeq 0.01$. With such small Y_α, the rate of the Higgs decay into N and ν will be as small as $\Gamma(H \to \mu\mu)$ and therefore negligible. With $g' < 10^{-4}$, the contribution from $\langle S \rangle$ to $m_{Z'}$ will also be negligible.

- Another scenario which has been proposed in Farzan and Heeck [25] invokes a new Higgs doublet H' which has $U(1)'$ charge equal to that of Ψ. The Yukawa coupling will be then equal to $\mathcal{L} = -\sum_\alpha y_\alpha \bar{L}_\alpha H'^T c \Psi$ which leads to

$$\kappa_\alpha = \frac{y_\alpha \langle H' \rangle}{\sqrt{2} m_\Psi}$$

where $\tan\beta = \langle H \rangle / \langle H' \rangle$. The VEV of H' can contribute to the Z' mass so we obtain

$$\cos\beta \leq 4 \times 10^{-5} \left(\frac{m_{Z'}}{10 \text{ MeV}}\right) \frac{1}{g_\Psi}. \tag{49}$$

Thus, to obtain sizeable κ_α (e.g., $\kappa_\alpha > 0.03$), we find

$$M_\Psi < \text{few GeV} \frac{m_{Z'}}{10 \text{ MeV}} \frac{0.2}{g' a_\Psi} \frac{0.03}{\kappa_\alpha}. \tag{50}$$

Moreover, the VEV of H' can induce $Z - Z'$ mixing on which there are strong bounds [201]. These bounds can be translated into $\cos\beta < 10^{-4}(m_{Z'}/10 \text{ MeV})(1/g_\Psi)$ which is slightly weaker than the bound in (49). The smallness of $\langle H' \rangle$, despite its relatively large mass, can be explained by adding a singlet scalar(s) of charge a_Ψ with $\mathcal{L} = -\mu S_1^\dagger H^\dagger H'$ which induces $\langle H' \rangle = -\mu \langle S_1 \rangle / (2M_{H'}^2)$. Taking $\langle S_1 \rangle \mu \ll M_{H'}^2$, we find $\cos\beta \ll 1$. The components of H' can be pair produced at colliders via electroweak interactions. They will then decay to Ψ and leptons. In particular, the charged component H^- can decay into charged lepton plus Ψ which appears as missing energy. Its signature will be similar to that of a charged slepton [25]. According to the present bounds [25, 202], $m_{H'} \gtrsim 300$ GeV.

Regardless of the mechanism behind the mixing between Ψ and ν, it will lead to the coupling of Z' to active neutrinos as follows

$$g' a_\Psi Z'_\mu \left(\sum_{\alpha,\beta} \kappa_\alpha^* \kappa_\beta \bar{\nu}_\alpha \gamma^\mu P_L \nu_\beta - \kappa_\alpha^* \bar{\nu}_\alpha \gamma^\mu P_L \Psi - \kappa_\alpha \bar{\Psi} \gamma^\mu P_L \nu_\alpha \right), \tag{51}$$

which leads to $\epsilon_{\alpha\beta}^u = \epsilon_{\alpha\beta}^d = \frac{g'^2 a_\Psi \kappa_\alpha^* \kappa_\beta}{6\sqrt{2} G_F m_{Z'}^2}$. Notice that if the mixing of Ψ with more than one flavor is nonzero, we can have lepton flavor violating NSI with $\epsilon_{\alpha\alpha}^{u(d)} \epsilon_{\beta\beta}^{u(d)} = |\epsilon_{\alpha\beta}^{u(d)}|^2$. If more than one Ψ is added, we may label the mixing of ith Ψ to ν_α with $\kappa_{i\alpha}$. The Schwartz inequality $(\sum_i \kappa_{i\alpha}^* \kappa_{i\beta})^2 < (\sum_i |\kappa_{i\alpha}|^2)(\sum_i |\kappa_{i\beta}|^2)$ then still applies

$$\epsilon_{\alpha\alpha}^{u(d)} \epsilon_{\beta\beta}^{u(d)} > (\epsilon_{\alpha\beta}^{u(d)})^2.$$

Taking $\kappa_{i\alpha} = \delta_{i\alpha}$, meaning that each Ψ_i mixes with only one ν_α, only diagonal elements of $\epsilon_{\alpha\beta}$ will be nonzero, preserving lepton flavors.

Notice that Ψ in our model decays into Z' and ν and appears as missing energy. Ψ should be heavier than MeV; otherwise, it can contribute to extra relativistic degrees of freedom in the early universe. Remember that we have found that $m_\Psi <$ few GeV. The mixing of active neutrinos with Ψ results in the violation of the unitarity of 3×3 PMNS matrix on which there are strong bounds [203–205]

$$|\kappa_e|^2 < 2.5 \times 10^{-3}, \ |\kappa_\mu|^2 < 4.4 \times 10^{-4} \text{ and}$$
$$|\kappa_\tau|^2 < 5.6 \times 10^{-3} \text{ at } 2\sigma \tag{52}$$

which immediately give

$$|\kappa_\mu \kappa_e| < 10^{-3}, \ |\kappa_\mu \kappa_\tau| < 1.6 \times 10^{-3} \text{ and}$$
$$|\kappa_e \kappa_\tau| < 3.7 \times 10^{-3} \text{ at } 2\sigma. \tag{53}$$

Under certain assumptions, Fernandez-Martinez et al. [203] also derives independent bound on $\kappa_\alpha \kappa_\beta^*|_{\alpha \neq \beta}$ from lepton flavor

violation (LFV) processes $l_\alpha^- \to l_\beta^- \gamma$, but these bounds are valid only for $m_\Psi \gg m_W$. For our case with $m_\Psi \ll m_W$, a GIM mechanism is at work and suppresses the contribution to $l_\alpha^- \to l_\beta^- \gamma$ from $\nu - \Psi$ mixing. In the case that the mixing comes from Yukawa coupling to H', because of the LFV induced by H' and Ψ coupling to more than one flavor, a new contribution to $l_\alpha^- \to l_\beta^- \gamma$ appears. As shown in [25], from $Br(\tau \to e\gamma) < 3.3 \times 10^{-8}$, $Br(\tau \to \mu\gamma) < 4.4 \times 10^{-8}$ [161] and $Br(\mu \to e\gamma) < 4.2 \times 10^{-13}$[206], one can respectively derive $|y_e y_\tau| < 0.46(m_{H^-}/(400 \text{ GeV}))^2$, $|y_\mu y_\tau| < 0.53(m_{H^-}/(400 \text{ GeV}))^2$ and $|y_e y_\mu| < 7 \times 10^{-4}(m_{H^-}/(400 \text{ GeV}))^2$. As demonstrated in Farzan and Heeck [25], except for $\epsilon_{e\mu}$ which is strongly constrained by the bound from $\mu \to e\gamma$ within the model described in Farzan and Heeck [25], all components of $\epsilon_{\alpha\beta}$ can be within the reach of current and upcoming long baseline neutrino experiments. If mixing is achieved via the mechanism described in Equation (48), no new bound from LFV rare decay applies and we can obtain all $\epsilon_{\alpha\beta}$ (including $\epsilon_{e\mu}$) of the order of

$$\epsilon_{\alpha\beta}^u = \epsilon_{\alpha\beta}^d = g' a_\Psi \left(\frac{g'}{10^{-5}} \right) \frac{\kappa_\alpha^* \kappa_\beta}{10^{-3}} \left(\frac{10 \text{ MeV}}{m_{Z'}} \right)^2. \qquad (54)$$

Notice that in this model, the coupling of Z' to neutrino pairs can be much larger than the coupling to quarks: $|g' a_\Psi \kappa_\alpha \kappa_\beta| \gg g'$, see Equation (51). The bounds from meson decays on Z' coupling to neutrino pairs have been studied in Bakhti and Farzan [173]. The results are shown in **Figures 10**, **11**. The strongest bound for $m_{Z'} \sim 10$ MeV is of order of 0.001, which can be readily satisfied if $\kappa_\alpha \kappa_\beta < 10^{-3}$. However, further data on $[\pi^+ \to e^+(\mu^+) + \text{missing energy}]$ or on $[K^+ \to e^+(\mu^+) + \text{missing energy}]$ can probe parts of the parameter space of interest to us.

4.3. Impact of Recent Results from COHERENT Experiment

Recently, the COHERENT experiment has released its first results confirming the SM prediction of elastic scattering of neutrinos off nuclei at 6.7σ, studying the interaction of ν_μ, $\bar{\nu}_\mu$ and ν_e flux from Spallation Neutron Source (SNS) at the Oak Ridge National Laboratory on a 14.6 kg CsI[Na] scintillator detector [126]. The preliminary results already set strong bounds on NSI.

Assuming the validity of the contact interaction approximation (i.e., assuming the mass of the mediator is heavier than ~ 10 MeV), Coloma et al. [127] shows that the recent COHERENT data rules out LMA-Dark solution. Liao and Marfatia [130], taking a universal coupling of Z' to SM fermions finds that

$$(g_\nu g_q)^{1/2} < 6 \times 10^{-5} \text{ for } m_{Z'} < 30 \text{ MeV at } 2\sigma. \qquad (55)$$

Let us discuss how this bound can constrain our model(s) for NSI. Regardless of the details of the underlying theory, we can write

$$(g_\nu g_q)^{1/2} = 5.47 \times 10^{-5} \sqrt{\epsilon_{\alpha\beta}} \left(\frac{m_{Z'}}{10 \text{ MeV}} \right)$$

where $g_q = g_B/3$ is the coupling of Z' boson to quarks and $(g_\nu)_{\alpha\beta}$ is its coupling to ν_α and ν_β. In the model described in section 4.1, $(g_\nu)_{\alpha\beta} = \delta_{\alpha\beta} a_\alpha g'$ and in the model of section 4.2, $(g_\nu)_{\alpha\beta} = g' a_\Psi \kappa_\alpha \kappa_\beta$. Remember that, in order for $\epsilon_{\alpha\beta}$ to show up in neutrino oscillation experiments, it should be non-universal. For example, the LMA-Dark solution requires $\epsilon_{\mu\mu} - \epsilon_{ee} = \epsilon_{\tau\tau} - \epsilon_{ee} \sim 1$. Setting $\epsilon_{ee} = 0$ and $\epsilon_{\mu\mu} \neq 0$, we expect the bound on $|\epsilon_{\mu\mu}|$ from the COHERENT experiment to be slightly weaker than that found in Liao and Marfatia [130] taking $\epsilon_{\mu\mu} = \epsilon_{ee} \neq 0$. Thus, the LMA-Dark solution still survives with the present COHERENT data but, further data from COHERENT as well as the data from upcoming reactor neutrino-nucleus coherent scattering experiments such as the setup described in Lindner et al. [193] can probe the most interesting part of the parameter space.
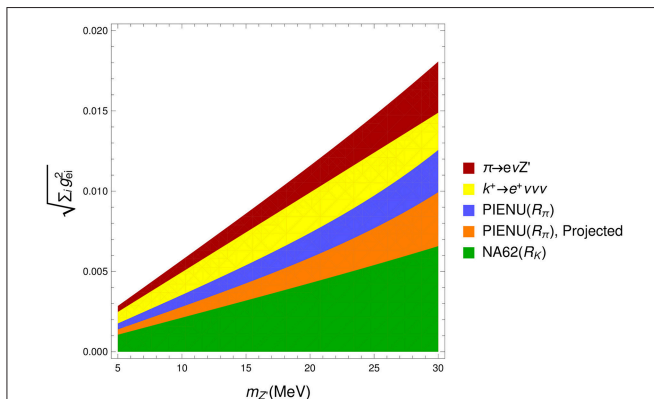

FIGURE 10 | 90% C.L. constraints on $\sqrt{\sum_i g_{ei}^2}$ vs. $m_{Z'}$ from constraints on $\pi \longrightarrow e\nu Z'$ [207] and $K^+ \longrightarrow e^+ \nu\nu\nu$ [208] branching ratios, from current and projected R_π measurement by PIENU [209] and from the R_K measurement by NA62 [210]. g_{ei} is the coupling of $Z'_\mu \bar{\nu}_e \gamma^\mu \nu_i$ where ν_i can be any neutrino state much lighter than ~ 100 MeV. Figure taken from Bakhti and Farzan [173] and reproduced with the permission of the American Physical Society.
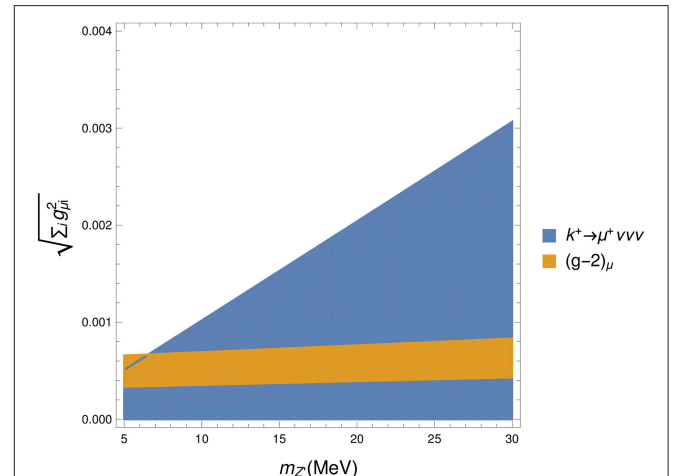

FIGURE 11 | 90% C.L. constraints on $\sqrt{\sum_i g_{\mu i}^2}$ vs. $m_{Z'}$ from $K^+ \longrightarrow \mu^+ \nu\nu\nu$ branching ratio [211]. The band shows the parameter space within L_μ gauge models (giving rise to equal couplings to μ and ν_μ) that can explain the $(g-2)_\mu$ anomaly [212]. $g_{\mu i}$ is the coupling of $Z'_\mu \bar{\nu}_\mu \gamma^\mu \nu_i$ where ν_i can be any neutrino state much lighter than 100 MeV. Figure taken from Bakhti and Farzan [173] and reproduced with the permission of the American Physical Society.

5. NSI AT UPCOMING LONG BASELINE EXPERIMENTS: T2HK, T2HKK, DUNE, JUNO, AND MOMENT

In recent years, rich literature has been developed on the possibility of detecting the NSI effects in upcoming long baseline neutrino experiments. In particular, degeneracies induced by the presence of NSI in the DUNE experiment have been scrutinized [15–18, 213–223]. In section 5.1, we review the effects of NSI at DUNE, T2HK and T2HKK experiments. In section 5.2, we show how intermediate baseline reactor experiments such as JUNO and RENO-50 can help to determine $\text{sign}(\cos 2\theta_{12})$ and therefore test the LMA-Dark solution. In section 5.3, we show how the MOMENT experiment can help to determine the octant of θ_{23} and the true value of δ despite the presence of NSI. Throughout this section, we set $\epsilon_{\mu\mu} = 0$ for definiteness and consistency with the majority of our references.

5.1. NSI at Upcoming Long Baseline Neutrino Experiments

Let us first briefly review the setups of the three upcoming state-of-the-art long baseline neutrino experiments which are designed to measure the yet unknown neutrino parameters with special focus on the Dirac CP-violating phase of the PMNS matrix.

- **DUNE:** The source of the DUNE experiment will be at the Fermilab and the detector will be located at Sanford Underground Research Facility (SURF) at Homestake mine in South Dakota [103]. The baseline will be 1,300 km. The far detector will be a 40 kton liquid Argon detector sitting on axis with the beam so the spectrum will be broad band. The energy of the neutrino beam will be around 3 GeV which comes from an 80 GeV proton beam with 1.47×10^{21} POT per year. A reasonable assumption for data taking is 3.5 years in each neutrino and antineutrinos modes.
- **T2HK:** The source of T2HK [224] will be upgraded 30 GeV JPARC beam with 2.7×10^{21} POT per year. The Hyper-Kamiokande detector with fiducial volume of 0.56 Mton [225] (25 times that of Super-Kamiokande) will be located in Kamiokande, 2.5° off axis so the spectrum will be narrow band. The energy of neutrinos will be around 0.6 GeV. The baseline of this experiment is 295 km. A reasonable assumption for data taking is the 2TankHK-staged configuration[11] for which the data taking time is 6 years for one tank plus another 4 years with second tank [221]. The ratio of running time in neutrino mode to that in the antineutrino mode is 1:3.
- **T2HKK:** This project is an extension of T2HK [218] with an extra detector in Korea with a baseline of 1,100 km. Two options with 2.5° off-axis-angle and 1.5° off-axis-angle have been discussed which respectively correspond to neutrino energies of 0.6 GeV and 0.8 GeV.

Notice that at T2HK, both energy of the neutrino beam and the baseline are lower than those at DUNE. We therefore expect the

---

[11]KEK Preprint 2016-21 and ICRR-Report-701-2016-1, https://lib-extopc.kek.jp/preprints/PDF/2016/1627/1627021.pdf.

DUNE experiment to be more sensitive to both standard and non-standard matter effects than T2HK and T2HKK. Although the baseline for the Korean detector of T2HKK is comparable to the DUNE baseline, the DUNE experiment will be more sensitive to matter effects than T2HKK, because the energy of the beam at T2HKK is lower. Detailed simulation confirms this expectation [221]. In the presence of NSI, new degeneracies will appear in long baseline neutrino experiments for determination of the value of δ, mass ordering and the octant of θ_{23}. One of the famous degeneracies is the so called generalized mass ordering degeneracy [11, 13, 19, 123, 221]. The oscillation probability remains invariant under the following simultaneous transformations

$$\theta_{12} \to \frac{\pi}{2} - \theta_{12}, \ \delta \to \pi - \delta, \ \Delta m_{31}^2 \to -\Delta m_{31}^2 + \Delta m_{21}^2,$$
$$\text{and } V_{eff} \to -S \cdot V_{eff}^* \cdot S \qquad (56)$$

where $S = \text{Diag}(1, -1, -1)$ and $(V_{eff})_{\alpha\beta} = \sqrt{2} G_F N_e [(\delta_{\alpha 1} \delta_{\beta 1}) + \epsilon_{\alpha\beta}]$ in which $\epsilon_{\alpha\beta} = \sum_{f \in \{e,u,d\}} (N_f/N_e) \epsilon_{\alpha\beta}^f$ depends on the composition of medium. Notice that the LMA-Dark solution with $\theta_{12} > \pi/4$ and $\epsilon^f \sim -1$ [13] is related to the generalized mass ordering transformation from the standard LMA solution with $\epsilon = 0$. For the Earth (with $N_p \simeq N_n$), we can write $N_u/N_e \simeq N_d/N_e = 3$. Notice however that the transformation in Equation (56) does not depend on the beam energy or baseline. As a result, by carrying out long baseline neutrino experiments on Earth with different baseline and beam energy configurations, this degeneracy cannot be resolved. Resolving this degeneracy requires media with different N_n/N_e composition. Notice that although the nuclear compositions of the Earth core and mantle are quite different, N_n/N_e is uniformly close to 1 across the Earth radius [113]. However, N_n/N_e in the Sun considerably differs from that in the Earth. Moreover, it varies from the Sun center (with $N_n/N_e \simeq 1/2$) to its outer region (with $N_n/N_e \simeq 1/6$) [60, 61]. As a result, the solar neutrino data can in principle help to solve this degeneracy. In fact, Gonzalez-Garcia and Maltoni [11] by analyzing solar data shows that the LMA solution with $\epsilon_{ee}^u \simeq 0.3$ is slightly favored over the LMA-Dark solution. The global analysis of solar, atmospheric and (very) long baseline data can in principle help to solve degeneracies. For the time being, however, since the terrestrial experiments are not precise enough to resolve the effects of $\text{sign}(\Delta m_{31}^2)$ and/or $\text{sign}(\cos 2\theta_{12})$, the generalized mass ordering degeneracy cannot be resolved.

At relatively low energy long baseline experiments such as T2HK and T2HKK for which the contribution to the oscillation probability from higher orders of $O(V_{eff}\epsilon/|\Delta m_{31}^2|)$ can be neglected, the appearance oscillation probability along the direction $\epsilon_{e\mu}/\epsilon_{e\tau} = \tan\theta_{23}$ will be equal to that for standard $\epsilon = 0$ [221]. The DUNE experiment being sensitive to higher orders of $(V_{eff}\epsilon/|\Delta m_{31}^2|)$ can solve this degeneracy [221]. At the DUNE experiment, another degeneracy appears when ϵ_{ee} and $\epsilon_{\tau e}$ are simultaneously turned on and the phase of $\epsilon_{e\tau}$ is allowed to be nonzero. As shown in **Figure 12**, (which corresponds to Figure 4 of Coloma [215] and confirmed in Figure 10 of Liao et al. [221]), in the presence of cancelation due to the phase of
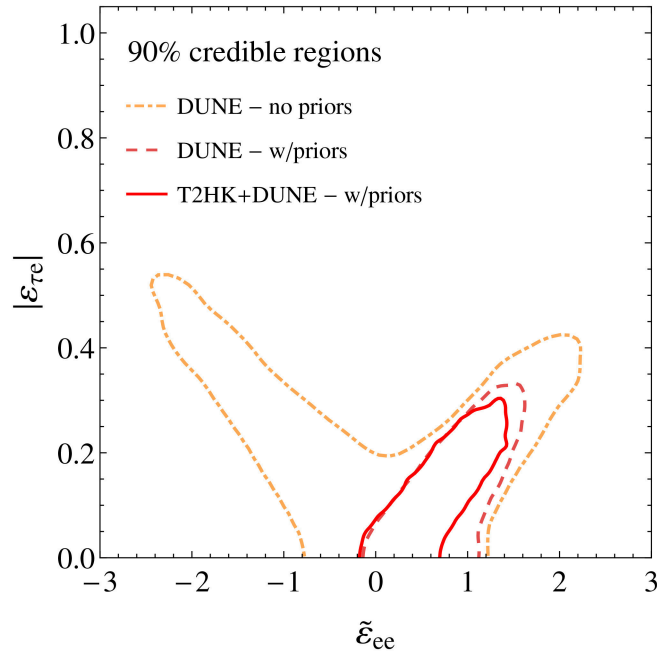
FIGURE 12 | 90% CL contours in the $|\epsilon_{\tau e}|$ and $\tilde{\epsilon}_{ee} = \epsilon_{ee} - \epsilon_{\mu\mu}$ plane for DUNE and DUNE+T2HK (see Equation 17 for the definition of ϵ). The phase of $\epsilon_{\tau e}$ is allowed to vary. Contours with priors take into account the present bounds from various neutrino oscillation experiments. This plot is taken from Coloma [215], published under the terms of the Creative Commons Attribution Noncommercial License and therefore no copyright permissions were required for its inclusion in this manuscript. We would like to thank P. Coloma for sending the original figure.

$\epsilon_{e\tau}$ for $|\epsilon_{e\tau}| \sim 0.2 - 0.3$, $|\epsilon_{ee}|$ as large as 2 cannot be disentangled from standard case with $\epsilon_{ee} = \epsilon_{e\tau} = 0$ at the DUNE experiment. However, this figure also demonstrates that when information on ϵ from already existent data is used as prior, the degeneracy can be considerably solved, ruling out the $\epsilon_{ee} < 0$ wing of solutions. That is because solar data rules out $\epsilon_{ee} < 0$ for $\theta_{12} < \pi/4$ [11]. NSI can induce degeneracies in deriving $\text{sign}(\cos 2\theta_{23})$. In principle, even with $\epsilon_{e\mu}$ ($\epsilon_{e\tau}$) as small as $O(0.01)$, the degeneracy due to the phase of $\epsilon_{e\mu}$ ($\epsilon_{e\tau}$) makes the determination of the octant of θ_{23} problematic [18]. Because of the generalized mass ordering degeneracy, the presence of NSI can also jeopardize determination of $\text{sign}(\Delta m_{31}^2)$ [226].

In summary, NSI induces degeneracies that makes determination of the true value of δ at DUNE impossible at $3\,\sigma$ C.L. The T2HKK experiment can considerably solve this degeneracy as demonstrated in **Figures 13**, **14** (corresponding to Figures 11 and 12 of Liao et al. [221]).

5.2. JUNO and RENO-50 Shedding Light on LMA-Dark

To determine the sign of Δm_{31}^2, two reactor neutrino experiments with baseline of ~ 50 km are proposed: The JUNO experiment in China which is planned to start data taking in 2020 and RENO-50 which is going to be an upgrade of the RENO experiment in South Korea[12]. In this section, we show that for known mass

---

[12]Joo [227] reports the current status of RENO-50.

ordering, these experiments can determine the octant of θ_{12}. At reactor experiments, since the energy is low, $|\Delta m_{31}^2|/E \gg \sqrt{2}G_F N_e$. Thus, the matter effects can be neglected and the survival probability can be written as

$$
\begin{aligned}
P(\bar{\nu}_e \to \bar{\nu}_e) &= \left| |U_{e1}|^2 + |U_{e2}|^2 e^{i\Delta_{21}} + |U_{e3}|^2 e^{i\Delta_{31}} \right|^2 \\
&= \left| c_{12}^2 c_{13}^2 + s_{12}^2 c_{13}^2 e^{i\Delta_{21}} + s_{13}^2 e^{i\Delta_{31}} \right|^2 \\
&= c_{13}^4 \left(1 - \sin^2 2\theta_{12} \sin^2 \frac{\Delta_{21}}{2} \right) + s_{13}^4 \\
&\quad + 2 s_{13}^2 c_{13}^2 \left[\cos \Delta_{31} (c_{12}^2 + s_{12}^2 \cos \Delta_{21}) \right. \\
&\quad \left. + s_{12}^2 \sin \Delta_{31} \sin \Delta_{21} \right],
\end{aligned} \tag{57}
$$

where $\Delta_{ij} = \Delta m_{ij}^2 L/(2E_\nu)$ in which L is the baseline. Notice that the first parenthesis (which could be resolved at KamLAND) is only sensitive to $\sin^2 2\theta_{12}$ and cannot therefore resolve the octant of θ_{12}. The terms in the last parenthesis, however, are sensitive to the octant of θ_{12}. To solve these terms two main challenges have to be overcome: (i) These terms are suppressed by $s_{13}^2 \sim 0.02$ so high statistics is required in order to resolve them. (ii) In the limit, $\Delta_{12} \to 0$, we can write $P(\bar{\nu}_e \to \bar{\nu}_e) = c_{13}^4 + s_{13}^4 + 2 s_{13}^2 c_{13}^2 \cos \Delta_{31}$ so the sensitivity to θ_{12} is lost. To determine θ_{12} baseline should be large enough (i.e., $L \gtrsim 10$ km). (iii) Condition $\Delta_{12} \gtrsim 1$ naturally implies $\Delta_{13} \gg 1$ so the terms sensitive to the octant of θ_{12} (and sign of Δm_{31}^2) oscillate rapidly. To resolve these terms, the energy resolution and accuracy of reconstruction of the total energy scale must be high. Notice that reactor experiments such
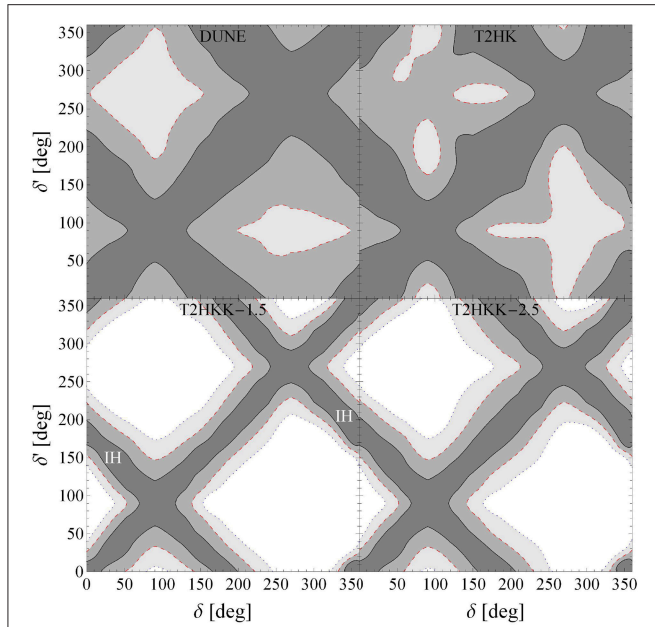
FIGURE 13 | 1σ, 2σ, and 3σ contours for extracted value of CP-violating phase δ' at DUNE, T2HK, T2HKK with $1.5°$ off-axis angle and T2HKK with $2.5°$ off-axis angle vs. true value of δ. Normal mass ordering is assumed and taken to be unknown. The values of ϵ_{ee}, $\epsilon_{e\mu}$ and $\epsilon_{e\tau}$ are allowed to vary. The parameters that are not shown are marginalized. This plot is taken from Liao et al. [221], published under the terms of the Creative Commons Attribution Noncommercial License and therefore no copyright permissions were required for its inclusion in this manuscript. We would like to thank D. Marfatia for sending the original figure.

FIGURE 14 | The same as **Figure 13** except that the mass ordering is assumed to be known. This plot is taken from Liao et al. [221], published under the terms of the Creative Commons Attribution Noncommercial License and therefore no copyright permissions were required for its inclusion in this manuscript. We would like to thank D. Marfatia for sending the original figure.
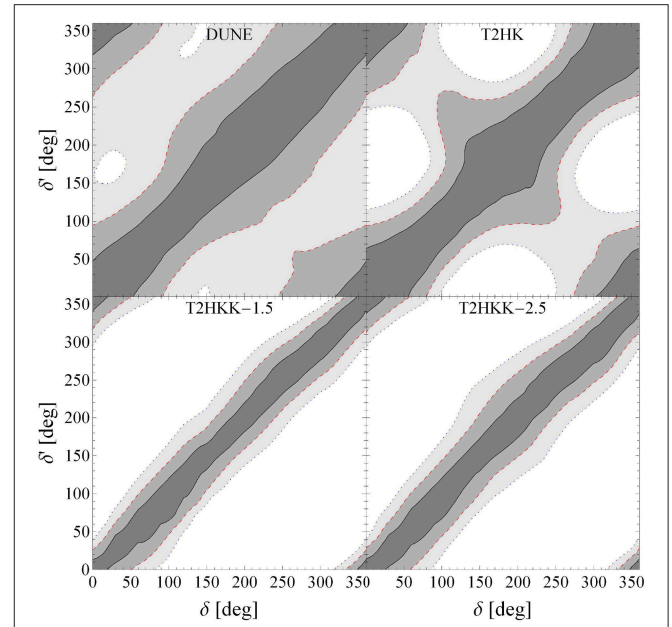
as Daya Bay satisfy the first condition and resolve the terms proportional to s_{13}^2, but cannot overcome the second challenge because at these experiments, $\Delta_{12} \ll 1$. At KamLAND, $\Delta_{12} > 1$ but the statistics was too low to resolve the s_{13}^2 terms. JUNO and RENO-50, being designed to be sensitive to these terms to determine $\text{sign}(\Delta m_{31}^2)$, can overcome all these three challenges. The detectors at JUNO and RENO-50 experiments will employ liquid scintillator technique with an impressive energy resolution of

$$\frac{\delta E_\nu}{E_\nu} \simeq 3\% \times \left(\frac{E_\nu}{\text{MeV}}\right)^{1/2}.$$

Moreover, the energy calibration error can be as low as 3%. Using the GLoBES software [228, 229], Bakhti and Farzan [19] shows how JUNO and RENO-50 experiments can test LMA-Dark solution with $\theta_{12} > \frac{\pi}{4}$. Results are shown in **Figures 15**, **16**. The star denotes the true value of Δm_{31}^2 and θ_{12}. In **Figures 15**, **16**, normal and inverted mass orderings are respectively assumed. Ellipses show 3σ C.L. contours, after 5 years of data taking. As seen from these figures, these upcoming experiments will be able to determine $|\Delta m_{31}^2|$ with much better accuracy than the present global data analysis so no prior on $|\Delta m_{31}^2|$ is assumed. The uncertainties of other relevant
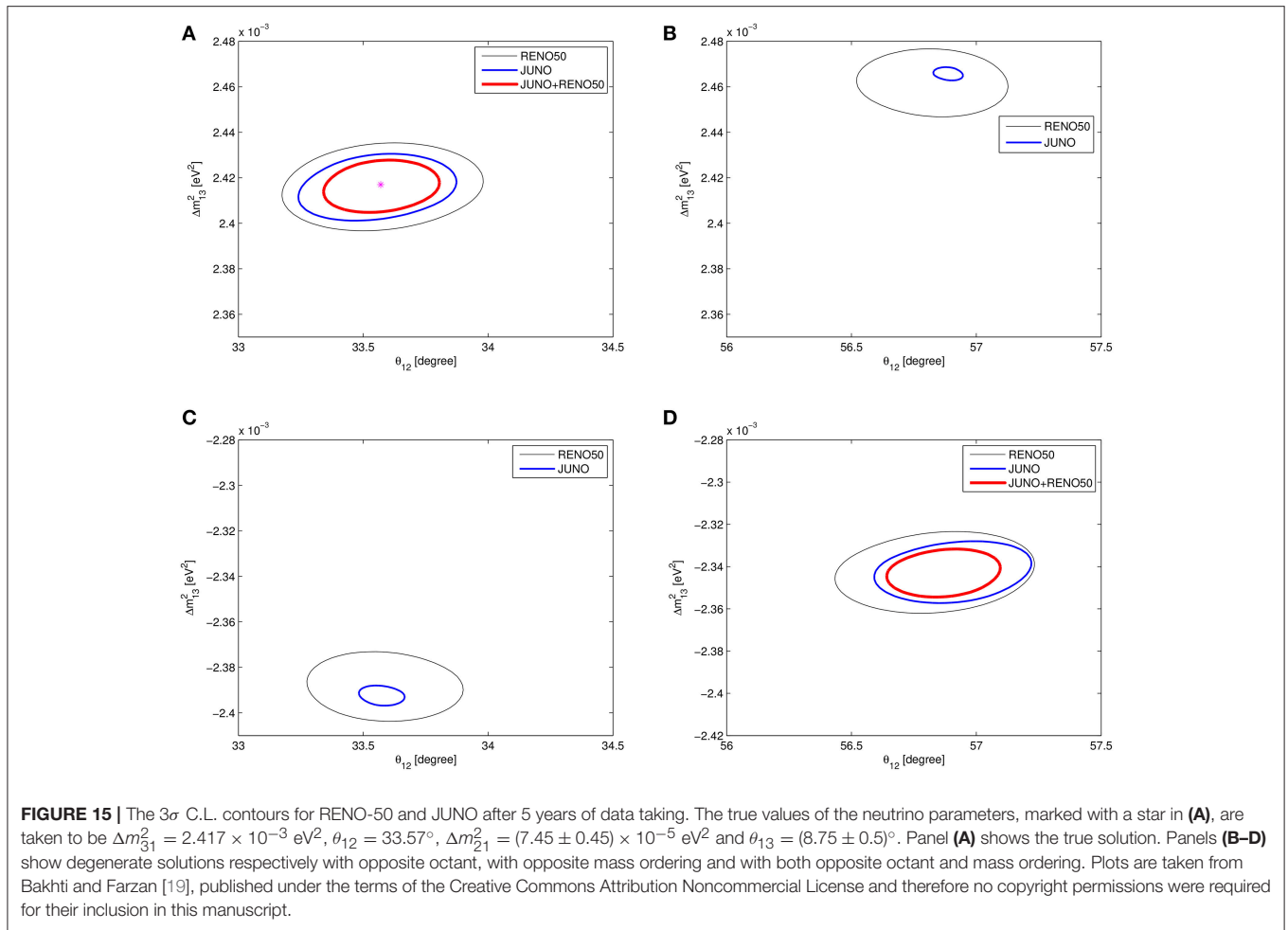
neutrino parameters are taken from [230] and are treated by pull-method.

For JUNO experiment, the uncertainties in the flux normalization and the initial energy spectrum at the source are taken respectively equal to 5 and 3%. RENO-50 enjoys having a near detector (the detectors of present RENO) which can measure the flux with down to O(0.3%) uncertainty. To perform the analysis, the energy range of 1.8–8 MeV is divided to 350 bins of 17.7 keV size. The pull-method is applied by defining

$$\chi^2 = \text{Min}|_{\theta_{pull},\alpha_i} \left[\sum_i \frac{[N_i(\theta_0, \bar{\theta}_{pull}) - N_i(\theta, \theta_{pull})(1 + \alpha_i)]^2}{N_i(\theta_0, \bar{\theta}_{pull})} \right.$$
$$\left. + \sum_i \frac{\alpha_i^2}{(\Delta \alpha_i)^2} + \frac{(\theta_{pull} - \bar{\theta}_{pull})^2}{(\Delta \theta_{pull})^2} \right], \qquad (58)$$

where N_i is the number of events at bin i. α_i is the pull parameter that accounts for the uncertainty in the initial spectrum at bin i. Pull parameters taking care of the other uncertainties are collectively denoted by θ_{pull}.

As seen from these figures, JUNO and RENO-50 can determine the octant of θ_{12} for a given mass ordering. This result is relatively robust against varying the calibration error but as expected, is extremely sensitive to the energy resolution. Increasing the uncertainty in energy resolution from 3 to 3.5%, Bakhti and Farzan [19] finds that JUNO and RENO-50 cannot determine the octant at 3σ C.L. after five years. As seen from the figures, JUNO and RENO-50 experiments cannot distinguish two solutions which are related to each other with

FIGURE 15 | The 3σ C.L. contours for RENO-50 and JUNO after 5 years of data taking. The true values of the neutrino parameters, marked with a star in **(A)**, are taken to be $\Delta m_{31}^2 = 2.417 \times 10^{-3}$ eV^2, $\theta_{12} = 33.57°$, $\Delta m_{21}^2 = (7.45 \pm 0.45) \times 10^{-5}$ eV^2 and $\theta_{13} = (8.75 \pm 0.5)°$. Panel **(A)** shows the true solution. Panels **(B–D)** show degenerate solutions respectively with opposite octant, with opposite mass ordering and with both opposite octant and mass ordering. Plots are taken from Bakhti and Farzan [19], published under the terms of the Creative Commons Attribution Noncommercial License and therefore no copyright permissions were required for their inclusion in this manuscript.

$\theta_{12} \leftrightarrow \pi/2 - \theta_{12}$ and $\Delta m_{31}^2 \rightarrow -\Delta m_{31}^2 + \Delta m_{21}^2$ which stems from the generalized mass ordering degeneracy that we discussed in section 5.1.

5.3. NSI at the MOMENT

The MOMENT experiment is a setup which has been proposed to measure the value of CP-violating phase, δ [231, 232]. MOMENT stands for MuOn-decay MEdium baseline NeuTrino beam. This experiment will be located in China. The neutrino beam in this experiment is provided by the muon decay. Beam can switch between muon decay ($\mu \rightarrow e\bar{\nu}_e\nu_\mu$) and antimuon decay ($\bar{\mu} \rightarrow e^+\nu_e\bar{\nu}_\mu$). The energies of neutrinos will be relatively low with a maximum energy at 700 MeV and peak energy at 150 MeV. The detector is going to be Gd doped water Cherenkov with fiducial mass of 500 kton, located at a distance of 150 km from the source. The detection modes are

$$\nu_e + n \rightarrow p + e^- \quad \bar{\nu}_\mu + n \rightarrow p + \mu^+$$
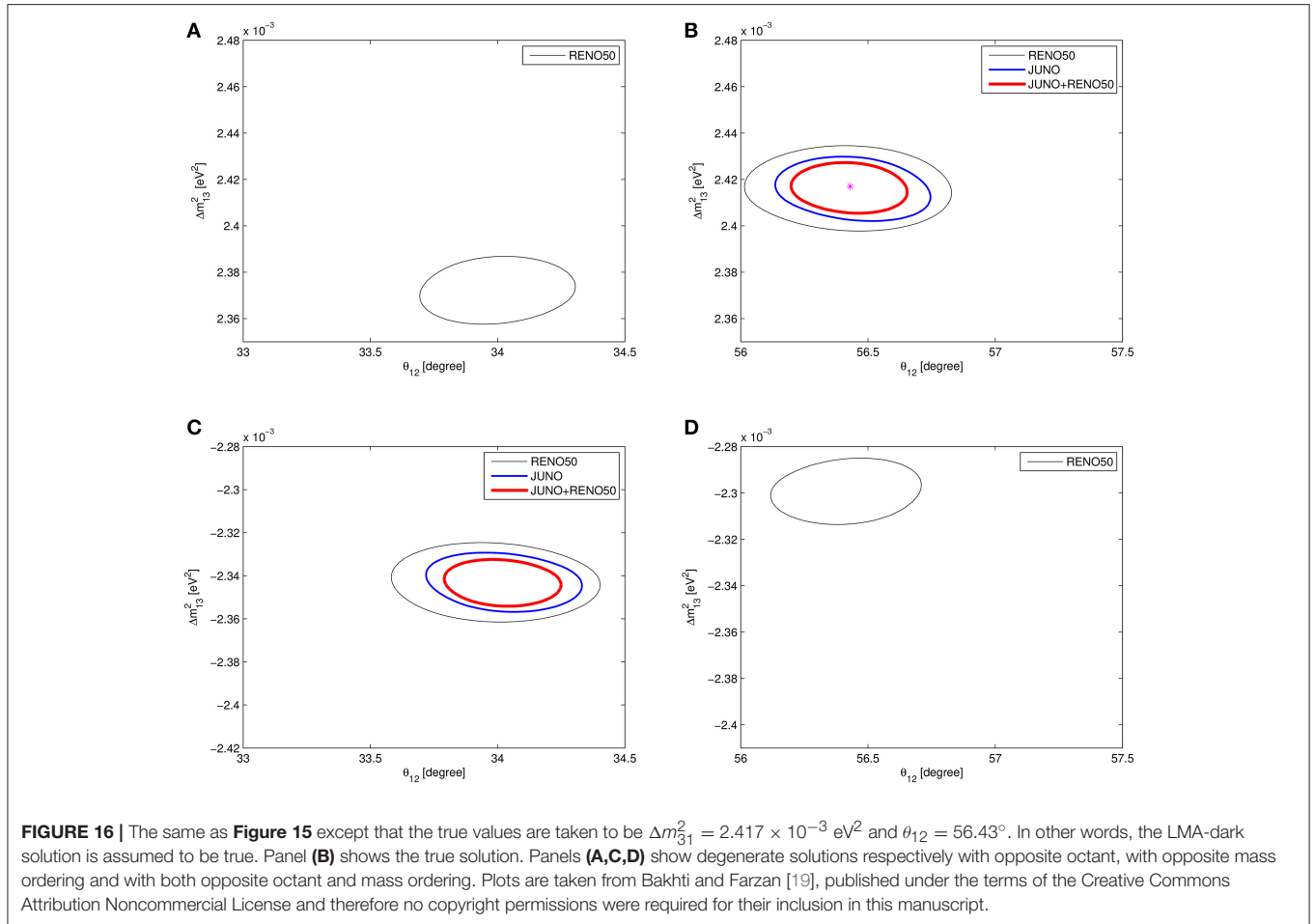
and

$$\bar{\nu}_e + n \rightarrow p + e^+ \quad \nu_\mu + n \rightarrow p + \mu^-.$$

Gd at the detector can capture the final neutron so although the detector lacks magnetic field, it can distinguish between

neutrino and antineutrino with Charge Identification (CI) of 80% [233]. The MOMENT experiment, with a baseline of 150 km and relatively low energy is not very sensitive to matter effects so it enjoys an ideal setup to determine δ and octant of θ_{23} without ambiguity induced by degeneracies with NSI. The potential of this experiment for determining δ and the octant of θ_{23} is studied in Bakhti and Farzan [234] using GLoBES [228, 229]. The unoscillated flux of each neutrino mode is taken to be 4.7×10^{11}m^{-2}year^{-1} and 5 years of data taking in each muon and antimuon modes is assumed. Uncertainties in flux normalization of $\bar{\nu}_e$ and ν_μ modes are taken to be correlated and equal to 5% but the uncertainties of fluxes from muon and antimuon modes are uncorrelated.

One of the main sources of background is atmospheric neutrinos. Since the neutrino beam at the MOMENT experiment will be sent in bunches, this source of background can be dramatically reduced. Reduction of background is parameterized by Suppression Factor (SF). Results of Bakhti and Farzan [234] are shown in **Figure 17**. The assumed true value of δ and θ_{23} are shown with a star. The mass ordering is taken to be normal and assumed to be known. All the appearance and disappearance modes are taken into account. In all these figures, the true values of ϵ are taken to be zero. In **Figures 17B–D**, pull method is

FIGURE 16 | The same as **Figure 15** except that the true values are taken to be $\Delta m_{31}^2 = 2.417 \times 10^{-3}$ eV^2 and $\theta_{12} = 56.43°$. In other words, the LMA-dark solution is assumed to be true. Panel **(B)** shows the true solution. Panels **(A,C,D)** show degenerate solutions respectively with opposite octant, with opposite mass ordering and with both opposite octant and mass ordering. Plots are taken from Bakhti and Farzan [19], published under the terms of the Creative Commons Attribution Noncommercial License and therefore no copyright permissions were required for their inclusion in this manuscript.

applied on $\epsilon = \sum_f (N^f/N_e)\epsilon^f$, taking 1σ uncertainties on ϵ as follows [11]

$$|\epsilon_{e\mu}| < 0.16, \; |\epsilon_{e\tau}| < 0.26 \text{ and } |\epsilon_{\mu\tau}| < 0.02 \qquad (59)$$

and

$$-0.018 < \epsilon_{\tau\tau} - \epsilon_{\mu\mu} < 0.054 \text{ and } 0.35 < \epsilon_{ee} - \epsilon_{\mu\mu} < 0.93. \quad (60)$$
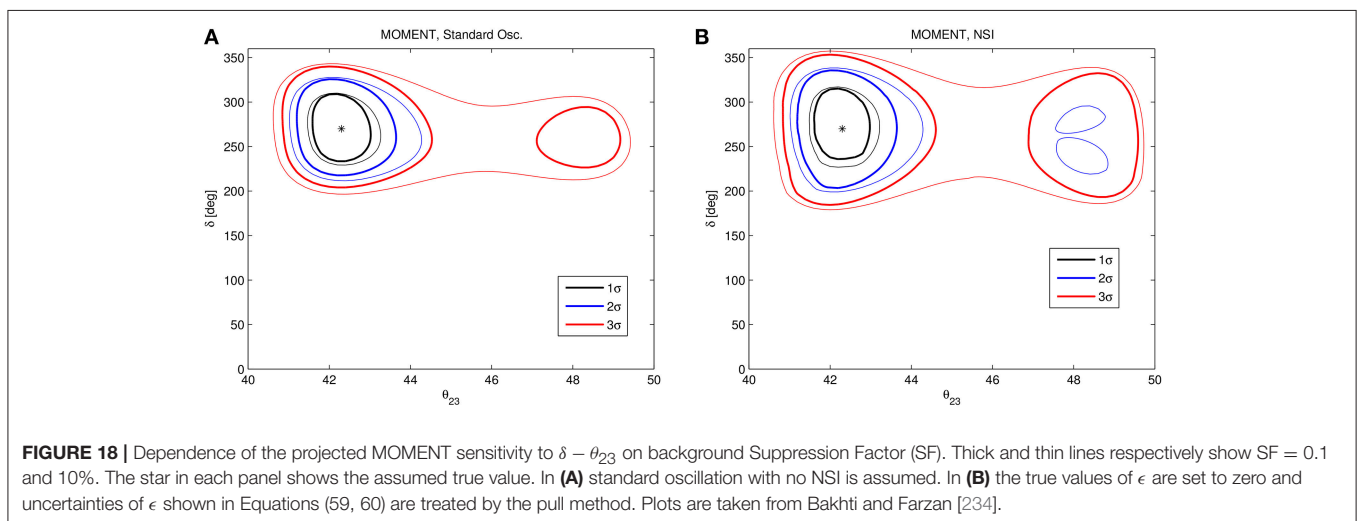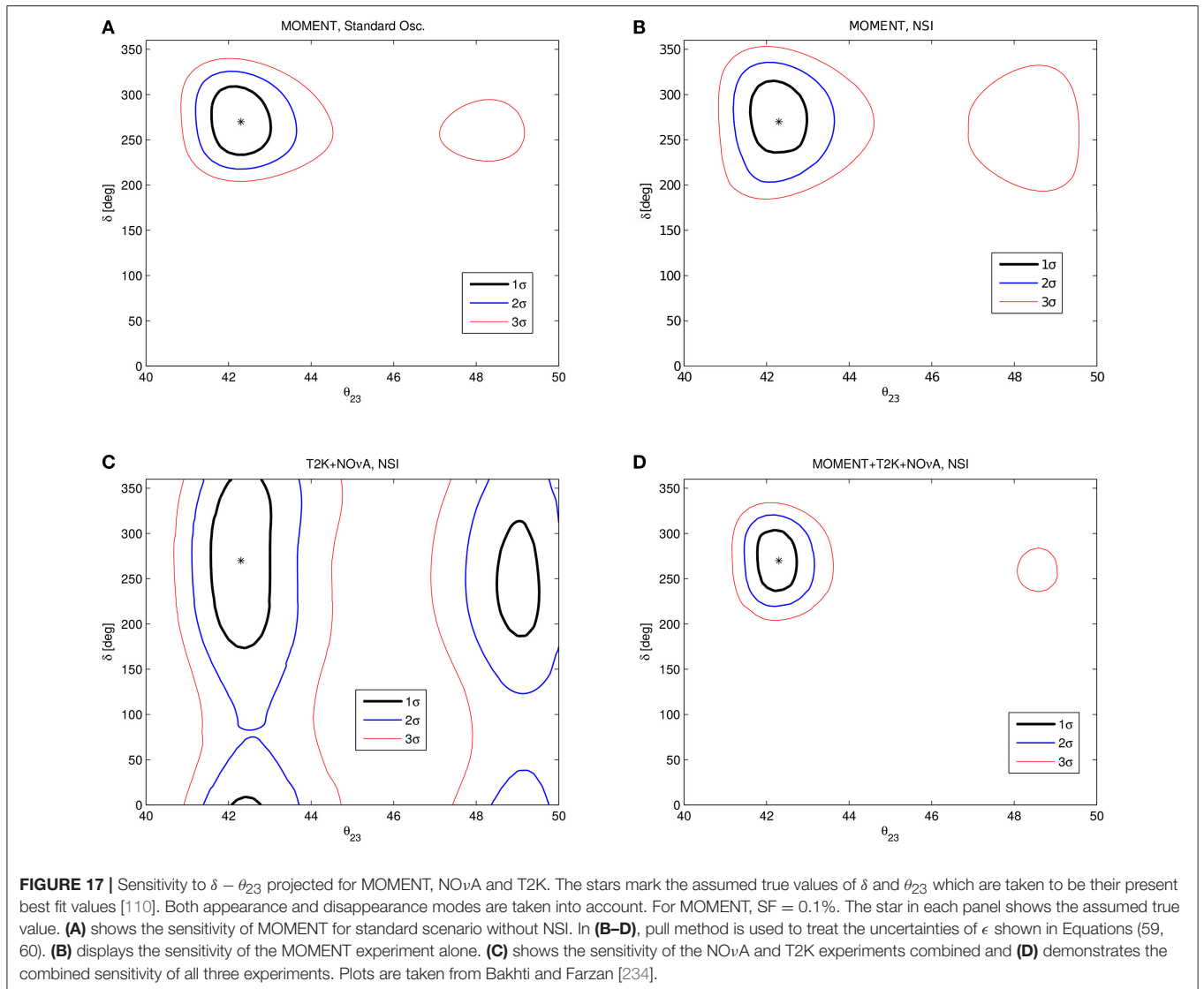
Results shown in **Figures 17C,D** assume that T2K (NOνA) takes data in neutrino mode for 2 (3) years and in antineutrino mode for 6 (3) years. For more details on the assumptions, see Bakhti and Farzan [234]. As seen from **Figure 17B**, turning on NSI, NOνA and T2K (even combined) cannot establish CP-violation even at $1\,\sigma$ C.L.: while the true value of δ is taken to be $270°$ (maximal CP-violation), $\delta = 0, 360°$ (CP-conserving) is within the $1\,\sigma$ C.L. contour. At 3σ C.L., these experiments cannot determine the octant of θ_{23}. Moreover, in the presence of NSI, these experiments cannot rule out the wrong octant even at $1\,\sigma$ C.L. But, comparing **Figure 17A** and **Figure 17B**, we observe that turning on NSI within range (59,60) does not considerably reduce the power of MOMENT to measure the CP-violating phase and rule out the wrong octant solution. In this figure, SF is taken to be 0.1% which is rather an optimistic

assumption. **Figure 18** shows that increasing SF up to 10%, the power of octant determination is significantly reduced but the determination of δ is not dramatically affected.

Similar result holds valid when instead of normal mass ordering, inverted mass ordering is taken (and again assumed that the ordering is known) [234]. Bakhti and Farzan [232] shows that the MOMENT experiment itself can determine the mass ordering. According to Bakhti and Farzan [234], as long as ϵ can vary in the range shown in Equations (59, 60), MOMENT maintains its power to determine the mass ordering. Of course, once we allow ϵ to vary in a wide range such that transformation in Equation (56) can be made, the power of mass ordering determination is lost due to the generalized mass ordering degeneracy.

6. SUMMARY

After multiple decades of experimental progress in the area of neutrino physics, the phenomenon of neutrino oscillations has been observed in a wide variety of experiments. The discovery of neutrino oscillations implies the existence of neutrino masses and therefore a need for an extension of the SM to include them. Many possibilities have been proposed so far, see for instance

FIGURE 17 | Sensitivity to $\delta - \theta_{23}$ projected for MOMENT, NOνA and T2K. The stars mark the assumed true values of δ and θ_{23} which are taken to be their present best fit values [110]. Both appearance and disappearance modes are taken into account. For MOMENT, SF = 0.1%. The star in each panel shows the assumed true value. **(A)** shows the sensitivity of MOMENT for standard scenario without NSI. In **(B–D)**, pull method is used to treat the uncertainties of ϵ shown in Equations (59, 60). **(B)** displays the sensitivity of the MOMENT experiment alone. **(C)** shows the sensitivity of the NOνA and T2K experiments combined and **(D)** demonstrates the combined sensitivity of all three experiments. Plots are taken from Bakhti and Farzan [234].

FIGURE 18 | Dependence of the projected MOMENT sensitivity to $\delta - \theta_{23}$ on background Suppression Factor (SF). Thick and thin lines respectively show SF = 0.1 and 10%. The star in each panel shows the assumed true value. In **(A)** standard oscillation with no NSI is assumed. In **(B)** the true values of ϵ are set to zero and uncertainties of ϵ shown in Equations (59, 60) are treated by the pull method. Plots are taken from Bakhti and Farzan [234].

King [235], Hirsch and Valle [236], Boucenna et al. [237], and Cai et al. [238]. Motivated by the two original *anomalies* in the solar and atmospheric neutrino sector, various other experiments have been proposed to search for neutrino oscillations in the solar and atmospheric neutrino flux as well as in man-made neutrino beams such as reactors or accelerators. The large amount of experimental data collected over more than 20 years has allowed a very precise determination of some of the parameters responsible for the oscillations. These include the solar mass splitting, Δm_{21}^2, the absolute value of the atmospheric mass splitting, $|\Delta m_{31}^2|$, as well as the solar (θ_{12}) and reactor (θ_{13}) mixing angles, measured with relative accuracies below 5%. Nevertheless, the current precision of atmospheric angle θ_{23} and the CP phase δ is not at that level. The sign of $\cos(2\theta_{23})$ or in other words the octant of θ_{23} is yet unknown. Moreover, although there are some hints for CP phase (δ) to be close to $3\pi/2$, its value is not yet established. The sign of Δm_{31}^2 or equivalently the scheme of mass ordering (normal vs. inverted) is also still unknown. In section 2, we have discussed the most relevant experimental information used in the global fits of neutrino oscillations [39–41] to obtain precise measurements of the oscillation parameters, exploiting the complementarity of the different data sets. The main results of these analysis have also been commented, with an emphasis on the still unknown parameters.

Since their discovery, neutrinos have always surprised us by showing unexpected characteristics. In the dawn of the neutrino precision era, it is intriguing to ask whether neutrinos have new interactions beyond those expected within the standard model of particles. Such new interactions can give a signal in different neutrino oscillation as well as non-oscillation experiments. No evidence for the presence of NSI has been reported so far. As a consequence of these negative searches, upper bounds on the magnitude of the new interactions can be set. In section 3, we have discussed the constraints on the NSI interactions, parameterized in terms of the $\epsilon_{\alpha\beta}$ couplings introduced in Equations (15) and (16). The presence of NSI has been extensively analyzed in the literature, at the level of the production, detection and propagation of neutrinos in matter. The most restrictive limits on NSI are summarized in **Tables 2–4**.

In principle, adding any new particle which couples both to neutrinos and to quarks will induce Non-Standard Interaction (NSI) for neutrinos. However, it is very challenging to build an electroweak symmetric model that leads to large enough NSI to be discernible at neutrino oscillation experiments without violating various bounds. We have discussed a class of models in which the new particle responsible for NSI is a light $U(1)'$ gauge boson Z' with mass 5 MeV − few 10 MeV with a coupling of order of $10^{-5} - 10^{-4}$ to quarks and neutrinos. Within this range of parameter space, the NSI effective coupling can be as large as the standard effective Fermi coupling, G_F.

The total flux of solar neutrino has been measured by SNO experiment via dissociation of Deuteron through axial part of neutral current interaction and has been found to be consistent with the standard model prediction. To avoid a deviation from this prediction, the coupling of quarks to the new gauge boson is taken to be non-chiral with equal $U(1)'$ charges for left-handed

and right-handed quarks. Moreover, the $U(1)'$ charges of up and down quarks are taken to be equal to make the charged current weak interaction term invariant under $U(1)'$. The $U(1)'$ charges of quarks is taken to be universal; otherwise, in the mass basis of quarks, we would have off-diagonal interactions leading to huge $q_i \rightarrow q_j Z'$ rate enhanced by $(m_{q_i}/m_{Z'})^2$. In summary, $U(1)'$ charges of quarks is taken to be proportional to their baryon number. We have discussed two different scenarios for $U(1)'$ charge assignment to leptons: (i) assigning $U(1)'$ charge to the SM fermion as $a_e L_e + a_\mu L_\mu + a_\tau L_\tau + B$ where L_α denotes lepton flavor α and B denotes Baryon number. With this assignment, lepton flavor will be preserved and both charged leptons and neutrinos obtain lepton flavor conserving NSI. A particularly interesting scenario is $a_e = 0$, $a_\mu = a_\tau = -3/2$ for which gauge symmetry anomalies automatically cancel without a need to add new specious. Choosing appropriate value of coupling [i.e., $4 \times 10^{-5}(m_{Z'}/10 \text{ MeV})$], the best fit to solar neutrino data with $\epsilon_{\mu\mu} - \epsilon_{ee} = \epsilon_{\tau\tau} - \epsilon_{ee} = -0.3$ can be reproduced. (ii) In the second scenario, the leptons are not charged under $U(1)'$. A new Dirac fermion, denoted by Ψ, with a mass of 1 GeV which is singlet under SM gauge group but charged under $U(1)'$ is introduced which mixes with neutrinos. As a result, neutrinos obtain coupling to Z' through mixing with the new fermion but charged leptons do not couple to Z' at the tree level. If the new fermion mixes with more than one flavor, both LFV and LFC NSI will be induced. Within this scenario, new fermions are needed to cancel the gauge anomalies. We have discussed different possibilities. To give masses to these new fermions, new scalars charged under $U(1)'$ are required whose VEV also gives a significant contribution to the mass of Z' boson.

We have suggested two mechanisms for inducing a mixing between Ψ and neutrinos: (1) Introducing a new Higgs doublet, H', with $U(1)'$ charge equal to that of Ψ which couples to left-handed lepton doublets and Ψ. H' obtains a VEV of few MeV which induces mixing. (2) Introducing a sterile neutrino, N (singlet both under SM gauge group and $U(1)'$) and a new scalar singlet with a $U(1)'$ charge equal to that of Ψ which couples to N and Ψ. Its VEV then induces the coupling.

Even though the mass of Z' particle is taken to be low (i.e., of order of solar neutrino energies and much smaller than the typical energies of atmospheric neutrinos or the energies of the neutrinos of long baseline experiments), the effect of new interaction on propagation of neutrinos in matter can be described by an effective four-Fermi Lagrangian integrating out Z' because at forward scattering of neutrinos off the background matter, the energy momentum transfer is zero. At high energy scattering experiments, such as NuTeV and CHARM, the energy momentum transfer, q^2, is much higher than $m_{Z'}^2$ so the effective four-Fermi coupling loses its viability. The amplitude of new effects will be suppressed by a factor of $\epsilon m_{Z'}^2/q^2 \ll 1$ relative to SM amplitude and will be negligible. Thus, unlike the case that the intermediate state responsible for NSI is heavy, these experiments cannot constrain $\epsilon \sim 1$. However, by studying scattering of low energy neutrinos ($E_\nu \sim$ few 10 MeV) off matter, these models can be tested. The current COHERENT experiment

and the upcoming CONUS experiment[13] are ideal set-ups to eventually test this model. An alternative way to test such models is to search for a dip in the energy spectrum of high energy cosmic neutrinos around few hundred TeV.

AUTHOR CONTRIBUTIONS

MT has contributed mainly to review the current status of neutrino oscillations as well as the current status of bounds on non-standard neutrino interactions. YF has contributed mainly to the review of models giving rise to sizeable non-standard neutrino interactions and the review of non-standard interaction searches at upcoming experiments.

---

[13]https://indico.cern.ch/event/606690/contributions/2591545/attachments/1499330/2336272/Taup2017_CONUS_talk_JHakenmueller.pdf.

REFERENCES

1. Davis R Jr, Harmer DS, Hoffman KC. Search for neutrinos from the sun. *Phys Rev Lett.* (1968) **20**:1205–9. doi: 10.1103/PhysRevLett.20.1205

2. Fukuda Y, et al. Evidence for oscillation of atmospheric neutrinos. *Phys Rev Lett.* (1998) **81**:1562–67. doi: 10.1103/PhysRevLett.81.1562

3. Abe Y, et al. Indication of reactor $\bar{\nu}_e$ disappearance in the double chooz experiment. *Phys Rev Lett.* (2012) **108**:131801. doi: 10.1103/PhysRevLett.108.131801

4. An FP, Bai JZ, Balantekin AB, Band HR, Beavis D, Beriguete M, et al. Observation of electron-antineutrino disappearance at Daya Bay. *Phys Rev Lett.* (2012) **108**:171803. doi: 10.1103/PhysRevLett.108.171803

5. Ahn JK, et al. Observation of reactor electron antineutrino disappearance in the RENO experiment. *Phys Rev Lett.* (2012) **108**:191802. doi: 10.1103/PhysRevLett.108.191802

6. Aliu E, et al. Evidence for muon neutrino oscillation in an accelerator-based experiment. *Phys Rev Lett.* (2005) **94**:081802. doi: 10.1103/PhysRevLett.94.081802

7. Michael DG, et al. Observation of muon neutrino disappearance with the MINOS detectors and the NuMI neutrino beam. *Phys Rev Lett.* (2006) **97**:191801. doi: 10.1103/PhysRevLett.97.191801

8. Smirnov AY. Solar neutrinos: oscillations or No-oscillations? arXiv:1609.02386.

9. Miranda OG, Tórtola MA, Valle JWF. Are solar neutrino oscillations robust? *J High Energy Phys.* (2006) **10**:008. doi: 10.1088/1126-6708/2006/10/008

10. Escrihuela FJ, Miranda OG, Tórtola MA, Valle JWF. Constraining nonstandard neutrino-quark interactions with solar, reactor and accelerator data. *Phys Rev D* (2009) **80**:105009. doi: 10.1103/PhysRevD.80.105009

11. Gonzalez-Garcia MC, Maltoni M. Determination of matter potential from global analysis of neutrino oscillation data. *J High Energy Phys.* (2013) **9**:152. doi: 10.1007/JHEP09(2013)152

12. Leitner R, Malinsky M, Roskovec B, Zhang H. Non-standard antineutrino interactions at Daya Bay. *J High Energy Phys.* (2011) **12**:001. doi: 10.1007/JHEP12(2011)001

13. Agarwalla SK, Bagchi P, Forero DV, Tórtola M. Probing non-standard interactions at daya bay. *J High Energy Phys.* (2015) **7**:60. doi: 10.1007/JHEP07(2015)060

14. Forero DV, Huber P. Hints for leptonic CP violation or New Physics? *Phys Rev Lett.* (2016) **117**:031801. doi: 10.1103/PhysRevLett.117.031801

15. Masud M, Chatterjee A, Mehta P. Probing CP violation signal at DUNE in presence of non-standard neutrino interactions. *J Phys G* (2016) **43**:095005. doi: 10.1088/0954-3899/43/9/095005

16. Masud M, Mehta P. Nonstandard interactions spoiling the CP violation sensitivity at DUNE and other long baseline experiments. *Phys Rev D* (2016) **94**:013014. doi: 10.1103/PhysRevD.94.013014

17. Liao J, Marfatia D, Whisnant K. Degeneracies in long-baseline neutrino experiments from nonstandard interactions. *Phys Rev D* (2016) **93**:093016. doi: 10.1103/PhysRevD.93.093016

18. Agarwalla SK, Chatterjee SS, Palazzo A. Degeneracy between θ_{23} octant and neutrino non-standard interactions at DUNE. *Phys Lett B* (2016) **762**:64–71. doi: 10.1016/j.physletb.2016.09.020

19. Bakhti P, Farzan Y. Shedding light on LMA-Dark solar neutrino solution by medium baseline reactor experiments: JUNO and RENO-50. *J High Energy Phys.* (2014) **7**:64. doi: 10.1007/JHEP07(2014)064

20. Aaboud M, Aad G, Abbott B, Abdinov O, Abeloos B, Abidi SH, et al. Search for new high-mass phenomena in the dilepton final state using 36 fb^{-1} of proton-proton collision data at $\sqrt{s} = 13$ TeV with the ATLAS detector. *J High Energy Phys.* (2017) **2017**:182. doi: 10.1007/JHEP10(2017)182

21. Buarque Franzosi D, Frandsen MT, Shoemaker IM. New or ν missing energy: discriminating dark matter from neutrino interactions at the LHC. *Phys Rev D* (2016) **93**:095001. doi: 10.1103/PhysRevD.93.095001

22. Berezhiani Z, Rossi A. Limits on the nonstandard interactions of neutrinos from e+ e− colliders. *Phys Lett B* (2002) **535**:207–18. doi: 10.1016/S0370-2693(02)01767-7

23. Friedland A, Graesser ML, Shoemaker IM, Vecchi L. Probing nonstandard standard model backgrounds with LHC monojets. *Phys Lett B* (2012) **714**:267–75. doi: 10.1016/j.physletb.2012.06.078

24. Farzan Y. A model for large non-standard interactions of neutrinos leading to the LMA-Dark solution. *Phys Lett B* (2015) **748**:311–5. doi: 10.1016/j.physletb.2015.07.015

25. Farzan Y, Heeck J. Neutrinophilic nonstandard interactions. *Phys Rev D* (2016) **94**:053010. doi: 10.1103/PhysRevD.94.053010

26. Farzan Y, Shoemaker IM. Lepton flavor violating non-standard interactions via light mediators. *J High Energy Phys.* (2016) **7**:33. doi: 10.1007/JHEP07(2016)033

27. Vanegas Forero D. *(Non)standard oscillations at current facilities.* PoSNOW2016:16 (2017).

28. Bakhti P, Khan AN, Wang W. Sensitivities to charged-current nonstandard neutrino interactions at DUNE. *J Phys G Nucl Part Phys.* (2017) **44**:125001. doi: 10.1088/1361-6471/aa9098

29. Khan AN, Tahir F. Nonstandard interactions and interference effect in low energy $\nu_e e$-scattering process. arXiv:1101.3191.

30. Kopp J, Machado PAN, Parke SJ. Interpretation of MINOS data in terms of non-standard neutrino interactions. *Phys Rev D* (2010) **82**:113002. doi: 10.1103/PhysRevD.82.113002

31. Bellazzini B, Grossman Y, Nachshon I, Paradisi P. Non-standard neutrino interactions at one loop. *J High Energy Phys.* (2011) **6**:104. doi: 10.1007/JHEP06(2011)104

32. Akhmedov E, Schwetz T. MiniBooNE and LSND data: non-standard neutrino interactions in a (3+1) scheme versus (3+2) oscillations. *J High Energy Phys.* (2010) **10**:115. doi: 10.1007/JHEP10(2010)115

33. Biggio C, Blennow M, Fernandez-Martinez E. General bounds on non-standard neutrino interactions. *J High Energy Phys.* (2009) **8**:90. doi: 10.1088/1126-6708/2009/08/090

34. Das A, Dighe A, Sen M. New effects of non-standard self-interactions of neutrinos in a supernova. *J Cosmol Astropart Phys.* (2017) **2017**:51. doi: 10.1088/1475-7516/2017/05/051

35. Dighe A, Sen M. Nonstandard neutrino self-interactions in a supernova and fast flavor conversions. *Phys Rev D* (2018) **97**:043011. doi: 10.1103/PhysRevD.97.043011

36. de Salas PF, Lineros RA, Tórtola M. Neutrino propagation in the galactic dark matter halo. *Phys Rev D* (2016) **94**:123001. doi: 10.1103/PhysRevD.94.123001

37. Brdar V, Kopp J, Liu J, Prass P, Wang X-P. Fuzzy dark matter and nonstandard neutrino interactions. *Phys Rev D* (2018) **97**:043001. doi: 10.1103/PhysRevD.97.043001

38. Mangano G, Miele G, Pastor S, Pinto T, Pisanti O, Serpico PD. Effects of non-standard neutrino-electron interactions on relic neutrino decoupling. *Nucl Phys B* (2006) **756**:100–16. doi: 10.1016/j.nuclphysb.2006.09.002

39. de Salas PF, Forero DV, Ternes CA, Tórtola M, Valle JW. Status of neutrino oscillations 2017. arXiv:1708.01186.

40. Capozzi F, Di Valentino E, Lisi E, Marrone A, Melchiorri A, Palazzo A. Global constraints on absolute neutrino masses and their ordering. *Phys Rev D* (2017) **95**:096014. doi: 10.1103/PhysRevD.95.096014

41. Esteban I, Gonzalez-Garcia MC, Maltoni M, Martinez-Soler I, Schwetz T. Updated fit to three neutrino mixing: exploring the accelerator-reactor complementarity. *J High Energy Phys.* (2017) **1**:87. doi: 10.1007/JHEP01(2017)087

42. Cleveland BT, Daily T, Davis R, Distel JR Jr, Lande K, Lee CK, et al. Measurement of the solar electron neutrino flux with the Homestake chlorine detector. *Astrophys J.* (1998) **496**:505–26. doi: 10.1086/305343

43. Kaether F, Hampel W, Heusser G, Kiko J, Kirsten T. Reanalysis of the GALLEX solar neutrino flux and source experiments. *Phys Lett B* (2010) **685**:47–54. doi: 10.1016/j.physletb.2010.01.030

44. Abdurashitov JN, Gavrin VN, Gorbachev VV, Gurkina PP, Ibragimova TV, Kalikhov AV, et al. Measurement of the solar neutrino capture rate with gallium metal. III: results for the 2002–2007 data-taking period. *Phys Rev C* (2009) **80**:015807. doi: 10.1103/PhysRevC.80.015807

45. Hirata KS, et al. Real time, directional measurement of B-8 solar neutrinos in the Kamiokande-II detector. *Phys Rev D* (1991) **44**:2241.

46. Hosaka J, et al. Solar neutrino measurements in super-Kamiokande-I. *Phys Rev D* (2006) **73**:112001. doi: 10.1103/PhysRevD.73.112001

47. Cravens JP, et al. Solar neutrino measurements in Super-Kamiokande-II. *Phys Rev D* (2008) **78**:032002. doi: 10.1103/PhysRevD.78.032002

48. Abe K, et al. Solar neutrino results in Super-Kamiokande-III. *Phys Rev D* (2011) **83**:052010.

49. Nakano Y. *PhD Thesis, University of Tokyo*. Available online at: http://www-sk.icrr.u-tokyo.ac.jp/sk/_pdf/articles/2016/doc_thesis_naknao.pdf (2016).

50. Abe K, et al. Solar neutrino measurements in super-kamiokande-IV. *Phys Rev D* (2016) **94**:052010. doi: 10.1103/PhysRevD.94.052010

51. Nakano Y. *Solar Neutrino Results from Super-Kamiokande*. Available online at: https://indico.cern.ch/event/432527/contributions/1072129/attachments/1319706/1979670/ichep2016_nakano_ver5.pdf (2016).

52. Wolfenstein L. Neutrino oscillations in matter. *Phys Rev D* (1978) **17**:2369–74. doi: 10.1103/PhysRevD.17.2369

53. Mikheev SP, Smirnov AY. Resonance amplification of oscillations in matter and spectroscopy of solar neutrinos. *Sov J Nucl Phys.* (1985) **42**:913–7.

54. Aharmim B, et al. An independent measurement of the total active B-8 solar neutrino flux using an array of He-3 proportional counters at the sudbury neutrino observatory. *Phys Rev Lett.* (2008) **101**:111301. doi: 10.1103/PhysRevLett.101.111301

55. Aharmim B, et al. Low energy threshold analysis of the phase I and phase II data sets of the sudbury neutrino observatory. *Phys Rev C* (2010) **81**:055504. doi: 10.1103/PhysRevC.81.055504

56. Bellini G, et al. Final results of Borexino Phase-I on low energy solar neutrino spectroscopy. *Phys Rev D* (2014) **89**:112007. doi: 10.1103/PhysRevD.89.112007

57. Bellini G, et al. Measurement of the solar 8B neutrino rate with a liquid scintillator target and 3 MeV energy threshold in the Borexino detector. *Phys Rev D* (2010) **82**:033006. doi: 10.1103/PhysRevD.82.033006

58. Bellini G, et al. Neutrinos from the primary proton–proton fusion process in the Sun. *Nature* (2014) **512**:383–6. doi: 10.1038/nature13702

59. Bahcall J. *J. Bahcall homepage*. Available online at: http://www.sns.ias.edu/~jnb/

60. Serenelli A, Basu S, Ferguson JW, Asplund M. New solar composition: the problem with solar models revisited. *Astrophys J.* (2009) **705**:L123–7. doi: 10.1088/0004-637X/705/2/L123

61. Vinyoles N, Serenelli AM, Villante FL, Basu S, Bergström J, Gonzalez-Garcia MC, et al. A new generation of standard solar models. *Astrophys J.* (2017) **835**:202. doi: 10.3847/1538-4357/835/2/202

62. Schwetz T, Tórtola MA, Valle JWF. Three-flavour neutrino oscillation update. *New J Phys.* (2008) **10**:113011. doi: 10.1088/1367-2630/10/11/113011

63. Eguchi K, et al. First results from KamLAND: evidence for reactor anti-neutrino disappearance. *Phys Rev Lett.* (2003) **90**:021802. doi: 10.1103/PhysRevLett.90.021802

64. Gando A, et al. Constraints on θ_{13} from a three-flavor oscillation analysis of reactor antineutrinos at KamLAND. *Phys Rev D* (2011) **83**:052002. doi: 10.1103/PhysRevD.83.052002

65. Apollonio M, et al. Search for neutrino oscillations on a long baseline at the CHOOZ nuclear power station. *Eur Phys J C* (2003) **27**:331–74. doi: 10.1140/epjc/s2002-01127-9

66. Piepke A. Final results from the Palo Verde neutrino oscillation experiment. *Prog Part Nucl Phys.* (2002) **48**:113–21. doi: 10.1016/S0146-6410(02)00117-5

67. Fogli GL, Lisi E, Marrone A, Palazzo A, Rotunno AM. Hints of $\theta_{13} > 0$ from global neutrino data analysis. *Phys Rev Lett.* (2008) **101**:141801. doi: 10.1103/PhysRevLett.101.141801

68. Maltoni M, Schwetz T. Three-flavour neutrino oscillation update and comments on possible hints for a non-zero θ_{13}. In: *Proceedings, 7th International Workshop on the Identification of Dark Matter (IDM 2008)* (Stockholm) (2008).

69. Maltoni M, Schwetz T, Tórtola MA, Valle JWF. Status of global fits to neutrino oscillations. *New J Phys.* (2004) **6**:122. doi: 10.1088/1367-2630/6/1/122

70. Goswami S, Smirnov AY. Solar neutrinos and 1-3 leptonic mixing. *Phys Rev D* (2005) **72**:053011. doi: 10.1103/PhysRevD.72.053011

71. Fogli GL, Lisi E, Marrone A, Palazzo A. Global analysis of three-flavor neutrino masses and mixings. *Prog Part Nucl Phys.* (2006) **57**:742–95. doi: 10.1016/j.ppnp.2005.08.002

72. Escamilla J, Latimer DC, Ernst DJ. Atmospheric neutrino oscillation data constraints on θ_{13}. *Phys Rev Lett.* (2009) **103**:061804. doi: 10.1103/PhysRevLett.103.061804

73. Gonzalez-Garcia MC, Maltoni M, Salvado J. Updated global fit to three neutrino mixing: status of the hints of $\theta_{13} > 0$. *J High Energy Phys.* (2010) **4**:56. doi: 10.1007/JHEP04(2010)056

74. Schwetz T, Tórtola M, Valle JWF. Global neutrino data and recent reactor fluxes: status of three-flavour oscillation parameters. *New J Phys.* (2011) **13**:063004. doi: 10.1088/1367-2630/13/6/063004

75. Fogli GL, Lisi E, Marrone A, Palazzo A, Rotunno AM. Evidence of $\theta_{13} > 0$ from global neutrino data analysis. *Phys Rev D* (2011) **84**:053007. doi: 10.1103/PhysRevD.84.053007

76. An FP, Balantekin AB, Band HR, Bishai M, Blyth S, Cao D, et al. Measurement of electron antineutrino oscillation based on 1230 days of operation of the Daya Bay experiment. *Phys Rev D* (2017) **95**:072006. doi: 10.1103/PhysRevD.95.072006

77. Parke S. What is Δm_{ee}^2? *Phys Rev D* (2016) **93**:053008. doi: 10.1103/PhysRevD.93.053008

78. Choi JH, et al. Observation of energy and baseline dependent reactor antineutrino disappearance in the RENO experiment. *Phys Rev Lett.* (2016) **116**:211801. doi: 10.1103/PhysRevLett.116.211801

79. Seo SH, et al. Spectral measurement of the electron antineutrino oscillation amplitude and frequency using 500 live days of RENO data. arXiv:1610.04326.

80. Meregaglia A. Multi-detector results from the Double Chooz experiment. Available online at: https://indico.in2p3.fr/event/13763/session/14/contribution/29/material/slides/0.pdf (2017).

81. Berger C, Fröhlich M, Nisius MR, Raupach F, Blum D, Bourdarios C, et al. A study of atmospheric neutrino oscillations in the FREJUS experiment. *Phys Lett B* (1990) **245**:305–10. doi: 10.1016/0370-2693(90)90150-5

82. Becker-Szendy R, Bionta RM, Bratton CB, Casper D, Claus R, Cortez B, et al. IMB-3: a large water Cherenkov detector for nucleon decay and neutrino interactions. *Nucl Instrum Meth A* (1993) **324**:363–82. doi: 10.1016/0168-9002(93)90998-W

83. Hirata KS, et al. Observation of a small atmospheric muon-neutrino / electron-neutrino ratio in Kamiokande. *Phys Lett B* (1992) **280**:146–52. doi: 10.1016/0370-2693(92)90788-6

84. Ashie Y, et al. Evidence for an oscillatory signature in atmospheric neutrino oscillation. *Phys Rev Lett.* (2004) **93**:101801. doi: 10.1103/PhysRevLett.93.101801

85. Koshio Y. Solar and atmospheric neutrino oscillations in Super-Kamiokande. *PoS* (2017) **NOW2016**:1.

86. Ageron M, et al. ANTARES: the first undersea neutrino telescope. *Nucl Instrum Meth A* (2011) **656**:11–38. doi: 10.1016/j.nima.2011.06.103

87. Adrian-Martinez S, et al. Measurement of atmospheric neutrino oscillations with the ANTARES neutrino telescope. *Phys Lett B* (2012) **714**:224–30. doi: 10.1016/j.physletb.2012.07.002

88. Abbasi R, et al. The design and performance of IceCube deepCore. *Astropart Phys.* (2012) **35**:615–24. doi: 10.1016/j.astropartphys.2012.01.004

89. Aartsen MG, et al. Determining neutrino oscillation parameters from atmospheric muon neutrino disappearance with three years of IceCube DeepCore data. *Phys Rev D* (2015) **91**:072004. doi: 10.1103/PhysRevD.91.072004

90. Aartsen MG, Ackermann M, Adams J, Aguilar JA, Ahlers M, Ahrens M, et al. Measurement of atmospheric neutrino oscillations at 6-56 GeV with IceCube DeepCore. *Phys Rev Lett.* (2018) **120**:071801. doi: 10.1103/PhysRevLett.120.071801

91. Ahn MH, et al. Measurement of neutrino oscillation by the K2K experiment. *Phys Rev D* (2006) **74**:072003. doi: 10.1103/PhysRevD.74.072003

92. Adamson P, et al. Measurement of neutrino and antineutrino oscillations using beam and atmospheric data in MINOS. *Phys Rev Lett.* (2013) **110**:251801. doi: 10.1103/PhysRevLett.110.251801

93. Adamson P, et al. Electron neutrino and antineutrino appearance in the full MINOS data sample. *Phys Rev Lett.* (2013) **110**:171801. doi: 10.1103/PhysRevLett.110.171801

94. Adamson P, et al. Combined analysis of ν_μ disappearance and $\nu_\mu \rightarrow \nu_e$ appearance in MINOS using accelerator and atmospheric neutrinos. *Phys Rev Lett.* (2014) **112**:191801. doi: 10.1103/PhysRevLett.112.191801

95. Abe K, et al. Combined analysis of neutrino and antineutrino oscillations at T2K. *Phys Rev Lett.* (2017) **118**:151801. doi: 10.1103/PhysRevLett.118.151801

96. Abe K, et al. Updated T2K measurements of muon neutrino and antineutrino disappearance using 1.5×10^{21} protons on target. *Phys Rev D* (2017) **96**:011102. doi: 10.1103/PhysRevD.96.011102

97. Barenboim G, Lykken JD. A Model of CPT violation for neutrinos. *Phys Lett B* (2003) **554**:73–80. doi: 10.1016/S0370-2693(02)03262-8

98. Barenboim G, Borissov L, Lykken JD. Neutrinos that violate CPT, and the experiments that love them. *Phys Lett B* (2002) **534**:106–13. doi: 10.1016/S0370-2693(02)01597-6

99. Barenboim G, Ternes CA, Tórtola M. Neutrinos, DUNE and the world best bound on CPT violation. arXiv:1712.01714.

100. Adamson P, et al. Measurement of the neutrino mixing angle θ_{23} in NOvA. *Phys Rev Lett.* (2017) **118**:151802. doi: 10.1103/PhysRevLett.118.151802

101. Adamson P, et al. Constraints on oscillation parameters from ν_e appearance and ν_μ disappearance in NOvA. *Phys Rev Lett.* (2017) **118**:231801. doi: 10.1103/PhysRevLett.118.231801

102. Hartz M. T2K neutrino oscillation results with data up to 2017 summer. Available online at: http://www.t2k.org/docs/talk/282 (2017).

103. Acciarri R, et al. Long-baseline neutrino facility (LBNF) and deep underground neutrino experiment (DUNE). arXiv:1512.06148.

104. Aartsen MG, et al. Letter of intent: the precision IceCube next generation upgrade (PINGU). arXiv:1401.2046.

105. Brunner J. KM3NeT - ORCA: measuring neutrino oscillations and the mass hierarchy in the Mediterranean Sea. *PoS* (2016) **ICRC2015**:1140.

106. An F, et al. Neutrino physics with JUNO. *J Phys G* (2016) **43**:030401. doi: 10.1088/0954-3899/43/3/030401

107. Kim SB. New results from RENO and prospects with RENO-50. *Nucl Part Phys Proc.* (2015) **265–6**:93–8. doi: 10.1016/j.nuclphysbps.2015.06.024

108. Forero DV, Tórtola M, Valle JWF. Neutrino oscillations refitted. *Phys Rev D* (2014) **90**:093006. doi: 10.1103/PhysRevD.90.093006

109. Capozzi F, Fogli GL, Lisi E, Marrone A, Montanino D, Palazzo A. Status of three-neutrino oscillation parameters, circa 2013. *Phys Rev D* (2014) **89**:093018. doi: 10.1103/PhysRevD.89.093018

110. Gonzalez-Garcia MC, Maltoni M, Schwetz T. Updated fit to three neutrino mixing: status of leptonic CP violation. *J High Energy Phys.* (2014) **11**:52. doi: 10.1007/JHEP11(2014)052

111. Ohlsson T. Status of non-standard neutrino interactions. *Rept Prog Phys.* (2013) **76**:044201. doi: 10.1088/0034-4885/76/4/044201

112. Miranda OG, Nunokawa H. Non standard neutrino interactions: current status and future prospects. *New J Phys.* (2015) **17**:95002. doi: 10.1088/1367-2630/17/9/095002

113. Lisi E, Montanino D. Earth regeneration effect in solar neutrino oscillations: an analytic approach. *Phys Rev D* (1997) **56**:1792–803. doi: 10.1103/PhysRevD.56.1792

114. Valle JWF. Resonant oscillations of massless neutrinos in matter. *Phys Lett B* (1987) **199**:432–6. doi: 10.1016/0370-2693(87)90947-6

115. Roulet E. MSW effect with flavor changing neutrino interactions. *Phys Rev D* (1991) **44**:R935–8.

116. Guzzo MM, Masiero A, Petcov ST. On the MSW effect with massless neutrinos and no mixing in the vacuum. *Phys Lett B* (1991) **260**:154–60. doi: 10.1016/0370-2693(91)90984-X

117. Barger VD, Phillips RJN, Whisnant K. Solar neutrino solutions with matter enhanced flavor changing neutral current scattering. *Phys Rev D* (1991) **44**:1629–43. doi: 10.1103/PhysRevD.44.1629

118. Guzzo M, de Holanda PC, Maltoni M, Nunokawa H, Tórtola MA, Valle JWF. Status of a hybrid three neutrino interpretation of neutrino data. *Nucl Phys B* (2002) **629**:479–90. doi: 10.1016/S0550-3213(02)00139-6

119. Friedland A, Lunardini C, Pena-Garay C. Solar neutrinos as probes of neutrino matter interactions. *Phys Lett B* (2004) **594**:347. doi: 10.1016/j.physletb.2004.05.047

120. Guzzo MM, de Holanda PC, Peres OLG. Effects of nonstandard neutrino interactions on MSW - LMA solution to the solar neutrino problems. *Phys Lett B* (2004) **591**:1–6. doi: 10.1016/j.physletb.2004.04.035

121. Palazzo A. Hint of non-standard dynamics in solar neutrino conversion. *Phys Rev D* (2011) **83**:101701. doi: 10.1103/PhysRevD.83.101701

122. Dorenbosch J, et al. Experimental verification of the universality of ν_e and ν_μ coupling to the neutral weak current. *Phys Lett B* (1986) **180**:303–7. doi: 10.1016/0370-2693(86)90315-1

123. Coloma P, Schwetz T. Generalized mass ordering degeneracy in neutrino oscillation experiments. *Phys Rev D* (2016) **94**:055005. doi: 10.1103/PhysRevD.94.055005

124. Coloma P, Denton PB, Gonzalez-Garcia MC, Maltoni M, Schwetz T. Curtailing the dark side in non-standard neutrino interactions. *J High Energy Phys.* (2017) **4**:116. doi: 10.1007/JHEP04(2017)116

125. Zeller GP, et al. A precise determination of electroweak parameters in neutrino nucleon scattering. *Phys Rev Lett.* (2002) **88**:091802. doi: 10.1103/PhysRevLett.88.091802

126. Akimov D, Albert JB, An P, Awe C, Barbeau PS, Becker B, et al. Observation of coherent elastic neutrino-nucleus scattering. *Science* (2017) **357**:1123–6. doi: 10.1126/science.aao0990

127. Coloma P, Gonzalez-Garcia MC, Maltoni M, Schwetz T. COHERENT enlightenment of the neutrino dark side. *Phys Rev D* (2017) **96**:115007. doi: 10.1103/PhysRevD.96.115007

128. Davidson S, Pena-Garay C, Rius N, Santamaria A. Present and future bounds on nonstandard neutrino interactions. *J High Energy Phys.* (2003) **3**:11. doi: 10.1088/1126-6708/2003/03/011

129. Biggio C, Blennow M, Fernandez-Martinez E. Loop bounds on non-standard neutrino interactions. *J High Energy Phys.* (2009) **3**:139. doi: 10.1088/1126-6708/2009/03/139

130. Liao J, Marfatia D. COHERENT constraints on nonstandard neutrino interactions. *Phys Lett B* (2017) **775**:54–7. doi: 10.1016/j.physletb.2017.10.046

131. Bolaños A, Miranda OG, Palazzo A, Tórtola MA, Valle JWF. Probing non-standard neutrino-electron interactions with solar and reactor neutrinos. *Phys Rev D* (2009) **79**:113012. doi: 10.1103/PhysRevD.79.113012

132. Berezhiani Z, Raghavan RS, Rossi A. Probing nonstandard couplings of neutrinos at the Borexino detector. *Nucl Phys B* (2002) **638**:62–80. doi: 10.1016/S0550-3213(02)00476-5

133. Agarwalla SK, Lombardi F, Takeuchi T. Constraining non-standard interactions of the neutrino with borexino. *J High Energy Phys.* (2012) **12**:79. doi: 10.1007/JHEP12(2012)079

134. Khan AN, McKay DW. $\sin^2(\theta)w$ estimate and bounds on nonstandard interactions at source and detector in the solar neutrino low-energy regime. *J High Energy Phys.* (2017) **7**:143. doi: 10.1007/JHEP07(2017)143

135. Fornengo N, Gonzalez-Garcia MC, Valle JW. On the interpretation of the atmospheric neutrino data in terms of flavor changing neutrino interactions. *J High Energy Phys.* (2000) **7**:6. doi: 10.1088/1126-6708/2000/07/006

136. Fornengo N, Maltoni M, Tomàs Bayo R, Valle JWF. Probing neutrino nonstandard interactions with atmospheric neutrino data. *Phys Rev D* (2002) **65**:013010. doi: 10.1103/PhysRevD.65.013010

137. Friedland A, Lunardini C, Maltoni M. Atmospheric neutrinos as probes of neutrino-matter interactions. *Phys Rev D* (2004) **70**:111301. doi: 10.1103/PhysRevD.70.111301

138. Friedland A, Lunardini C. A Test of tau neutrino interactions with atmospheric neutrinos and K2K. *Phys Rev D* (2005) **72**:053009. doi: 10.1103/PhysRevD.72.053009

139. Mitsuka G, et al. Study of non-standard neutrino interactions with atmospheric neutrino data in super-kamiokande I and II. *Phys Rev D* (2011) **84**:113008. doi: 10.1103/PhysRevD.84.113008

140. Gonzalez-Garcia MC, Maltoni M, Salvado J. Testing matter effects in propagation of atmospheric and long-baseline neutrinos. *J High Energy Phys.* (2011) **5**:75. doi: 10.1007/JHEP05(2011)075

141. Esmaili A, Smirnov AY. Probing non-standard interaction of neutrinos with iceCube and deepCore. *J High Energy Phys.* (2013) **6**:26. doi: 10.1007/JHEP06(2013)026

142. Aartsen MG, et al. Search for nonstandard neutrino interactions with IceCube deepCore. arXiv:1709.07079.

143. Salvado J, Mena O, Palomares-Ruiz S, Rius N. Non-standard interactions with high-energy atmospheric neutrinos at IceCube. *J High Energy Phys.* (2017) **1**:141. doi: 10.1007/JHEP01(2017)141

144. Choubey S, Ohlsson T. Bounds on non-standard neutrino interactions using PINGU. *Phys Lett B* (2014) **739**:357–64. doi: 10.1016/j.physletb.2014.11.010

145. Choubey S, Ghosh A, Ohlsson T, Tiwari D. Neutrino physics with non-standard interactions at INO. *J High Energy Phys.* (2015) **12**:126. doi: 10.1007/JHEP12(2015)126

146. Gonzalez-Garcia MC, Maltoni M, Martinez-Soler I, Song N. . Non-standard neutrino interactions in the Earth and the flavor of astrophysical neutrinos. *Astropart Phys.* (2016) **84**:15–22. doi: 10.1016/j.astropartphys.2016.07.001

147. An FP, et al. Measurement of the reactor antineutrino flux and spectrum at daya bay. *Phys Rev Lett.* (2016) **116**:061801. doi: 10.1103/PhysRevLett.116.061801

148. Abe Y, et al. Improved measurements of the neutrino mixing angle θ_{13} with the Double Chooz detector. *J High Energy Phys.* (2014) **10**:86. doi: 10.1007/JHEP10(2014)086

149. Ohlsson T, Zhang H. Non-standard interaction effects at reactor neutrino experiments. *Phys Lett B* (2009) **671**:99–104. doi: 10.1016/j.physletb.2008.12.005

150. Girardi I, Meloni D. Constraining new physics scenarios in neutrino oscillations from Daya Bay data. *Phys Rev D* (2014) **90**:073011. doi: 10.1103/PhysRevD.90.073011

151. Khan AN, McKay DW, Tahir F. Sensitivity of medium-baseline reactor neutrino mass-hierarchy experiments to nonstandard interactions. *Phys Rev D* (2013) **88**:113006. doi: 10.1103/PhysRevD.88.113006

152. Kopp J, Lindner M, Ota T, Sato J. Non-standard neutrino interactions in reactor and superbeam experiments. *Phys Rev D* (2008) **77**:013007. doi: 10.1103/PhysRevD.77.013007

153. Ohlsson T, Zhang H, Zhou S. Nonstandard interaction effects on neutrino parameters at medium-baseline reactor antineutrino experiments. *Phys Lett B* (2014) **728**:148–55. doi: 10.1016/j.physletb.2013.11.052

154. Adamson P, et al. Search for flavor-changing non-standard neutrino interactions by MINOS. *Phys Rev D* (2013) **88**:072011. doi: 10.1103/PhysRevD.88.072011

155. Adamson P, et al. Search for flavor-changing nonstandard neutrino interactions using ν_e appearance in MINOS. *Phys Rev D* (2017) **95**:012005. doi: 10.1103/PhysRevD.95.012005

156. Liao J, Marfatia D, Whisnant K. Nonmaximal neutrino mixing at NOνA from nonstandard interactions. *Phys Lett B* (2017) **767**:350–353. doi: 10.1016/j.physletb.2017.02.024

157. Girardi I, Meloni D, Petcov ST. The daya bay and T2K results on $\sin^2 2\theta_{13}$ and non-standard neutrino interactions. *Nucl Phys B* (2014) **886**:31–42. doi: 10.1016/j.nuclphysb.2014.06.014

158. Blennow M, Choubey S, Ohlsson T, Raut SK. Exploring source and detector non-standard neutrino interactions at ESSνSB. *J High Energy Phys.* (2015) **9**:96. doi: 10.1007/JHEP09(2015)096

159. Ge SF, Smirnov AY. Non-standard interactions and the CP phase measurements in neutrino oscillations at low energies. *J High Energy Phys.* (2016) **10**:138. doi: 10.1007/JHEP10(2016)138

160. Khan AN. Global analysis of the source and detector nonstandard interactions using the short baseline $\nu - e$ and $\bar{\nu} - e$ scattering data. *Phys Rev D* (2016) **93**:093019. doi: 10.1103/PhysRevD.93.093019

161. Patrignani C, et al. Review of particle physics. *Chin Phys.* (2016) **40**:100001. doi: 10.1088/1674-1137/40/10/100001

162. Barranco J, Miranda OG, Moura CA, Valle JWF. Constraining non-standard neutrino-electron interactions. *Phys Rev D* (2008) **77**:093014. doi: 10.1103/PhysRevD.77.093014

163. Deniz M, et al. Constraints on non-standard neutrino interactions and unparticle physics with neutrino-electron scattering at the Kuo-Sheng nuclear power reactor. *Phys Rev D* (2010) **82**:033004. doi: 10.1103/PhysRevD.82.033004

164. Khan AN, McKay DW, Tahir F. Short baseline reactor $\bar{\nu} - e$ scattering experiments and nonstandard neutrino interactions at source and detector. *Phys Rev D* (2014) **90**:053008. doi: 10.1103/PhysRevD.90.053008

165. Escrihuela FJ, Tórtola M, Valle JWF, Miranda OG. Global constraints on muon-neutrino non-standard interactions. *Phys Rev D* (2011) **83**:093002. doi: 10.1103/PhysRevD.83.093002

166. Astier P, et al. Final NOMAD results on muon-neutrino → tau-neutrino and electron-neutrino → tau-neutrino oscillations including a new search for tau-neutrino appearance using hadronic tau decays. *Nucl Phys B* (2001) **611**:3–39. doi: 10.1016/S0550-3213(01)00339-X

167. Astier P, et al. Search for nu(mu) → nu(e) oscillations in the NOMAD experiment. *Phys Lett B* (2003) **570**:19–31. doi: 10.1016/j.physletb.2003.07.029

168. Eitel K. Latest results of the KARMEN2 experiment. *Nucl Phys Proc Suppl.* (2001) **91**:191–7. doi: 10.1016/S0920-5632(00)00940-3

169. Forero DV, Huang WC. Sizable NSI from the SU(2)$_L$ scalar doublet-singlet mixing and the implications in DUNE. *J High Energy Phys.* (2017) **3**:18. doi: 10.1007/JHEP03(2017)018

170. Babu KS, Friedland A, Machado PAN, Mocioiu I. Flavor gauge models below the fermi scale. *J High Energy Phys.* (2017) **12**:96. doi: 10.1007/JHEP12(2017)096

171. Harnik R, Kopp J, Machado PAN. Exploring nu signals in dark matter detectors. *JCAP* (2012) **1207**:26. doi: 10.1088/1475-7516/2012/07/026

172. Batley JR, et al. Search for the dark photon in π^0 decays. *Phys Lett B* (2015) **746**:178–85. doi: 10.1016/j.physletb.2015.04.068

173. Bakhti P, Farzan Y. Constraining secret gauge interactions of neutrinos by meson decays. *Phys Rev D* (2017) **95**:095008. doi: 10.1103/PhysRevD.95.095008

174. Belotsky KM, Sudarikov AL, Khlopov AY. Constraint on anomalous 4nu interaction. *Phys Atom Nucl.* (2001) **64**:1637–42. doi: 10.1134/1.1409505

175. Laha R, Dasgupta B, Beacom JF. Constraints on new neutrino interactions via light abelian vector bosons. *Phys Rev D* (2014) **89**:093025. doi: 10.1103/PhysRevD.89.093025

176. Barger V, Chiang CW, Keung WY, Marfatia D. Constraint on parity-violating muonic forces. *Phys Rev Lett.* (2012) **108**:081802. doi: 10.1103/PhysRevLett.108.081802

177. Kamada A, Yu HB. Coherent propagation of PeV neutrinos and the Dip in the neutrino spectrum at iceCube. *Phys Rev D* (2015) **92**:113004. doi: 10.1103/PhysRevD.92.113004

178. Davoudiasl H, Lee HS, Marciano WJ. Muon $g − 2$, rare kaon decays, and parity violation from dark bosons. *Phys Rev D* (2014) **89**:095006. doi: 10.1103/PhysRevD.89.095006

179. Huang GY, Ohlsson T, Zhou S. Observational constraints on secret neutrino interactions from big bang nucleosynthesis. arXiv:1712.04792.

180. Das CR, Pulido J. Possible trace of neutrino nonstandard interactions in the supernova. *J Phys Conf Ser.* (2012) **375**:042040. doi: 10.1088/1742-6596/375/1/042040

181. Esteban-Pretel A, Tomas R, Valle JWF. Probing non-standard neutrino interactions with supernova neutrinos. *Phys Rev D* (2007) **76**:053001. doi: 10.1103/PhysRevD.76.053001

182. Jegerlehner F, Nyffeler A. The Muon g-2. *Phys Rept.* (2009) **477**:1–110. doi: 10.1016/j.physrep.2009.04.003

183. Dutta B, Liao S, Strigari LE, Walker JW. Non-standard interactions of solar neutrinos in dark matter experiments. *Phys Lett B* (2017) **773**:242–6. doi: 10.1016/j.physletb.2017.08.031

184. Cerdeño DG, Fairbairn M, Jubb T, Machado PAN, Vincent AC, Boehm C. Physics from solar neutrinos in dark matter direct detection experiments. *J High Energy Phys.* (2016) **5**:118. doi: 10.1007/JHEP05(2016)118

185. Aristizabal Sierra D, Rojas N, Tytgat MHG. Neutrino non-standard interactions and dark matter searches with multi-ton scale detectors. arXiv:1712.09667.

186. Shoemaker IM. COHERENT search strategy for beyond standard model neutrino interactions. *Phys Rev D* (2017) **95**:115028. doi: 10.1103/PhysRevD.95.115028

187. Akimov D, et al. The COHERENT experiment at the spallation neutron source. arXiv:1509.08702.

188. Wong HT. Ultra-low-energy germanium detector for neutrino-nucleus coherent scattering and dark matter searches. *Mod Phys Lett A* (2008) **23**:1431–42. doi: 10.1142/S0217732308027801

189. Aguilar-Arevalo A, et al. The CONNIE experiment. *J Phys Conf Ser.* (2016) **761**:012057. doi: 10.1088/1742-6596/761/1/012057

190. Aguilar-Arevalo A, et al. Results of the engineering run of the Coherent Neutrino Nucleus Interaction Experiment (CONNIE). *JINST* (2016) **11**:P07024. doi: 10.1088/1748-0221/11/07/P07024

191. Agnolet G, et al. Background studies for the MINER coherent neutrino scattering reactor experiment. *Nucl Instrum Meth A* (2017) **853**:53–60. doi: 10.1016/j.nima.2017.02.024

192. Billard J, Carr R, Dawson J, Figueroa-Feliciano E, Formaggio JA, Gascon J, et al. Coherent neutrino scattering with low temperature bolometers at chooz reactor complex. *J Phys G Nucl Part Phys.* (2017) **44**:105101. doi: 10.1088/1361-6471/aa83d0

193. Lindner M, Rodejohann W, Xu XJ. Coherent neutrino-nucleus scattering and new neutrino interactions. *J High Energy Phys.* (2017) **3**:97. doi: 10.1007/JHEP03(2017)097

194. Barranco J, Miranda OG, Rashba TI. Probing new physics with coherent neutrino scattering off nuclei. *J High Energy Phys.* (2005) **12**:21. doi: 10.1088/1126-6708/2005/12/021

195. Kerman S, Sharma V, Deniz M, Wong HT, Chen JW, Li HB, et al. Coherency in neutrino-nucleus elastic scattering. *Phys Rev D* (2016) **93**:113006. doi: 10.1103/PhysRevD.93.113006

196. Mishra SR, et al. Neutrino tridents and W Z interference. *Phys Rev Lett.* (1991) **66**:3117–20. doi: 10.1103/PhysRevLett.66.3117

197. Geiregat D, et al. First observation of neutrino trident production. *Phys Lett B* (1990) **245**:271–5. doi: 10.1016/0370-2693(90)90146-W

198. Altmannshofer W, Gori S, Pospelov M, Yavin I. Neutrino trident production: a powerful probe of new physics with neutrino beams. *Phys Rev Lett.* (2014) **113**:091801. doi: 10.1103/PhysRevLett.113.091801

199. Ge SF, Lindner M, Rodejohann W. Atmospheric trident production for probing new physics. *Phys Lett B* (2017) **772**:164–8. doi: 10.1016/j.physletb.2017.06.020

200. Trocino D. Searches for invisible decay modes of the Higgs boson with the CMS detector. *Nucl Part Phys. Proc.* (2016) **273–275**:758–63. doi: 10.1016/j.nuclphysbps.2015.09.116

201. Davoudiasl H, Lee HS, Marciano WJ. 'Dark' Z implications for parity violation, rare meson decays, and higgs physics. *Phys Rev D* (2012) **85**:115019. doi: 10.1103/PhysRevD.85.115019

202. Khachatryan V, et al. Searches for electroweak production of charginos, neutralinos, and sleptons decaying to leptons and W, Z, and Higgs bosons in pp collisions at 8 TeV. *Eur Phys J C* (2014) **74**:3036. doi: 10.1140/epjc/s10052-014-3036-7

203. Fernandez-Martinez E, Hernandez-Garcia J, Lopez-Pavon J. Global constraints on heavy neutrino mixing. *J High Energy Phys.* (2016) **8**:33. doi: 10.1007/JHEP08(2016)033

204. Escrihuela FJ, Forero DV, Miranda OG, Tórtola M, Valle JWF. On the description of nonunitary neutrino mixing. *Phys Rev D* (2015) **92**:053009. doi: 10.1103/PhysRevD.92.053009

205. Escrihuela FJ, Forero DV, Miranda OG, Tórtola M, Valle JWF. Probing CP violation with non-unitary mixing in long-baseline neutrino oscillation experiments: DUNE as a case study. *New J Phys.* (2017) **19**:093005. doi: 10.1088/1367-2630/aa79ec

206. Baldini AM, et al. Search for the lepton flavour violating decay $\mu^+ \to e^+\gamma$ with the full dataset of the MEG experiment. *Eur Phys J C* (2016) **76**:434. doi: 10.1140/epjc/s10052-016-4271-x

207. Picciotto CE, et al. Searches for majoron production and other processes associated with $\pi \to \nu_e$ decay. *Phys Rev D* (1988) **37**:1131.

208. Heintze J, et al. A measurement of the K+ → e+ neutrino gamma structure decay. *Nucl Phys B* (1979) **149**:365–80. doi: 10.1016/0550-3213(79)90001-4

209. Aguilar-Arevalo A, et al. Improved measurement of the $\pi \to e\nu$ branching ratio. *Phys Rev Lett.* (2015) **115**:071801. doi: 10.1103/PhysRevLett.115.071801

210. Lazzeroni C, et al. Precision measurement of the ratio of the charged kaon leptonic decay rates. *Phys Lett B* (2013) **719**:326–36. doi: 10.1016/j.physletb.2013.01.037

211. Pang CY, Hildebrand RH, Cable GD, Stiening R. Search for rare k+ decays. i. k+ → mu+ nu anti-nu nu. *Phys Rev D* (1973) **8**:1989–2003.

212. Pospelov M. Secluded U(1) below the weak scale. *Phys Rev D* (2009) **80**:095002. doi: 10.1103/PhysRevD.80.095002

213. Blennow M, Choubey S, Ohlsson T, Pramanik D, Raut SK. A combined study of source, detector and matter non-standard neutrino interactions at DUNE. *J High Energy Phys.* (2016) **8**:90. doi: 10.1007/JHEP08(2016)090

214. Masud M, Mehta P. Nonstandard interactions and resolving the ordering of neutrino masses at DUNE and other long baseline experiments. *Phys Rev D* (2016) **94**:053007. doi: 10.1103/PhysRevD.94.053007

215. Coloma P. Non-standard interactions in propagation at the deep underground neutrino experiment. *J High Energy Phys.* (2016) **3**:16. doi: 10.1007/JHEP03(2016)016

216. Oki H, Yasuda O. Sensitivity of the T2KK experiment to the non-standard interaction in propagation. *Phys Rev D* (2010) **82**:073009. doi: 10.1103/PhysRevD.82.073009

217. Fukasawa S, Ghosh M, Yasuda O. Sensitivity of the T2HKK experiment to nonstandard interactions. *Phys Rev D* (2017) **95**:055005. doi: 10.1103/PhysRevD.95.055005

218. Abe K, et al. Physics potentials with the second hyper-kamiokande detector in Korea. arXiv:1611.06118.

219. de Gouvêa A, Kelly KJ. Non-standard neutrino interactions at DUNE. *Nucl Phys B* (2016) **908**:318–35. doi: 10.1016/j.nuclphysb.2016.03.013

220. Huitu K, Kärkkäinen TJ, Maalampi J, Vihonen S. Constraining the nonstandard interaction parameters in long baseline neutrino experiments. *Phys Rev D* (2016) **93**:053016. doi: 10.1103/PhysRevD.93.053016

221. Liao J, Marfatia D, Whisnant K. Nonstandard neutrino interactions at DUNE, T2HK and T2HKK. *J High Energy Phys.* (2017) **1**:71. doi: 10.1007/JHEP01(2017)071

222. Masud M, Bishai M, Mehta P. Extricating new physics scenarios at DUNE with high energy beams. arXiv:1704.08650.

223. Rout J, Masud M, Mehta P. Can we probe intrinsic CP and T violations and nonunitarity at long baseline accelerator experiments? *Phys Rev D* (2017) **95**:075035. doi: 10.1103/PhysRevD.95.075035

224. Abe K, et al. Physics potential of a long-baseline neutrino oscillation experiment using a J-PARC neutrino beam and Hyper-Kamiokande. *PTEP* (2015) **2015**:053C02. doi: 10.1093/ptep/ptv061

225. Kearns E, et al. Hyper-kamiokande physics opportunities. In *Proceedings, 2013 Community Summer Study on the Future of U.S. Particle Physics: Snowmass on the Mississippi (CSS2013): July 29-August 6, 2013*. Minneapolis, MN (2013).

226. Deepthi KN, Goswami S, Nath N. Can nonstandard interactions jeopardize the hierarchy sensitivity of DUNE? *Phys Rev D* (2017) **96**:075023. doi: 10.1103/PhysRevD.96.075023

227. Joo KK. New results from RENO & prospects with RENO-50. *J Phys Conf Ser.* (2017) **888**:012012. doi: 10.1088/1742-6596/888/1/012012

228. Huber P, Lindner M, Winter W. Simulation of long-baseline neutrino oscillation experiments with GLoBES (General Long Baseline Experiment Simulator). *Comput Phys Commun.* (2005) **167**:195. doi: 10.1016/j.cpc.2005.01.003

229. Huber P, Kopp J, Lindner M, Rolinec M, Winter W. New features in the simulation of neutrino oscillation experiments with GLoBES 3.0: general long baseline experiment simulator. *Comput Phys Commun.* (2007) **177**:432–8. doi: 10.1016/j.cpc.2007.05.004

230. Gonzalez-Garcia MC, Maltoni M, Salvado J, Schwetz T. Global fit to three neutrino mixing: critical look at present precision. *J High Energy Phys.* (2012) **12**:123. doi: 10.1007/JHEP12(2012)123

231. Cao J, et al. Muon-decay medium-baseline neutrino beam facility. *Phys Rev.* (2014) **17**:090101. doi: 10.1103/PhysRevSTAB.17.090101

232. Blennow M, Coloma P, Fernandez-Martinez E. The MOMENT to search for CP violation. *J High Energy Phys.* (2016) **3**:197. doi: 10.1007/JHEP03(2016)197

233. Huber P, Schwetz T. A Low energy neutrino factory with non-magnetic detectors. *Phys Lett B* (2008) **669**:294–300. doi: 10.1016/j.physletb.2008.10.009

234. Bakhti P, Farzan Y. CP-violation and non-standard interactions at the MOMENT. *J High Energy Phys.* (2016) **7**:109. doi: 10.1007/JHEP07(2016)109

235. King SF. Neutrino mass models. *Rept Prog Phys.* (2004) **67**:107–58. doi: 10.1088/0034-4885/67/2/R01

236. Hirsch M, Valle JWF. Supersymmetric origin of neutrino mass. *New J Phys.* (2004) **6**:76. doi: 10.1088/1367-2630/6/1/076

237. Boucenna SM, Morisi S, Valle JWF. The low-scale approach to neutrino masses. *Adv High Energy Phys.* (2014) **2014**:831598. doi: 10.1155/2014/831598

238. Cai Y, Herrero García J, Schmidt MA, Vicente A, Volkas RR. From the trees to the forest: a review of radiative neutrino mass models. *Front Phys.* (2017) **5**:63. doi: 10.3389/fphy.2017.00063